ACTA CLIMATOLOGICA ET CHOROLOGICA

TOMUS XLVII–XLVIII.

ACTA CLIMATOLOGICA ET CHOROLOGICA

TOMUS XLVII-XLVIII.

CONTENTS

SYNOPTIC STUDY OF THE HEAVIEST SNOWFALLS IN POZNAŃ SINCE 1960/61 TO 2009/2010

E BEDNORZ

Department of Climatology, Adam Mickiewicz University, ul. Dzięgielowa 27, 61-680 Poznań, Poland
E-mail: ewabedno@amu.edu.pl

Summary: Composite maps of the sea level pressure and 500 hPa geopotential heights means and anomalies were constructed for the days with the high snow accumulation in Poznań. Similar maps of the air temperature at the isobaric level 850 hPa and of precipitable water content were presented. Additionally, 48-hours back trajectories of air masses for chosen days with the most effective snowfalls were constructed, using the NOAA HYSPLIT model. Negative anomalies of sea level pressure and 500 hPa heights, which mean low pressure systems spreading over Europe, are the basic condition of abundant snowfalls in Poznań. Snowfalls may appear as a result of fronts in the colder parts of Mediterranean cyclones with the dynamic warm and humid air of distant southern origin climbing upwards on the cooler and more stabile polar air masses from the north or east. The alternative location of snow-bringing low pressure systems is the Baltic Sea region.

Key words: snowfalls in Poland, air circulation, synoptic conditions, back trajectories

1. INTRODUCTION

Winter in the European moderate zone is a very changeable season, with mild periods alternating with the cold ones, the latest being often accompanied with snowfalls or even heavy snowstorms. These severe weather events may have a strong economic impact. Abundant snowfalls, often simultaneous with low temperatures, may cause traffic hazards, communication problems, and power shortages; consequently, they can paralyze community life. The European community experienced such events for example in the end of November 2005 after short but strong snowstorms which took place in Germany and Western Europe. Dramatic events took place in Bavaria in January 2006 when a deep snow accumulation after heavy snowfalls crushed building structures, and caused the collapse of the roof of the ice rink, and also in Katowice (Poland), where the exhibition hall collapsed during the racing pigeon show. Both tragedies brought many deaths and injuries.

Serious social and economic effects justify research into the synoptic reasons for heavy snowstorms, as it may be helpful in forecasting such weather events. Snow occurrence is determined by the air temperature, precipitation and, indirectly, by the inflow of particular air masses. The atmospheric circulation is a driving factor for weather conditions in winter and it is responsible for the above mentioned intra-seasonal variability of the winter weather in the moderate zone. The aim of this study is to find the daily circulation patterns and daily synoptic conditions responsible for abundant snowfalls in Poznań, resulting in daily increase in snow cover depth by at least 10 cm. Closer analysis of synoptic conditions of heavy

snowfalls may be helpful in recognizing circumstances of these phenomena, however rare, but having a strong economic impact.

The analysis of severe snowstorms formation in Europe has already been performed in a regional scale, for example for the Swedish east coast (Andersson and Nilsson 1990, Andersson and Gustafsson 1993). The synoptic classification of severe snowstorms in Austria has been worked out by Spreitzhofer (1999a, 1999b). Bednorz (2008) has found circulation patterns responsible for heavy snowfalls in the German-Polish lowlands. Babolcsai and Hirsch (2006) have worked out detailed characteristics and synoptic classification of heavy snowfall events in Budapest for the period 1953-2003, consisting of eight weather types. Most of them were connected with different kinds of Mediterranean cyclones and additionally with secondary lows in north-western Europe. In this study the detailed analysis was performed for Poznań, located in the central Europe.

The extent of the seasonal snow cover is going to decrease in central Europe, according to climate projections (EEA 2012, 2013). The increase in winter precipitation expected in most models will not mean more snow on the ground, as snow cover is sensitive to winter temperature as well as to snowfalls (Raisanen 2008, Raisanen and Eklund 2012). Number of days with snowfall above 10 cm will increase only in the north and they will probably decrease in other parts of Europe. Also the reduced number of snow cover days is expected in the analyzed region (Kjelstrom et al. 2011). In such context research on the synoptic conditions of high snow occurrence in a central European station seems to be justified.

2. MATERIAL AND METHODS

In this study, the intensity of snowfalls was evaluated by the increase in the snow cover depth accumulated on the ground. Snow depth observations at the meteorological stations are taken once a day at 6:00 UTC with 1 cm precision. The days when the snow has a depth of ≥ 1 cm are considered as the days with snow cover. For the purpose of the study, the days during which snow cover depth increased by ≥ 10 cm were selected. Changes in the snow cover depth were calculated by subtracting the snow cover depth of a given day from the snow cover depth of the following day. Daily data of snow cover depth in the station of Poznań Ławica, regarding 50 winter seasons from December to March 1960/1961-2009/2010, was derived from the Institute of Meteorology and Water Management dataset. Besides, the extreme 2-, 3-, 4- and 5-days lasting events of snow accumulation were identified.

In order to describe the circulation, daily sea level pressure (SLP) and 500 hPa geopotential heights (Z500) data were selected from the National Centers for Environmental Prediction (NCEP) – National Center for Atmospheric Research (NCAR) reanalysis data (Kalnay et al. 1996). From the same source, grid-based temperature values at isobaric level 850 hPa (T850) and the content of precipitable water (PW), were obtained and used in the study. The PW index designates the mass of water contained in the column of air above the unit surface area, irrespective of the state of aggregation, and is expressed in kg m^{-2} (Wibig and Siedlecki 2007).

Firstly, the correlation coefficients between the daily snow increases, reaching and exceeding the critical values of 5 cm and 10 cm and the daily values of SLP and Z500 in the grid points in the area 35-70°N latitude by 35°W-40°E longitude were calculated and

mapped. Rikiishi and Sakakibara (2004), analyzing the intensity of snow accumulation in the territory of the former Soviet Union, have calculated the pentad differences in the depth of snow cover and referred these to atmospheric circulation.

Furthermore, composite maps of the SLP Z500 means and anomalies were constructed for the days with increase in the snow cover depth of $\geq$ 10 cm. Anomalies were computed as differences between composite values and multiannual means of the winter season. Similar anomaly maps of T850 and PW were constructed. The composite analysis has been used previously to identify the atmospheric circulation patterns associated with heavy snowfalls in the mountains (Birkeland and Mock 1996). Finally, 48-hours back trajectories of air masses for three chosen days with the most effective snowfalls (i.e. days with the highest snow accumulation), were constructed, using the NOAA HYSPLIT model (Rolph 2012, Draxler and Rolph 2012, http://ready.arl.noaa.gov/HYSPLIT.php). The model analyzed the movement of air masses for three altitudes above sea level: 300-500 meters (corresponding to the medium level of the mixing layer), 1500-2000 meters (corresponding to the mean altitude of isobaric surface 850 hPa) and 4000-5000 meters (corresponding to the altitude of isobaric surface 700-500 hPa). An analysis of air trajectories at the three altitudes provided significant input to the information obtained from synoptic maps and made it possible to identify the probable source area of air masses causing snowfalls. This method is often used to detect the source area of pollution deposit (Avila and Alarcon 1999, Salvador et al. 2010).

Additionally, the synoptic maps from 00:00 UTC for the days with extreme snow accumulation were collected from the Institute of Meteorology and Water Management database and used to identify the precise synoptic conditions of the selected cases of extreme snowfalls.

3. RESULTS

Poznań is situated in the least snowy region in Poland, where the mean annual number of days with snow cover does not reach 50 days (Bednorz 2011). The Poznań Ławica station experiences on the average 48 days with snow cover a year, however there are on the average 17 days with snow accumulation noted in the station.

16 cases of snowfalls resulting in a snow depth daily increase by at least 10 cm were identified in Poznań during 50 winter seasons 1960/61 - 2009/10 (Table 1). Four of them were noted in the snowy period of the 1960s and three in the beginning of the 1970s. Seven cases were reported in the 1980s, four of them happened in the snowy season 1985/86. The further two decades, regarded as not snowy ones, experienced only two events of extreme snow accumulation in Poznań. The maximum daily snow accumulation, resulting in snow cover depth increase by 17 cm, was recorded in the beginning of March 1965. Snowfalls could persist for more than one day when the low pressure systems with the snow-bringing fronts moved over Central-Europe. Therefore the cases when a great amount of snow came in a short time period (from 2 to 5 days) were also identified (Table 2). The 2-days snowfall exceeding 10 cm may happen once a year on the average and the 3-days snowfall of the same effectiveness (i.e. causing the increase in snow cover depth by at least 10 cm) may happen twice a year. However, the annual number of cases of snowfalls lasting 1-5 days and resulting in snow cover increase by $\geq$ 10 cm, varies from year to year (Fig. 1). In the least snowy winters (i.e. 1972/1973, 1983/1984, 1988/1989, 1996/1997, 1997/1998, 2000/2001, 2002/2003, 2007/2008, 2008/2009) there were no such days at all, while in the most snowy

winters (i.e. 1968/1069, 1969/1970, 1978/1979, 1985/1986, 1987/1988) there were over a dozen of such cases. In the last two decades (1990-2010) the number of abundant snowfall events has been smaller than in the 1960s and 1980s, however there is no statistically significant trend of changes in the 50-years period. Events of snowfalls lasting several days and causing at least 20 cm snow accumulation are very rare and they happened in the seasons 1964/65, 1969/70 and in December 2001.

Table 1 Events of the daily snow cover increase by ≥ 10 cm in Poznań in winters 1960/61-2009/10

Data	Daily snow cover increase in cm
03-03-1965	17
08-03-1966	10
26-12-1968	10
26-11-1969	11
16-01-1970	14
02-03-1970	11
29-11-1973	10
29-12-1985	10
26-01-1986	11
19-02-1986	11
10-04-1986	13
12-01-1987	12
30-01-1988	13
08-03-1988	11
19-11-1993	10
20-02-1996	10

Table 2 Number of cases with the highest snow cover increase in Poznań in winters 1960/61-2009/10

Length of the period	Snow cover increase by		
	≥ 10 cm	≥ 15 cm	≥ 20 cm
1 day	16	1	0
2 days	50	4	1
3 days	98	10	2
4 days	165	19	9
5 days	246	22	9

The correlation coefficients between the daily snow increases by at least 5 cm and the daily values of SLP and Z500 in the grid points show distinctly the areas of negative relationships, which indicate instant pressure decreases, accompanying abundant snowfalls (Fig. 2, left). The centre of the negative correlation falls to the south of Europe, exactly to the Venice Bay on the Adriatic Sea. The same computing performed for 16 cases of the highest snow accumulation allowed to produce the second correlation map (Fig. 2, right), where two centers of negative correlation appear, one of them located south of Poland, and the other one west to the British Islands.

Abundant snowfalls in Poznań, resulting in a snow cover depth increase by at least 10 cm are coexistent with a deep and vast low pressure system extending over Central-Europe (Fig. 3, left). Negative SLP anomalies exceed -12 hPa over the cyclone centre, while Z500 lowers by over 200 gpm (Fig. 3, right). The negative center of the SLP correlation field is shifted towards the south-east, regarding the negative center of the Z500. At the same time, higher-than-normal pressure is observed over the northern Atlantic, with a centre of positive anomalies (> 9 hPa) right over Island, which may be associated with the negative phase of the North Atlantic Oscillation (NAO). Contours of Z500 constructed for the days with snow

cover increase by at least 10 cm bend to the north over the Atlantic and to the south in central Europe, suggesting northerly and northwesterly flow in the middle troposphere over Western-Europe. At the same time, such pressure pattern indicates eastern and northeastern airflow in the lower troposphere. High pressure trough extending over Scandinavia may intensify the eastern and northeastern airflow over the Baltic Sea and northern Poland.
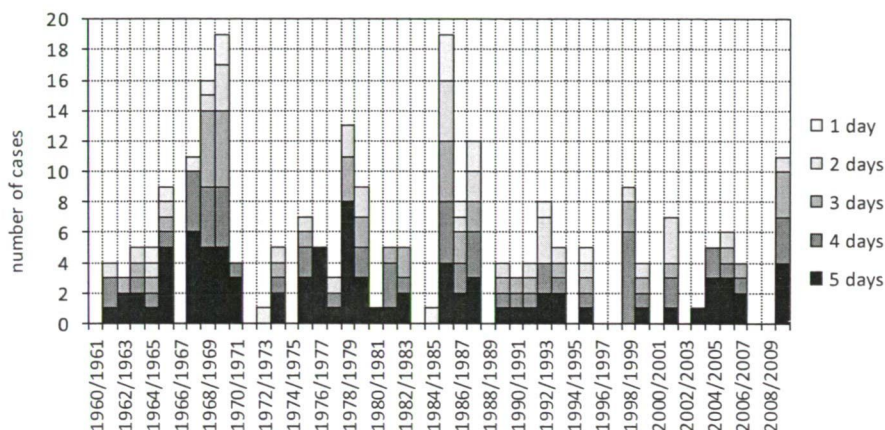
Fig. 1 Seasonal number of cases with snow cover increase by ≥ 10 cm during 1-, 2-, 3-, 4-, and 5-days periods
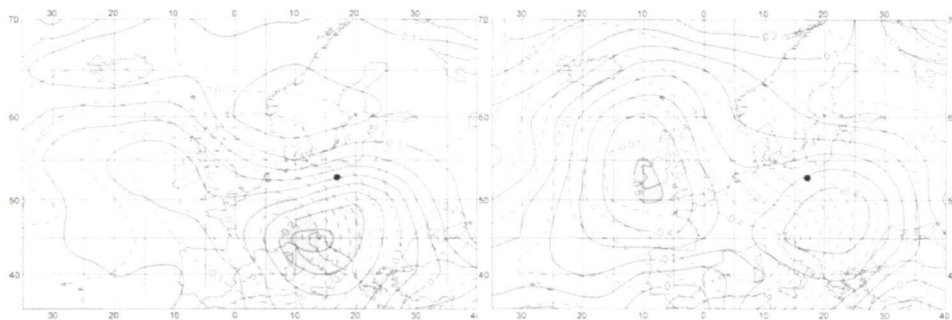
Fig. 2 Correlation coefficients between the daily values of SLP (solid lines) Z500 (dashed lines) and the daily snow increases of at least 5 cm (left) and 10 cm (right) in Poznań. Statistically significant values are shaded, location of Poznań marked with a dot

Contours of Z500, cutting the central European low meridionally, allow distinguishing a colder part of the SLP low in the north and a warmer part in the south. In the colder part, higher air density decreases the Z500, which is more than 300 gpm lower than in the southern part. Poznań is placed in the cold northeastern section of the low pressure system. Strong negative anomalies of T850 are observed over entire Europe, excluding the southeastern outskirts (Fig. 4). Temperature is lower than normal by 3-6 deg over central Europe and by 7-8 deg in the northern Europe. Negative PW anomalies are correlated to low temperatures over Europe and they are distributed similarly.
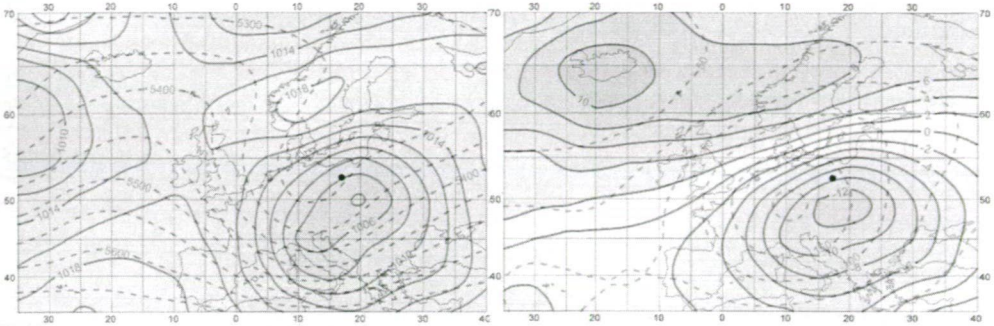
Fig. 3 Composite map (left) and anomaly map (right) of SLP (solid lines) and Z500 (dashed lines) for
the days with snow cover increase by at least 10 cm in Poznań.
Location of Poznań is marked with a dot
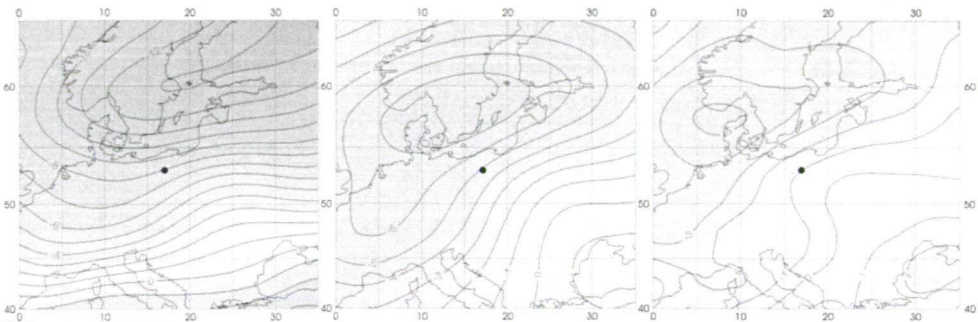
Fig. 4 Composite map (left) and anomaly map (middle) of T850 and anomaly map of PW (right) for
the days with snow cover increase by at least 10 cm in Poznań.
Location of Poznań is marked with a dot

Obviously, the circulation patterns observed during the selected 16 days of snow depth increase by at least 10 cm in Poznań were not identical. The detailed analysis of several synoptic maps allowed finding differences in the position of cyclonic centers over Europe. The synoptic map of 12 January 1987 represents the typical location of a low-pressure system for most of analyzed cases. It spreads in the south of Europe, in the Mediterranean region, with one center located over the Balkan Peninsula and a secondary centre over Italy and the Adriatic Sea (Fig. 5). At the same time a strong anticyclonal ridge spreads latitudinally over Scandinavia and northeastern Europe. The air pressure in a local centre over central Scandinavia exceeds 1050 hPa. The high pressure system over Northern-Europe preserves very cold air, of the polar continental origin, coming from the eastern direction in the lower troposphere. On the other hand the south cyclone is a reservoir of warm air from the Mediterranean. The meeting of these two elements results in heavy snowfalls in Central-Europe. The described processes signify warm front structure, with the dynamic warm and humid air of distant southern origin climbing upwards on the cooler and more stable polar continental air masses from the east. The demonstration of such a situation is shown at back trajectories at Fig. 5 drawn for the snowstorms on 12-13 Jan 1987 (12 cm of the new fallen snow). A quite similar situation took place on the 19-20 Feb 1986 (11 cm of the new fallen snow), with the cyclonal systems in the south of Europe and anticyclonal centre over northeastern Europe (Fig. 6).

Fig. 5 Synoptic map and the 48-hours back trajectories of air particles at heights of 300 m (triangles), 2000 m (squares) and 4000 m (circles) above ground level for 12-13 January 1987

Fig. 6 Synoptic map and the 48-hours back trajectories of air particles at heights of 500 m (triangles), 2000 m (squares) and 5000 m (circles) above ground level for 20 February 1986

The situations, when the cyclones, bringing heavy snowfalls to Poznań spread over Central-Europe are distinctly rarer. Only 30% of all distinguished cases of abundant snowfalls are caused by low pressure systems with heir centers located right over Poland, over northern Germany or northeast of Poland, as shown at Fig. 7. The small, but rather deep centre formed over the Baltic Sea and east thereof causes the northern flow of the arctic air to entire Poland at all tropospheric levels (Fig. 7). This time the Baltic Sea is a source region for the abundant snowfalls (11 cm of the new snow), as may be concluded from the back trajectories of the air masses.
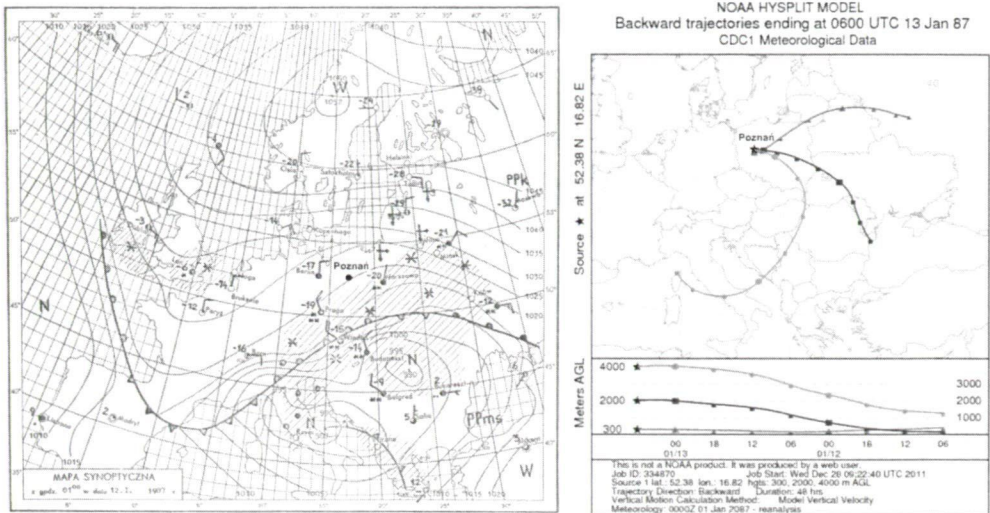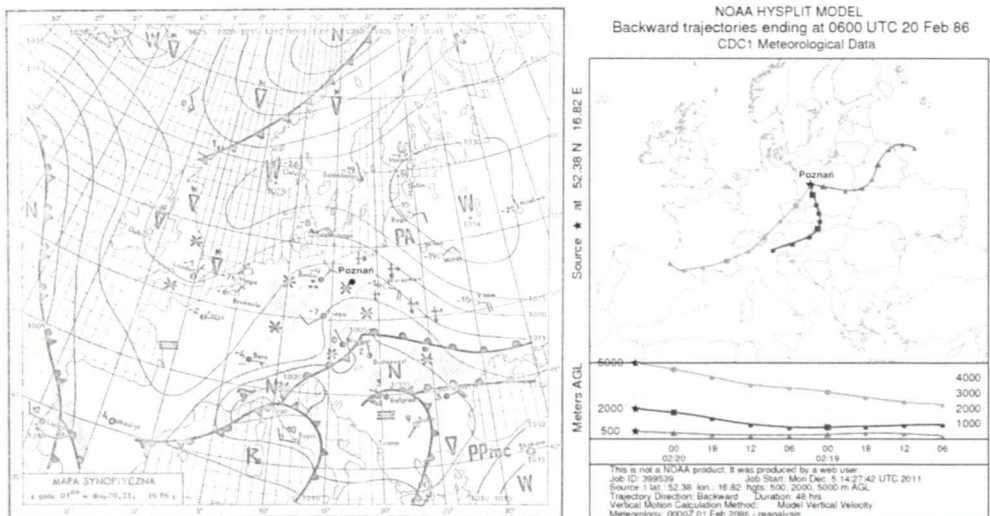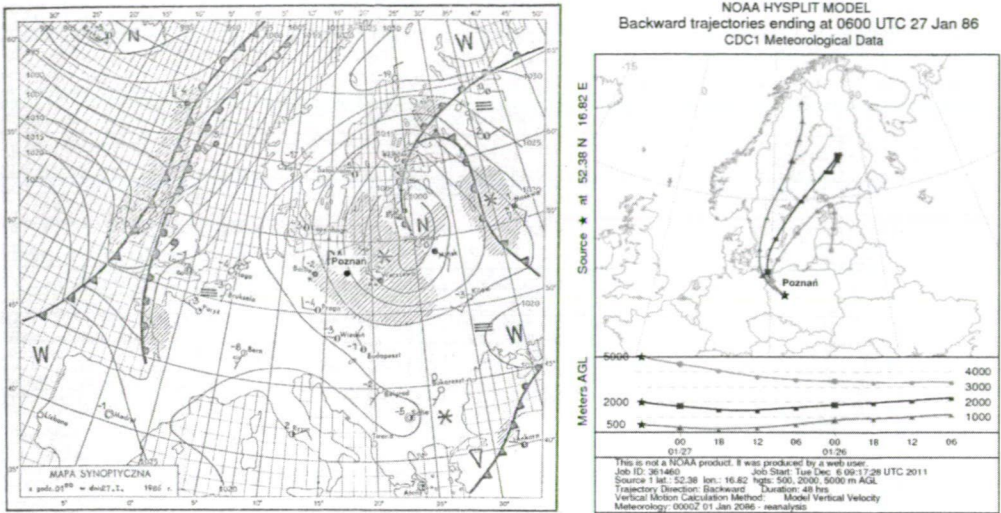
Fig. 7 Synoptic map and the 48-hours back trajectories of air particles at heights of 500 m (triangles), 2000 m (squares) and 5000 m (circles) above ground level for 27 January 1986

4. DISCUSSION AND CONCLUSIONS

Abundant snowfalls in Poznań, resulting in high snow accumulation and increase in snow cover depth, are associated with negative anomalies of both SLP and Z500 over the central and southern part of the continent, which means widespread low pressure systems over Southern-Europe. Snowfalls, which are directly determined by the air temperature and precipitation and indirectly by the inflow of particular air masses, appear as a result of fronts in the colder parts of Mediterranean cyclones. Low pressure centers are often situated over the Balkan Peninsula or over Italy and the Adriatic Sea. At the same time the high pressure system spreads over Scandinavia and northeastern Europe. Such pressure pattern causes the southeastern air inflow over Poland. The eastern sector of inflow dominates in the lower troposphere, bringing dry, but very cold polar continental air, while in the upper troposphere the southern inflow of warm and humid air of a Mediterranean origin is observed. The structure described in the study signifies the warm front, with the dynamic warm and humid air of distant southern origin climbing upwards on the cooler and more stable polar continental air masses from the east. The meeting of these two elements results in snowstorms in Central-Europe.

The alternative, although rarer location of low pressure systems causing abundant snowfalls in Poznań is northeastwards of Poland or right over Central-Europe, with the Baltic Sea or Atlantic Ocean being a source region of the humid and relatively cold air.

The described pressure patterns and anomalies causing abundant snowfalls in Poznań, namely the cyclonal activity over the continent and simultaneous weakening of Icelandic Low, correspond to the negative NAO phase, which has been proven to contribute to a large snow cover extent in Europe (Gutzler and Rosen 1992, Clark et al. 1999, Bednorz 2002, Falarz 2007, 2013). It has been also proved that during the negative phase of NAO the number of Mediterranean cyclones, which contribute to abundant snowfalls in central Europe, is

larger compared to the positive NAO phase (increase by 20%) and the mean European cyclone path is shifted southwards (Pinto et al. 2009, Nissen et al. 2010, Lionello (ed.) 2012).

The positive phase of NAO results in less snowy winters in western Poland, whereas the negative phase increases the probability of snowy winters (Bednorz 2002). The key to explain such a relationship is the air temperature. NAO is well known to have a significant impact on European air temperatures (Hurrell 1995). The predominant westerly air flow caused by the strong subtropical Azores High and the deep polar Icelandic Low at the positive phase of NAO brings mild maritime air over Europe and causes an increase in the air temperature. In Poznań, where average air temperatures in winter months are slightly below zero (Jan -1.6°C, Feb -0.9°C) such increases usually mean going above the melting point and they result in thaws. During the negative phase of NAO, the northeast and east flow is predominant. They bring the north arctic air or the cold continental air from the winter Siberian High to western Poland.

Heavy snowfalls in Poznań may appear only at the condition of negative temperature anomalies, extending over most of the continent (Bednorz 2011). However, despite of high humidity of snow-bringing air masses, the content of PW in the atmosphere over Poland during the days of high snow accumulation is not higher than average. It is because PW and the air temperature are positively correlated and the highest degree of relationship is observed in winter in the middle and high latitudes (Smith 1966, Viswanadham 1981).

Similar low pressure systems (one with a centre over the Baltic Sea and the other the Mediterranean) were defined by Spreitzhofer (1999b, 2000) as typical weather patterns related to intense snowfalls in Austria. Also Scherrer and Appenzeller (2006) defined cyclonic activity over southeastern Europe being one of important factors causing snowfalls in the Swiss Alps.

Concluding, the atmospheric circulation and consequently the synoptic conditions are the main factors contributing to the occurrence of the extreme winter weather events i.e. heavy snowfalls in central Europe. Therefore, analyses of the circulation and synoptic conditions associated with heavy snowfalls, as undertaken in this study, may improve forecasts of snowstorms occurrence and may give a chance to protect the community from their economic impact.

REFERENCES

Andersson T, Gustafsson N (1993) Coast of departure and coast of arrival. two important concepts for the formation and structure of convective snowbands over seas and lakes. Mon Weather Rev 122:1036-1049

Andersson T, Nilsson S (1990) Topographically induced snowbands over the Baltic Sea and their precipitation distribution. Weather Forecast 5:299-312

Avila A, Alarcon M (1999) Relationship between precipitation chemistry and meteorological situations at a rural site in NE Spain. Atmos Environ 33:1663-1677

Babolcsai G, Hirsch T (2006) Characteristics and synoptic classification of heavy snowfall events in Budapest for the period 1953-2003. Part I. Időjárás 110:1-13

Bednorz E (2002) Snow cover in western Poland and macro-scale circulation conditions. Int J Climatol 22:533-541

Bednorz E (2008) Synoptic reasons for heavy snowfalls in the Polish-German lowlands. Theor Appl Climatol 92:133-140

Bednorz E (2011) Synoptic conditions of snow cover occurrence in central European lowlands. Int J Climatol 31:1108-1118.

Birkeland KW, Mock CJ (1996) Atmospheric circulation patterns associated with heavy snowfall events, Bridger Bowl, Montana, U.S.A. Mt Res Dev 16:281-286

Clark MP, Serreze MC, Robinson AD (1999) Atmospheric controls on Eurasian snow extent. Int J Climatol 19:27-40

Draxler RR, Rolph GD (2012) HYSPLIT (HYbrid Single-Particle Lagrangian Integrated Trajectory). Model access via NOAA ARL READY Website. (http://ready.arl.noaa.gov/HYSPLIT.php). NOAA Air Resources Laboratory, Silver Spring, MD

European Environment Agency (2012) Climate change, impacts and vulnerability in Europe 2012 - An indicator-based report. Report No 12 Copenhagen

European Environment Agency (2013) Adaptation in Europe. Report No 3 Copenhagen

Falarz M (2007) Snow cover variability in Poland in relation to the macro and mesoscale atmospheric circulation in the twentieth century. Int J Climatol 27:2069-2081

Falarz M (2013) Seasonal stability of snow cover in Poland in relation to the atmospheric circulation. Theor Appl Climatol 111:21-28

Gutzler DS, Rosen RD (1992) Interannual variability of wintertime snow-cover across the Northern Hemisphere. J Climate 5:1441-1447

Hurrell JW (1995) Decadal trends in the North Atlantic Oscillation: regional temperatures and precipitation. Science 269:676-679

Kalnay E, Kanamitsu M, Kistler R, Collins W, Deaven D, Gandin L, Iredell M, Saha S, White G, Woollen J, Zhu Y, Leetmaa A, Reynolds R, Chelliah M, Ebisuzaki W, Higgins W, Janowiak, J, Mo KC, Ropelewski C, Wang J, Jenne R, Joseph D (1996) The NMC/NCAR 40-Year Reanalysis Project. B Am Meteorol Soc 77:437-471

Kjellström E, Nikulin G, Hansson U, Strandberg G, Ullerstig A (2011) 21st century changes in the European climate: uncertainties derived from an ensemble of regional climate model simulations. Tellus 63A:24-40

Nissen KM, Leckebusch GC, Pinto JG, RenggliD, Ulbrich S, Ulbrich U (2010) Cyclones causing wind storms in the Mediterranean:characteristics, trends and links to large-scale patterns. Nat Hazard Earth Sys 10:1379-1391

Pinto JG, Zachaqias S, Fink AH, Leckebusch GC, Ulbrich U (2009) Factors contributing to the development of extreme North Atlantic cyclones and their relationship with the NAO. Clim Dynam 32:711-737

Raisanen J (2008) Warmer climate: less or more snow? Clim Dynam 30:307-319

Raisanen J, Eklund J (2012) 21st century changes in snow climate in Northern Europe: a high-resolution view from ENSEMBLES regional climate models. Clim Dynam 38:2575-2591

Rikhiishi K, Sakakibara J (2004) Seasonal cycle of the snow coverage in the former Soviet Union and its relation with atmospheric circulation. Ann Glaciol 38:106-114

Rolph GD (2012) Real-time Environmental Applications and Display sYstem (READY) Website (http://ready.arl.noaa.gov). NOAA Air Resources Laboratory, Silver Spring, MD

Salvador P, Artinano B, Pio C, Afonso J, Legrand M, Puxbaum H, Hammer S (2010) Evaluation of aerosol sources at European high altitude background sites with trajectory statistical methods. Atmos Environ 44:2316-2329

Scherrer SC, Appenzeller C (2006) Swiss Alpine snow pack variability: major patterns and links to local climate and large-scale flow. Clim Res 32:187-199

Smith WL (1966) Note on the relationship between total precipitable water and surface dew point. J Appl Meteorol 5:726-727

Spreitzhofer G (1999a) Synoptic classification of severe snowstorms over Austria. Meteorol Z 8:3-15

Spreitzhofer G (1999b) Spatial, temporal and intensity characteristics of heavy snowfall events over Austria. Theor Appl Climatol 62:209-219

Spreitzhofer G (2000) On the characteristics of heavy multiple day snowfalls in the Eastern Alps. Nat Hazards 21:35-53

Lionello P (2012) The climate of the Mediterranean Region. From the past to the future. Elsevier, Oxford

Viswanadham Y (1981) The relationship between total precipitable water and surface dew point. J Appl Meteorol 20:3-8

Wibig J, Siedlecki M (2007) Przestrzenny i czasowy rozkład zawartości wody opadowej. [Spatial and temporal pattern of precipitable water. (in Polish)] In: K. Piotrowicz, R. Twardosz (eds), Wahania klimatu w różnych skalach przestrzennych i czasowych. [Fluctuations of climate in various spatial and temporal scales. (in Polish)] Instytut Geografii i Gospodarki Przestrzennej Uniwersytetu Jagiellońskiego, Kraków. 195-202

PREDICTING DAILY RAGWEED POLLEN CONCENTRATIONS USING NEURAL NETWORKS AND TREE ALGORITHMS OVER LYON (FRANCE) AND SZEGED (HUNGARY)

Z CSÉPE[1], L MAKRA[1], D VOUKANTSIS[2], I MATYASOVSZKY[3], G TUSNÁDY[4], K KARATZAS[2] and M THIBAUDON[5]

[1]*Department of Climatology and Landscape Ecology, University of Szeged, P.O.B. 653, 6701, Szeged, Hungary*
[2]*Department of Mechanical Engineering, Informatics Systems & Applications Group, Aristotle University, P.O. Box 483, 54124 Thessaloniki, Greece*
[3]*Department of Meteorology, Eötvös Loránd University, Pázmány Péter st. 1/A, 1117 Budapest, Hungary*
[4]*Mathematical Institute of the Hungarian Academy of Sciences, P.O.B. 127, 1364 Budapest, Hungary*
[5]*RNSA (Aerobiology Network of France), La Parličre, 69610 Saint Genis l'Argentière, France*
E-mail: csepe.zoltan@gmail.com

Summary: Forecasting ragweed pollen concentration is a useful tool for sensitive people in order to prepare in time for high pollen episodes. The aim of the study is to use methods of Computational Intelligence (CI) (Multi-Layer Perceptron, M5P, REPTree, DecisionStump and MLPRegressor) for predicting daily values of *Ambrosia* pollen concentrations and alarm levels for 1-7 days ahead for Szeged (Hungary) and Lyon (France), respectively. Ten-year daily mean ragweed pollen data (within 1997-2006) are considered for both cities. 10 input variables are used in the models including pollen level or alarm level on the given day, furthermore the serial number of the given day of the year within the pollen season and altogether 8 meteorological variables. The study has novelties as (1) daily alarm thresholds are predicted in the aerobiological literature for the first time; (2) data-driven modelling methods including neural networks have never been used in forecasting daily *Ambrosia* pollen concentration; (3) algorithm J48 has never been used in palynological forecasts; (4) we apply a rarely used technique, namely factor analysis with special transformation, to detect the importance of the influencing variables in defining the pollen levels for 1-7 days ahead. When predicting pollen concentrations, for Szeged Multi-Layer Perceptron models deliver similar results with tree-based models 1 and 2 days ahead; while for Lyon only Multi-Layer Perceptron provides acceptable result. When predicting alarm levels, the performance of Multi-Layer Perceptron is the best for both cities. It is presented that the selection of the optimal method depends on climate, as a function of geographical location and relief. The results show that the more complex CI methods perform well, and their performance is case-specific for ≥2 days forecasting horizon. A determination coefficient of 0.98 (*Ambrosia*, Szeged, one day and two days ahead) using Multi-Layer Perceptron ranks this model the best one in the literature.

Key words: ragweed pollen allergy, forecasting, factor analysis with special transformation, neural networks, multi-layer perceptron, tree based methods

1. INTRODUCTION

The warming of the climate system is obvious, as it is now evident from observations of increases in global average air and ocean temperatures, the widespread melting of snow and ice, and rising global average sea level (IPCC 2013). Recent climate warming is associated with the modification of the distribution areas of plants producing allergenic pollen (Laaidi et al. 2011, Ziska et al. 2011), furthermore, with an earlier onset (Frei 2008, Rodríguez-Rajo et al. 2011), and earlier end dates (Stach et al. 2007, Recio et al. 2010), a longer pollen season (Stach et al. 2007, Ariano et al. 2010), an increase in the total annual

pollen load (Cristofori et al. 2010, Ariano et al. 2010, Laaidi et al. 2011), as well as an increase of patient number sensitized to pollen throughout the year (Ariano et al. 2010).

The genus of ragweed (*Ambrosia spp*) comprises 42 species. They are the best known weeds for the most severe and widespread allergies caused by its pollen (Béres et al. 2005). However, in Europe, common ragweed *(Ambrosia artemisiifolia)* is predominant of all *Ambrosia* species (Makra et al. 2005, Bullock et al. 2010, Vinogradova et al. 2010). The most important habitat areas of common ragweed in Europe are the Rhône valley in France (Chauvel et al. 2006, Gladieux et al. 2011), north-western Milan and south Varese (Lombardy, Po River valley) in Italy (Bonini et al. 2012), the Pannonian Plain including Hungary and some parts of Serbia, Croatia, Slovenia, Slovakia and Romania (Kiss and Béres 2006, Makra et al. 2005), furthermore Ukraine (Rodinkova et al. 2012) and the south-western part of European Russia (Reznik 2009).

Advanced techniques such as neural networks, multi-layer perceptron and the support vector regression learning methods have been useful procedures for forecasting air quality parameters (Juhos et al. 2009, Vlachogianni et al. 2011, Voukantsis et al. 2011, Kassomenos et al. 2013). However, methods of Computational Intelligence (CI) have only been scarcely applied in airborne pollen related studies. They were used for forecasting (a) daily pollen concentrations (Delaunay et al. 2004, cedar pollen; Aznarte et al. 2007, olive pollen; Rodríguez-Rajo et al. 2010, Poaceae pollen; Voukantsis et al. 2010, Oleaceae, Poaceae and Urticaceae pollen; Puc 2012; *Betula* pollen), (b) pollen-induced symptoms (Voukantsis et al. 2013), (c) risk level of *Betula* pollen in the air (Castellano-Méndez et al. 2005) and (d) the severity of the Poaceae pollen season (Sánchez Mesa et al. 2005). Furthermore, Aznarte et al. (2007) used neuro-fuzzy models for forecasting olive pollen concentrations. The above applications of neural networks and neuro-fuzzy models produced better results than traditional statistical methods (Sánchez Mesa et al. 2005).

These methods of Computational Intelligence 1) can deal with the complexity of the mechanisms concerning the release and dispersion of the airborne pollen, 2) can be applied for different tasks (e.g. optimization and forecasting), 3) are computationally efficient and can be easily integrated into the operational use of the models (Voukantsis et al. 2010).

In this paper we use factor analysis with special transformation, a technique for detecting the importance of the influencing variables in defining the pollen levels for 1-7 days ahead. Furthermore, data-oriented models are applied for (1) predicting daily concentration of ragweed pollen that shows the highest allergenicity of all taxa and (2) comparing the efficiency of different prediction techniques over two heavily polluted areas in Europe, i.e. over Lyon (France) and Szeged (Hungary), respectively. The main objectives are: i) development of accurate forecasting models for operational use, ii) evaluation of CI methods that have not been previously applied for *Ambrosia* pollen, such as Multi-Layer Perceptron and regression trees and iii) obtaining a forecast of highest accuracy among CI methods based on input data of former prediction algorithms. Note that (1) data-driven modeling methods including neural networks have never been used in forecasting daily *Ambrosia* pollen concentration, (2) daily alarm thresholds are predicted in the aerobiological literature for the first time; furthermore (3) algorithm J48 has never been used in palynological forecasts.

2. MATERIALS

2.1. Location and data

2.1.1. Study area

Two European cities, namely Lyon (Rhône Valley, France) and Szeged (Pannonian Plain, Hungary) were selected as they show high ragweed pollen levels in Europe.

These cities differ in their topography and climate as well as in ragweed pollen characteristics. Szeged (46.25°N, 20.10°E), the largest settlement in South-eastern Hungary, is located at the confluence of the rivers Tisza and Maros (Fig. 1). The city is the centre of the Szeged region with 203,000 inhabitants. In the Köppen system the climate of Szeged is the

Fig. 1 The geographical positions of Lyon and Szeged

Ca type (warm, temperate climate), with relatively mild and short winters and hot summers (Köppen, 1931). Lyon (45.77°N, 4.83°E) lies in the Rhône-Alpes of France.

The city is located in the Rhône valley at the confluence of the Rhône and Saône rivers with a population of 1.8 million (Fig. 1). In the Köppen system its climate is of the Cbf type. That is, it has a temperate oceanic climate with mild winters and cool-to-warm summers, as well as a uniform annual precipitation distribution (Köppen, 1931).

2.1.2. Pollen and meteorological data

Ten-year (1997-2006) daily mean ragweed pollen data were considered for both Szeged and Lyon. Ragweed pollen concentrations or ragweed pollen alarm threshold values for 1, 2, …, 7 days after the given day were used as resultant variables. Ragweed pollen levels or ragweed pollen alarm thresholds on the given day; furthermore, the serial number of the given day of the year within the pollen season and altogether 8 meteorological variables on the given day were selected as influencing variables. The meteorological variables include daily values of mean temperature (T_{mean},°C), minimum temperature (T_{min},°C) and maximum temperature (T_{max},°C), daily temperature range ($\Delta T=T_{max}-T_{min}$,°C), daily mean relative humidity (RH, %), daily total radiation (TR, $W \cdot m^{-2}$), daily means of air pressure (P, mm) and wind speed (WS, $m \cdot s^{-1}$). For Lyon, daily data of total radiation were absent hence they were replaced with daily sunshine duration (SD, hour).

Alarm levels of *Ambrosia* pollen used in Hungary are as follows (Mányoki et al. 2011). Level 0: there is no *Ambrosia* pollen in the air. Level 1: (1-9 pollen grains m^{-3} of air): (very low pollen concentration, it produces no symptoms. Level 2: (10-29 pollen grains m^{-3} of air): low pollen concentration, it may cause symptoms. Level 3: (30-49 pollen grains m^{-3} of air): medium pollen concentration, it may generate symptoms even for less sensitive people. Level 4: (50-99 pollen grains m^{-3} of air): medium high pollen concentration, it may induce medium strong reactions even for less sensitive people. Level 5: (100-199 pollen

grains m^{-3} of air): high pollen concentration, it may provoke strong or very strong symptoms for all sensitive people. Level 6: (200-499 pollen grains m^{-3} of air): very high pollen concentration, health state of sensitive people may turn critical, asthmatic symptoms may also occur. Level 7: (500-999 pollen grains m^{-3} of air): exceptionally high pollen concentration, it may provoke acute symptoms inducing serious deterioration in the quality of life. Level 8: (>1000 pollen grains m^{-3} of air): extreme pollen concentration, excessively strong symptoms (Mányoki et al. 1011). The data were separated into two parts: the training set (1997-2004) to develop forecasting models, and the test set (2005-2006) to validate these models.

2.2. Methods

The study applies the factor analysis with special transformation. Furthermore, the following CI methods are evaluated for the task. Multi-layer perceptron (MLP) (Haykin 1999) models are artificial neural network models capable of modelling complex and highly nonlinear processes. Two types of neural networks are applied: a complex (MLP with more than one hidden layer) and a less complex (MLPRegressor with only one hidden layer) version. For predicting both the daily pollen concentrations and daily alarm levels of ragweed, several tree algorithms (M5P, REPTree, DecisionStump and J48) are used. These algorithms have not yet been used for the above tasks. The models have been developed in Matlab with WEKA implementation of the above algorithms, found in Hall et al. (2009).

2.2.1. Factor analysis with special transformation

Factor analysis identifies linear relationships among examined variables and thus helps to reduce the dimensionality of the initial database without substantial loss of information. Factor analysis was applied to our initial datasets consisting daily values of 11 correlated variables [10 explanatory variables including the serial number of the days in the year, 8 meteorological and 1 pollen variable (*Ambrosia* pollen level or alarm level) and 1 resultant variable (*Ambrosia* pollen level or alarm level for 1-7 target days, respectively)] in order to transform the original variables into fewer uncorrelated variables. These new variables, called factors, can be viewed as latent variables explaining the joint behaviour of the day in the year, furthermore the meteorological elements and the pollen variables. The number of retained factors can be determined by different criteria. The most common and widely accepted one is to specify a least percentage (80%) of the total variance of the original variables that has to be explained (Jolliffe 1993) by the factors. After performing the factor analysis, a special transformation of the retained factors was made to discover to what degree the above-mentioned explanatory variables affect the resultant variable and to give a rank of their influence (Jahn and Vahle 1968). When performing factor analysis on the standardized variables, factor loadings are correlation coefficients between the factors and the original variables. Consequently, if the resultant variable is strongly correlated with a factor and an explanatory variable is highly correlated with this factor, then the explanatory variable is also highly correlated with the resultant variable. Hence, it is advisable to combine all the factors together with the resultant variable into one new factor. It is effective to do so that only one factor has big contribution to the resultant variable and the remaining factors are uncorrelated with the resultant variable. This latter procedure is called special transformation (Jahn and Vahle 1968).

2.2.2. Multi-layer Perceptron (MLP)

MLP (Haykin 1999) is the most successful implementation of feedforward artificial neural networks and have been widely applied in the field of environmental science for classification, regression and function approximation problems. MLP can model complex and highly non-linear processes through the topology of the network. Multi-Layer Perceptron comprises an input and an output layer with one or more hidden layers of nonlinearly-activation functions. These capabilities have already been successfully utilized in previous studies in order to forecast pollen concentrations (e.g. Voukantsis et al. 2010), therefore MLP is an important procedure and this is the first occasion for using this method for predicting daily concentrations and daily alarm thresholds of ragweed pollen.

In the study, the MLP model always has more than one hidden layer and MLP has several parameters that need to be set. They are training time, learning rate, hidden layers and neurons in the layers. Training time was 1500, learning rate started from 0.3 and it was reduced in each step. This helps to stop the network from diverging from the target output as well as improve the general performance. The number of hidden layers is generated automatically by WEKA. MLP was applied with the same options for predicting both the daily pollen concentrations and daily alarm thresholds of ragweed.

2.2.3. MLPRegressor and MLPClassifier

Both classes are built-in WEKA modelling softwares (Hall et al. 2009). These algorithms are special parts of Multi-Layer Perceptrons. They always have only one hidden layer, where the number of neurons is user specific. Both use optimization by minimizing the squared error plus a quadratic penalty with the BFGS method. All parameters are standardized, including the target variable. The activation function is a logistic function. MLPRegressor and MLPClassifier are applied for predicting the daily pollen concentrations and daily alarm thresholds of ragweed, respectively.

2.2.4. Tree-based algorithms

This procedure is a reproduction of Quinlan's M5 algorithm (Quinlan 1992) being a combination of decision trees and multivariate regression models. Contrary to other regression trees the leaves of the M5P tree structure consist of MLR models. So, it is possible to model local linearity within the data similarly to piecewise linear functions. This is the first study applying M5P to model daily ragweed pollen data.

DecisionStump builds a decision tree with a single split point. It makes (1) regression based on mean-squared errors or (2) classification based on entropy depending on the data type to be forecasted.

REPTree is a fast decision tree learner. It builds a decision tree using information gain or makes a regression tree from the variance. It applies pruning with backfitting for reducing error.

J48 is an implementation of C4.5 algorithm in the WEKA data mining pool. C4.5 builds decision trees from a set of training data in the same way as ID3 using the concept of information entropy. J48 classifier achieves fast execution times and adequate scales of large datasets (Quinlan 1993).

3. RESULTS AND DISCUSSION

3.1. Performance evaluation

The importance of the serial number of the day in the year, furthermore daily values of eight meteorological variables and *Ambrosia* pollen level were analysed in determining a future day pollen level for 1-7 days ahead using factor analysis with special transformation (Tables 1-2). When comparing the results very little similarity was received for the two cities. The importance of the serial number of the day of the year shows a tendency of higher weights towards increasing target days for both Szeged and Lyon; however, this effect is more remarkable for Szeged. From the meteorological influencing variables, only TR and *Ambrosia* pollen level showed similarly significant positive weights with values of the same magnitude in determining a future day pollen level (Tables 1-2). The weights of actual day *Ambrosia* pollen level emerge extraordinarily from all variables indicating its high significance for both cities. This confirms former findings according to which the most decisive influencing variable of all is the actual day *Ambrosia* pollen level for assigning pollen levels 1-7 days ahead (Makra et al. 2011, Makra and Matyasovszky 2011).

For Szeged, T_{mean}, T_{max} and ΔT indicate significant and substantially higher positive weights compared to Lyon. While the importance of RH and WS can be negligible for Szeged, these parameters show highly relevant negative associations in the formation of pollen levels 1-7 days ahead for Lyon. P shows notable negative and positive weights for Szeged and Lyon, respectively. The here-mentioned definite difference in the weights and signs of the influencing variables for the two cities can be explained by their different climate and relief. The temperate oceanic climate of Lyon with cool-to-warm summers confirms the role of humidity parameters (RH) here, while the location of the city in the Rhone valley on the foothills of High Alps emphasizes the weight of the wind (WS). The warm, temperate climate of Szeged highlights the importance of the temperature parameters (T_{mean}, T_{max}, T_{min} and ΔT) and shows insignificant weights for the humidity (RH), while the central location of the city in the Pannonian Plain makes negligible the role of the wind (WS) (Tables 1-2).

3.2. Performance of the forecasting models

The following statistical indices were used to compare the performance of the models: (1) correlation coefficient as a measure of the strength; (2) Root Mean Square Error (RMSE) and (3) Mean Absolute Error (MAE) as measures of the error in the forecast.

For Szeged, MLP provides the best results for the forecasting horizon (1-7 days) that is confirmed by former studies (Sánchez-Mesa et al. 2002, Voukantsis et al. 2010). 1-day forecast indicates the best performance. This can be explained by the close association between the pollen concentrations of consecutive days and the predominant role of local pollen release in the measured pollen concentration in Szeged (Makra et al. 2010). The efficiency of MLPRegressor declines intensely when forecasting more than 2 days ahead due to its simpler construction (Table 3, Fig. 2). Considering decision trees, performance of REPTree decreases for >1-day forecasts, while DecisionStump provides an overall weak result for the forecasting horizon. MLPRegressor serves the best performance for 1 and 2-day ahead forecasts; however, when the forecasting horizon exceeds 2 days, the accuracy of the predictions sharply decreases. High values of RMSE and MAE can be attributed to the very high variability of the daily ragweed pollen concentrations. There are no periods in the pollen season that can be approximated linearly with high confidence.
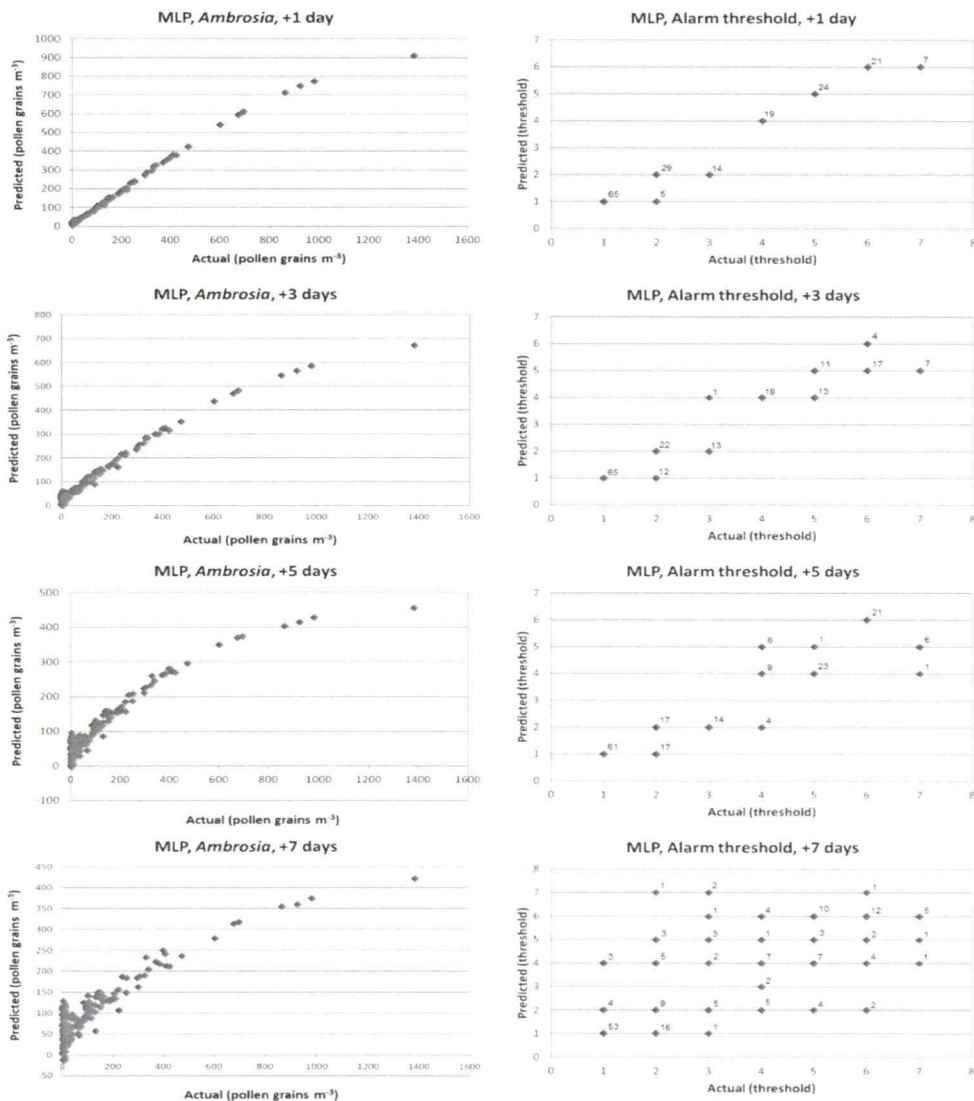
Fig. 2 Scatter plots, Szeged. Selected scatter plots of actual and predicted *Ambrosia* pollen concentrations (MLP), as well as alarm thresholds (MLP). The forecasting horizon is given in days

23

Z Csépe, L Makra, D Voukantsis, I Matyasovszky, G Tusnády, K Karatzas, and M Thibaudon

Table 1 Special transformation, Szeged. Relevance of the influencing variables in defining the resultant variable (pollen levels) 1-7 days ahead and the rank of importance of the influencing variables for determining the resultant variable (thresholds of significance: *italic:* $x_{0.05} = 0.064$; **bold:** $x_{0.01} = 0.084$)

[1]Day	[2]Day weight	rank	[3]T_{mean} weight	rank	[4]T_{max} weight	rank	[5]T_{min} weight	rank	[6]ΔT weight	rank	[7]RH weight	rank	[8]TR weight	rank	[9]P weight	rank	[10]WS weight	rank	Ambrosia weight	rank
+1	0.00	7	**0.13**	7	**0.14**	7	0.06	7	**0.10**	4	-0.01	6	**0.11**	7	*-0.07*	4	*0.07*	1	**0.96**	1
+2	-0.02	6	**0.16**	6	**0.17**	6	*0.07*	6	**0.11**	3	-0.02	3	**0.13**	6	-0.06	6	0.06	2	**0.93**	2
+3	-0.04	5	**0.18**	5	**0.19**	5	0.09	4	**0.12**	2	-0.02	2	**0.15**	5	*-0.08*	3	0.05	3	**0.90**	3
+4	-0.06	4	**0.20**	4	**0.21**	4	0.09	5	**0.15**	1	-0.03	1	**0.17**	1	-0.07	5	0.02	4	**0.87**	4
+5	*-0.08*	3	**0.21**	3	**0.21**	3	0.14	3	0.09	5	-0.01	5	**0.15**	4	-0.05	7	-0.01	5	**0.84**	5
+6	**-0.13**	2	**0.26**	2	**0.25**	2	0.19	2	*0.07*	6	0.00	7	**0.16**	3	**-0.10**	1	0.01	6	**0.81**	6
+7	**-0.17**	1	**0.29**	1	**0.27**	1	0.25	1	0.03	7	0.01	4	**0.16**	2	-0.09	2	0.00	7	**0.78**	7

[1]: target day of the forecast; [2]: serial number of the day in the year; [3]: daily mean temperature (°C); [4]: daily maximum temperature (°C); [5]: daily minimum temperature (°C); [6]: daily temperature range (°C); [7]: daily relative humidity (%); [8]: daily total radiation (W·m^{-2}); [9]: daily mean air pressure (hPa); [10]: daily wind speed (m·s^{-1})

Table 2 Special transformation, Lyon. Relevance of the influencing variables in defining the resultant variable (pollen levels) 1-7 days ahead and the rank of importance of the influencing variables for determining the resultant variable (thresholds of significance: *italic:* $x_{0.05} = 0.064$; **bold:** $x_{0.01} = 0.084$)

[1]Day	[2]Day weight	rank	[3]T_{mean} weight	rank	[4]T_{max} weight	rank	[5]T_{min} weight	rank	[6]ΔT weight	rank	[7]RH weight	rank	[8]TR weight	rank	[9]P weight	rank	[10]WS weight	rank	Ambrosia weight	rank
+1	0.05	2	**0.12**	1	**0.11**	1	0.09	5	*0.08*	1	**-0.14**	5	**0.17**	5	0.03	7	-0.02	7	**0.87**	1
+2	0.04	4	0.06	5	0.05	2	*0.07*	7	0.03	6	**-0.17**	3	**0.24**	2	**0.16**	2	**-0.11**	4	**0.71**	2
+3	0.01	6	0.05	7	0.04	4	*0.08*	6	0.01	7	**-0.18**	1	**0.26**	1	**0.16**	1	**-0.13**	2	**0.69**	4
+4	-0.01	7	0.06	6	0.03	7	0.13	4	-0.03	5	**-0.17**	2	**0.18**	4	0.10	3	-0.09	6	**0.70**	3
+5	-0.03	5	*0.07*	4	0.03	6	0.14	3	-0.03	4	**-0.15**	4	**0.19**	3	0.10	4	**-0.11**	3	**0.66**	5
+6	-0.05	3	*0.08*	3	0.04	5	0.17	2	-0.03	2	**-0.12**	6	**0.17**	6	0.11	5	-0.10	5	**0.62**	7
+7	*-0.07*	1	**0.09**	2	0.04	3	0.17	1	-0.03	3	**-0.11**	7	0.10	7	0.05	6	**-0.14**	1	**0.62**	6

[1]: target day of the forecast; [2]: serial number of the day in the year; [3]: daily mean temperature (°C); [4]: daily maximum temperature (°C); [5]: daily minimum temperature (°C); [6]: daily temperature range (°C); [7]: daily relative humidity (%); [8]: daily total radiation (W·m^{-2}); [9]: daily mean air pressure (hPa); [10]: daily wind speed (m·s^{-1})

Table 3 Statistical evaluation of the *Ambrosia* pollen concentration forecasting models for Szeged in terms of the correlation coefficient (r), the Root Mean Square Error (RMSE) and the Mean Absolute Error (MAE). T indicates the forecasting horizon (in days). (MLP: Multi-Layer Perceptron model, M5P: Regression tree model, REPTree: regression tree model, DecisionStump: decision tree model and MLPRegressor: Multi-Layer Perceptron model)

T	MLP			M5P			REPTree			DecisionStump			MLPRegressor		
(day)	r	RMSE	MAE	r	RMSE	MAE	r	RMSE	MAE	r	RMSE	MAE	r	RMSE	MAE
+1	0.99	45.08	17.11	0.98	52.34	18.60	0.95	63.69	24.25	0.75	128.86	78.95	0.97	60.89	20.28
+2	0.99	66.66	27.54	0.83	115.81	38.30	0.85	110.29	38.11	0.64	150.69	64.11	0.97	76.02	34.72
+3	0.98	80.08	33.79	0.82	117.62	46.30	0.80	123.15	45.26	0.63	152.21	64.09	0.61	153.23	56.85
+4	0.96	94.02	40.69	0.78	126.04	54.91	0.71	138.79	58.79	0.63	153.05	64.97	0.54	162.09	61.61
+5	0.94	111.30	50.43	0.59	153.11	73.12	0.69	143.99	59.74	0.62	154.44	65.28	0.42	175.27	73.71
+6	0.92	121.51	58.88	0.53	161.07	81.92	0.49	166.75	77.98	0.60	157.77	66.24	0.65	149.11	71.15
+7	0.90	127.13	63.34	0.43	172.45	83.79	0.43	174.15	75.35	0.60	157.97	66.34	0.54	161.88	80.57

Table 4 Statistical evaluation of the *Ambrosia* pollen alarm level forecasting models for Szeged in terms of the correlation coefficient (r), the Root Mean Square Error (RMSE) and the Mean Absolute Error (MAE). T indicates the forecasting horizon (in days). (MLP: Multi-Layer Perceptron model, J48: decision tree model, REPTree: decision tree model, DecisionStump: decision tree model and MLPClassifier: Multi-Layer Perceptron model)

T	MLP			J48			REPTree			DecisionStump			MLPClassifier		
(day)	r	RMSE	MAE	r	RMSE	MAE	r	RMSE	MAE	r	RMSE	MAE	r	RMSE	MAE
+1	0.98	0.37	0.14	0.94	0.70	0.44	0.98	0.40	0.16	0.74	1.32	0.92	0.98	0.37	0.14
+2	0.95	0.67	0.40	0.91	0.88	0.52	0.96	0.60	0.32	0.74	1.32	0.92	0.96	0.62	0.37
+3	0.96	0.67	0.38	0.87	1.01	0.63	0.90	0.93	0.58	0.74	1.32	0.93	0.90	0.94	0.53
+4	0.80	1.19	0.73	0.85	1.08	0.73	0.91	0.85	0.54	0.74	1.32	0.93	0.81	1.22	0.70
+5	0.94	0.77	0.46	0.79	1.26	0.87	0.92	0.78	0.46	0.73	1.32	0.94	0.82	1.14	0.78
+6	0.82	1.18	0.78	0.73	1.39	0.95	0.83	1.10	074	0.73	1.32	0.94	0.86	1.05	0.67
+7	0.76	1.36	0.88	0.72	1.41	0.93	0.77	1.32	0.92	0.73	1.32	0.95	0.74	1.39	1.02

Z Csépe, L Makra, D Voukantsis, I Matyasovszky, G Tusnády, K Karatzas, and M Thibaudon

Table 5 Statistical evaluation of the *Ambrosia* pollen concentration forecasting models for Lyon in terms of the correlation coefficient (r), the Root Mean Square Error (RMSE) and the Mean Absolute Error (MAE). T indicates the forecasting horizon (in days). (MLP: Multi-Layer Perceptron model, M5P: Regression tree model, REPTree: regression tree model, DecisionStump: decision tree model and MLPRegressor: Multi-Layer Perceptron model)

T (day)	r	MLP RMSE	MAE	r	M5P RMSE	MAE	r	REPTree RMSE	MAE	r	DecisionStump RMSE	MAE	r	MLPRegressor RMSE	MAE
+1	0.96	33.53	12.73	0.97	28.26	11.62	0.70	48.99	15.89	0.81	45.88	18.39	0.36	62.09	22.44
+2	0.91	48.31	21.67	0.68	52.14	21.05	0.42	60.85	23.63	0.43	60.13	23.33	0.59	56.29	20.08
+3	0.81	53.59	24.74	0.64	55.12	22.76	0.57	56.42	20.21	0.43	60.88	25.20	0.33	62.86	25.72
+4	0.74	63.17	29.13	0.29	63.06	24.80	0.41	60.85	24.47	0.43	60.63	24.19	0.01	70.02	29.37
+5	0.64	58.82	26.67	0.19	65.15	26.80	0.42	59.91	22.83	0.35	62.18	25.65	-0.01	73.23	32.35
+6	0.78	55.92	24.81	0.43	59.93	23.81	0.33	62.05	24.75	0.35	62.15	25.54	0.01	72.99	32.16
+7	0.92	51.67	22.47	0.80	52.29	21.84	0.34	61.75	23.94	0.34	62.06	25.33	0.12	69.23	30.04

Table 6 Statistical evaluation of the *Ambrosia* pollen alarm level forecasting models for Lyon in terms of the correlation coefficient (r), the Root Mean Square Error (RMSE) and the Mean Absolute Error (MAE). T indicates the forecasting horizon (in days). (MLP: Multi-Layer Perceptron model, J48: decision tree model, REPTree: decision tree model, DecisionStump: decision tree model and MLPClassifier: Multi-Layer Perceptron model)

| T (day)	r	MLP RMSE	MAE	r	J48 RMSE	MAE	r	REPTree RMSE	MAE	r	DecisionStump RMSE	MAE	r	MLPClassifier RMSE	MAE
+1	0.91	1.12	0.53	0.80	1.05	0.46	0.84	0.75	0.29	-	1.48	0.69	0.73	0.97	0.40
+2	0.65	1.31	0.62	0.35	1.67	0.85	0.52	1.22	0.48	-	1.48	0.70	0.51	1.20	0.58
+3	0.26	1.60	0.80	0.17	1.66	0.90	–	1.48	0.70	-	1.48	0.70	0.44	1.29	0.60
+4	0.39	1.41	0.67	0.63	1.07	0.49	0.47	1.33	0.63	-	1.48	0.70	0.45	1.35	0.60
+5	0.26	1.45	0.70	0.37	1.32	0.72	0.65	1.11	0.51	-	1.48	0.70	0.59	1.23	0.54
+6	0.46	1.40	0.68	0.38	1.28	0.61	0.52	1.23	0.52	-	1.48	0.70	0.31	1.30	0.68
+7	-	1.48	0.71	0.38	1.49	0.75	0.48	1.32	0.62	-	1.48	0.70	0.14	1.43	0.74
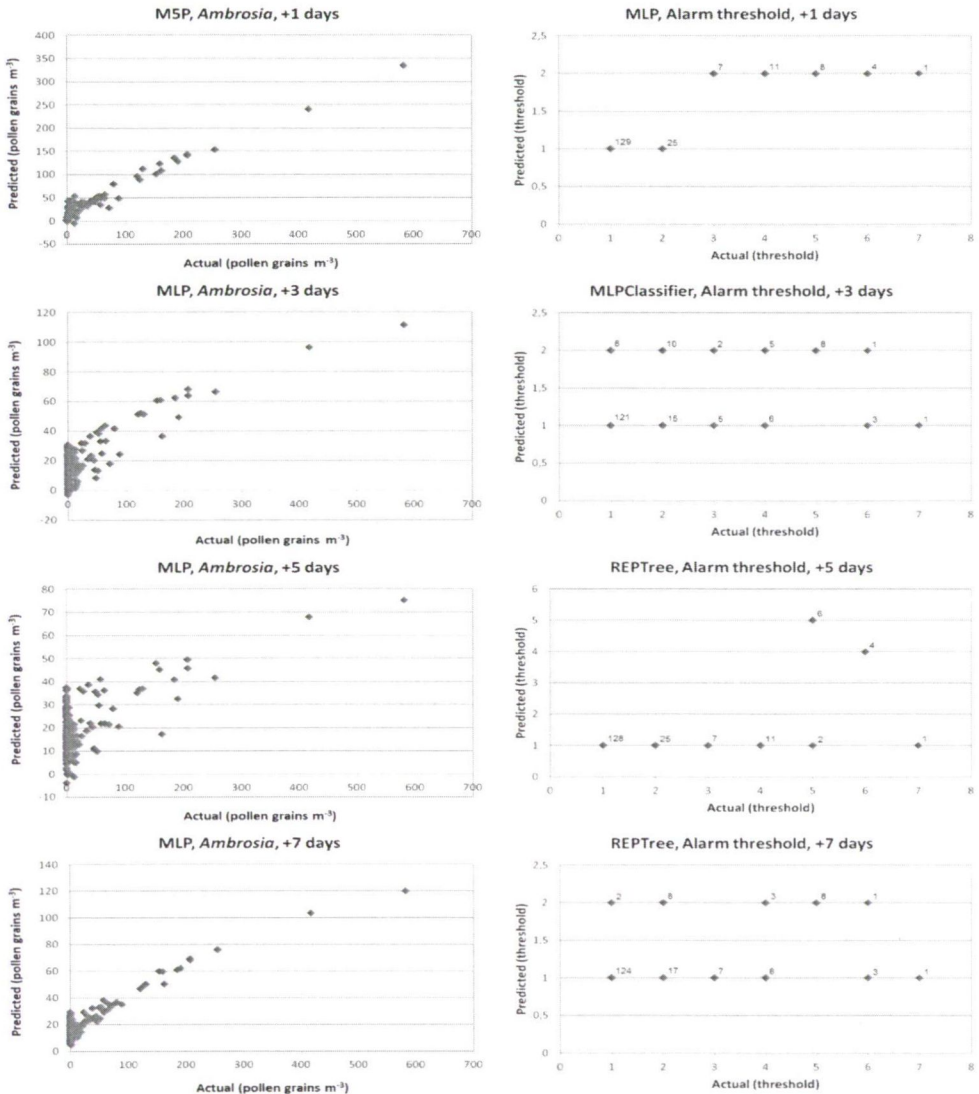
Fig. 3 Scatter plots, Lyon. Selected scatter plots of actual and predicted *Ambrosia* pollen
concentrations (M5P, MLP), as well as alarm thresholds (MLP, MLPClassifier, REPTree). The
forecasting horizon is given in days

This is why M5P is not a reliable method for >2 days forecasts. Based on the scatter plots, when the forecasting horizon expands, (1) the accuracy of the forecast weakens and (2) the best method (MLP) increasingly underestimates the pollen concentration (Fig. 2). Note that for the remaining methods, under- and overestimation may occur at both the beginning and end of the pollen season. However, MLP underestimates consistently regardless the day of the pollen season and the length of the forecasting horizon. On the whole, all the methods analysed in the study (except for the simplest DecisionStump) perform well for 1 and 2-day ahead forecasts for Szeged.

Note, however, that MLP provides a correlation coefficient 0.96 even for the 4-day forecast and the efficiency of the prediction does not decrease below r=0.90 even for 7-day forecast. For the remaining methods the accuracy of the forecasts for >2 days ahead indicate sharp decrease (Table 3, Fig. 2).

Predicting alarm levels is another area of pollen forecasts. Their fast and efficient prediction serves a simple and easily traceable tool for sensitive people in preparing for days of high pollen load. In order to better predict *Ambrosia* pollen alarm levels introduced for Hungary (Mányoki et al. 2011), the original 0-1 and 7-8 categories were aggregated. In the scatter plots of forecasting alarm levels for both Szeged and Lyon, the horizontal axis indicates the observed alarm level, while the vertical axis shows the forecasted alarm level. Starting from the actual day several alarm levels can be expected on the target day depending on the initial day, and the forecasts for the target day can result in different alarm levels. Note that with the increase of the forecasting horizon the uncertainty of the alarm level increases. The numbers beside the forecasted alarm levels indicate their total occurrences for the data set (Figs. 2-3).

MLP shows the best results for the alarm levels of Szeged. The decision tree based REPTree model provides better or similarly good performance compared to the MLP since alarm levels form classes for which RAPTree is very sensitive. Besides these methods the simply constructed MLPClassifier, that has a faster run-time compared to MLP, is also capable of predicting alarm levels with good performance. When forecasting 1-day alarm level, three methods (MLP, REPTree and MLPClassifier) show the same efficacy (Table 4). 1, 2 and 3-day ahead predictions of alarm levels perform well, while forecasts for >3 days ahead indicate substantial decrease for all the methods applied. Note that MLP provides good result even for a 5-day forecast, as well; whereas, the performance of DecisionStump is the worst due to the construction of the method: it carries out only one single split (Table 4, Fig. 2).

For Lyon, MLP provides the best performance of all the procedures. One-layer MLPRegressor is the least efficient and, similarly to the case of Szeged, DecisionStump is not capable of predicting alarm levels. As wind speed shows significant negative associations with the measured pollen concentrations for 1-7 days ahead (Table 2), this parameter strongly degrades the performance of the methods (Tables 5-6, Fig. 3).

The procedures perform well for Szeged, but they are not really efficient for Lyon. For the latter case, neither pollen concentrations nor alarm levels show a definite annual course, due to the substantially smaller pollen concentrations, furthermore different climate and relief in Lyon compared to those of Szeged (Tables 5-6). The predictability of alarm levels for Lyon is quite weak that can be explained with the following reasons: (1) alarm levels introduced for Hungary cannot be applied well for Lyon due to the different distribution of pollen concentrations for the two cities, (2) the structure of the association between the influencing and resultant variables are different for Szeged and Lyon (Tables 1-2, Tables 5-6, Fig. 3).

Uncertainties in the accuracy of the forecasts can be explained by the lack of sufficient number of influencing variables including the fact that environmental associations of ragweed pollen level have not been fully discovered yet. For example, high air pollutant concentrations are likely to have either short or long term impact on pollen levels (Minero et al. 1998; Jäger et al. 1991), especially in a polluted urban environment like Szeged and Lyon. The results show that the learning strategies of the algorithms can perform well, but the really good model is MLP for predicting both pollen concentrations and alarm levels for each city. Based on the results for Szeged and Lyon we can perform accurate forecasts of the daily pollen concentrations and alarm levels for several days ahead. The efficiency of the models belongs to the best ones compared to those reported in the literature. When forecasting, the following values of r^2 (i.e. squared

correlations) of one day ahead forecasts were received: 0.60 for Poaceae using neural networks (Sánchez-Mesa et al. 2002); 0.93 again for Poaceae using neural networks (Rodríguez-Rajo et al. 2010); 0.45 for grass pollen (whole season) using correlation analysis (Stach et al. 2008) and 0.79 for Poaceae using Multiple Linear Regression (Voukantsis et al. 2010). Our study provides a coefficient of determination of 0.98 (*Ambrosia,* Szeged, one day and two days ahead) using Multi-Layer Perceptron that ranks this model the best one in the literature.

3.3. Model fitting on the days of the highest pollen levels

Pollen concentrations on the days exhibiting the highest pollen levels during a 7-day period were predicted and analysed for both cities (Fig. 4).

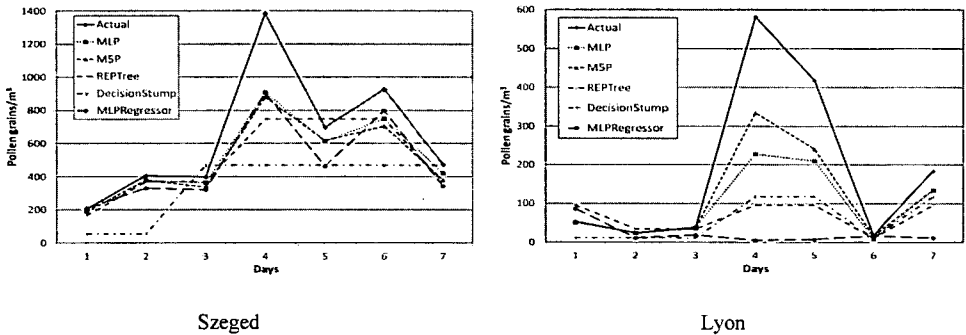Szeged   Lyon

Fig. 4 One-day forecasts for a seven-day period encompassing the day of the highest pollen load of *Ambrosia* (Actual: measured pollen concentrations, MLP: Multi-Layer Perceptron model, M5P: regression tree model, REPTree: decision tree model, DecisionStump: decision tree model, MLPRegressor: Multi-Layer Perceptron model)

For example, regarding the absolute maximum pollen counts within the 10-year period examined, for Szeged and Lyon the best 1-day forecast is provided by MLP (actual value: 1385 pollen grains m^{-3}; forecasted value: 910 pollen grains m^{-3}) and M5P (actual value: 582 pollen grains m^{-3}; forecasted value: 335 pollen grains m^{-3}), respectively. However, all methods underestimate the pollen concentrations in these episodic situations.

The message of the above experiment is that MLP, M5P and MLPRegressor follow well the annual course of the pollen concentration. This is important information as the usefulness of a good forecast is much higher for the days of the highest pollen concentrations than for those of small pollen levels at the beginning and end of the pollen season. Accordingly, these methods can help in developing personalized information services that could improve the overall quality of life for sensitized people.

4. CONCLUSIONS

We applied Computational Intelligence procedures in order to predict daily values of *Ambrosia* pollen concentrations and alarm levels for Szeged (Hungary) and Lyon (France). Despite the difficulties in the availability of daily pollen levels (they are at disposal only after a week), forecasts of daily ragweed pollen concentrations and alarm levels were successful

for 1-7 days ahead for both cities. The importance of the influencing variables (the serial number of the day in the year, meteorological and pollen variables) in forming the resultant variable (pollen levels or alarm levels for 1-7 days ahead) was analysed. The weights of *Ambrosia* pollen level emerge extraordinarily from all variables indicating its high significance in determining pollen levels (alarm levels) for 1-7 days ahead for both cities. The weights of the rest of influencing variables are different for the two cities. For instance, the most important variables are temperature-related ones for Szeged, while relative humidity and wind speed have the most important role in forming pollen concentrations in Lyon.

For Szeged, Multi-Layer Perceptron models provide results similar with tree-based models for predicting pollen concentration 1 and 2-days ahead, while for more than two days ahead they deliver better results than tree-based models. For Lyon, only the Multi-Layer Perceptron gives acceptable result for predicting pollen levels 1 and 2-days ahead. Concerning the alarm levels, the efficiency of the procedures differs substantially.

When fitting the models to the days of the highest pollen levels the more complex CI methods proved better for both cities. MLP and M5P methods provided the best results for Szeged and Lyon, respectively. We have shown that the selection of the optimal method depends on climate as a function of geographical location and relief.

Results received can be utilized by the national pollen information services. Total medical costs of ragweed pollen can be substantially reduced if sensitized people can be prepared in time for serious ragweed pollen episodes. Decision-makers are responsible for introducing regulations and actions in order to facilitate the problem caused by ragweed pollen. Furthermore, it is the responsibility of aero-biologists to develop personalized information services in order to improve the overall quality of life of sensitized people. Note however, that due to the restrictions of the pollen sampling procedure (daily pollen counts are available after a 7-day period) the applicability of the present or any other statistical models for operative pollen forecast is limited in time. This problem can only be solved if instruments based on a totally new principle will be introduced measuring "in situ" pollen counts.

The methods applied are sensitive to the number of the influencing parameters. A further aim is to use much more influencing parameters (including further meteorological parameters, in addition chemical air pollutants, land use, relief, etc.) in order to develop a general model for different locations.

REFERENCES

Ariano R, Canonica GW, Passalacqua G (2010) Possible role of climate changes in variations in pollen seasons and allergic sensitizations during 27 years. Ann Allerg Asthma Im 104:215-222

Aznarte JL, Sánchez JMB, Lugilde DN, Fernández CDL, de la Guardia CD, Sánchez FA (2007) Forecasting airborne pollen concentration time series with neural and neuro-fuzzy models. Expert Syst Appl 32:1218-1225

Béres I, Novák R, Hoffmanné Pathy Zs, Kazinczi G (2005) Az ürömlevelű parlagfű (Ambrosia artemisiifolia L.) elterjedése, morfológiája, biológiája, jelentősége és a védekezés lehetőségei. [Distribution, morphology,

biology and importance of common ragweed (Ambrosia artemisiifolia L.) and protection facilities. (in Hungarian)] Gyomnövények, Gyomirtás 6:1-48

Bonini M, Albertini R, Brighetti MA, Ugolotti M, Travaglini A (2012) RIMA-Italian Monitoring Network in Aerobiology. Ragweed pollen spreading in Italy. Second International Ragweed Conference, Lyon, France

Bullock JM, Chapman D, Schafer S, Roy D, Girardello M, Haynes T, Beal S, Wheeler B, Dickie I, Phang Z, Tinch R, Čivić K, Delbaere B, Jones-Walters L, Hilbert A, Schrauwen A, Prank M, Sofiev M, Niemelä S, Räisänen P, Lees B, Skinner M, Finch S, Brough C (2010) Assessing and controlling the spread and the effects of common ragweed in Europe. Final report: ENV.B2/ETU/2010/0037, Natural Environment Research Council, UK, 456

Castellano-Méndez M, Aira MJ, Iglesias I, Jato V, González-Manteiga W (2005) Artificial neural networks as a useful tool to predict the risk level of Betula pollen in the air. Int J Biometeorol 49:310-316

Chauvel B, Dessaint F, Cardinal-Legrand C, Bretagnolle F (2006) The historical spread of Ambrosia artemisiifolia L. in France from herbarium records. J Biogeogr 33:665-673

Cristofori A, Cristofolini F, Gottardini E (2010) Twenty years of aerobiological monitoring in Trentino (Italy): assessment and evaluation of airborne pollen variability. Aerobiologia 26:253-261

Delaunay JJ, Seymour C, Fouillet V (2004) Investigation of short-range cedar pollen forecasting. Phys Rev E 70: Article No. 066214

Frei T (2008) Climate change and its impact on airborne pollen in Basel, Switzerland 1969-2007. Allergologie 31:165-169

Gladieux P, Giraud T, Kiss L, Genton BJ, Jonot O, Shykoff JA (2011) Distinct invasion sources of common ragweed (Ambrosia artemisiifolia) in Eastern and Western Europe. Biol Invasions 13:933-944

Hall M, Frank E, Holmes G, Pfahringer B, Reutemann P, Witten IH (2009) The WEKA data mining software: an update. SIGKDD Explorations 11:10-18

Haykin S (1999) Neural Networks: a Comprehensive Foundation, 2nd ed. Upper Saddle River, Prentice Hall, NJ

IPCC (2013) Summary for policymakers. Climate Change 2013. Stocker TF, Qin D,Plattner GP, Tignor MMB, Allen SK, Boschung J, Nauels A, Xia Y, Bex V, Midgley PM (eds) The Physical Science Basis. Contribution of Working Group I to the Fifth Assessment Report of the Intergovernmental Panel on Climate Change, (Cambridge University Press, Cambridge, UK).

Jahn W, Vahle H (1968) Die Faktoranalyse und ihre Anwendung. Verlag die Wirtschaft, Berlin

Jäger S, Spieksma FTM, Nolard N (1991) Fluctuations and trend in airborne concentrations of some abundant pollen types, monitored at Vienna, Leiden and Brussels. Grana 30:309-312

Jolliffe IT (1993) Principal component analysis: A beginner's guide – II. Pitfalls, myths and extensions. Weather 48:246-253

Juhos I, Makra L, Tóth B (2009) The behaviour of the multi-layer perceptron and the support vector regression learning methods in the prediction of NO and NO_2 concentrations in Szeged, Hungary. Neural Comput Appl 18:193-205

Kiss L, Béres I (2006) Anthropogenic factors behind the recent population expansion of common ragweed (*Ambrosia artemisiifolia L.*) in Eastern Europe: is there a correlation with political transitions? J Biogeogr 33:2156-2157

Köppen W (1931) Grundriss Der Klimakunde. Walter De Gruyter & Co, Berlin

Laaidi M, Chinet T, Aegerter P (2011) Pollen allergies, pollution and climate: Literature review. Revue Française D'Allergologie 51:622-628

Makra L, Juhász M, Béczi R, Borsos E (2005) The history and impacts of airborne Ambrosia (Asteraceae) pollen in Hungary. Grana 44:57-64

Makra L, Sánta T, Matyasovszky I, Damialis A, Karatzas K, Bergmann KC, Vokou D (2010) Airborne pollen in three European cities: Detection of atmospheric circulation pathways by applying three-dimensional clustering of backward trajectories. J Geophys Res-Atmos 115:D24220

Makra L, Matyasovszky I, Thibaudon M, Bonini M (2011) Forecasting ragweed pollen characteristics with nonparametric regression methods over the most polluted areas in Europe. Int J Biometeorol 55:361-371

Makra L, Matyasovszky I (2011) Assessment of the daily ragweed pollen concentration with previous-day meteorological variables using regression and quantile regression analysis for Szeged, Hungary. Aerobiologia 27:247-259

Mányoki G, Apatini D, Magyar D, Páldy A (2011) A parlagfüpollen becsült országos eloszlása a Parlagfü Pollen Riasztási Rendszer (PPRR) szerint. (Assessed incidence of ragweed in Hungary according to the Ragweed Pollen Alarm System (RPAS). In: Apatini D (ed) Az ÁNTSZ Aerobiológiai Hálózatának tájékoztatója, éves jelentés, kézirat. [Report of the Aerobiological Network of ÁNTSZ, annual report (in Hungarian)], manuscript. OKI, Budapest, 81

Minero FJG, Iglesias I, Jato V, Aira MJ, Candau P, Morales J, Tomas C (1998) Study of the pollen emissions of Urticaceae, Plantaginaceae and Poaceae at five sites in western Spain. Aerobiologia 14:117-129

Puc M (2012) Artificial neural network model of the relationship between Betula pollen and meteorological factors in Szczecin (Poland). Int J Biometeorol 56:395-401

Quinlan RJ (1992) Learning with continuous classes. In: Proc. of the 5th Australian Joint Conference on Artificial Intelligence, Singapore, 343-348

Quinlan RJ (1993) C4.5: Programs for Machine Learning. Morgan Kaufmann Publishers, San Mateo, CA

Recio M, Docampo S, García-Sánchez J, Trigo MM, Melgar M, Cabezudo B (2010) Influence of temperature, rainfall and wind trends on grass pollination in Malaga (western Mediterranean coast). Agr Forest Meteorol 150:931-940

Reznik S (2009) Common ragweed (Ambrosia artemisiifolia L.) in Russia: spread, distribution, abundance, harmfulness and control measures. Ambroisie, The first international ragweed review 26

Rodinkova V, Palamarchuk O, Kremenska L (2012) The most abundant Ambrosia pollen count is associated with the southern, eastern and the northern-eastern Ukraine. Alergologia et Immunologia 9:181

Rodríguez-Rajo FJ, Astray G, Ferreiro-Lage JA, Aira MJ, Jato-Rodriguez MV, Mejuto JC (2010) Evaluation of atmospheric Poaceae pollen concentration using a neural network applied to a coastal Atlantic climate region. Neural Networks 23:419-425

Rodríguez-Rajo FJ, Aira MJ, Fernandez-Gonzalez M, Seijo C, Jato V (2011) Recent trends in airborne pollen for tree species in Galicia, NW Spain. Clim Res 48:281-291

Sánchez-Mesa JA, Galán C, Martínez-Heras JA, Hervás-Martínez C (2002) The use of a neural network to forecast daily grass pollen concentration in a Mediterranean region: the southern part of the Iberian Penisula. Clin Exp Allergy 32:1606-1612

Sánchez Mesa JA, Galán C, Hervás C (2005) The use of discriminant analysis and neural networks to forecast the severity of the Poaceae pollen season in a region with a typical Mediterranean climate. Int J Biometeorol 49:355-362

Stach A, García-Mozo H, Prieto-Baena JC, Czarnecka-Operacz M, Jenerowicz D, Silny W, Galán C (2007) Prevalence of Artemisia species pollinosis in western Poland: Impact of climate change on aerobiological trends, 1995-2004. J Invest Allerg Clin 17:39-47

Stach A, Smith M, Baena JCP, Emberlin J (2008) Long-term and short-term forecast models for Poaceae (grass) pollen in Poznań, Poland, constructed using regression analysis. Environ Exp Bot 62:323-332

Vinogradova YR, Majorov SR, Khorun LV (2010) Black Book of Central Russia: Alien Species of flora of Central Russia (in Russian). Moscow: GEOS

Vlachogianni A, Kassomenos P, Karppinen A, Karakitsios S, Kukkonen J (2011) Evaluation of a multiple regression model for the forecasting of the concentrations of NOx and PM10 in Athens and Helsinki. Sci Total Environ 409:1559-1571

Voukantsis D, Niska H, Karatzas K, Riga M, Damialis A, Vokou D (2010) Forecasting daily pollen concentrations using data-driven modeling methods in Thessaloniki, Greece. Atmos Environ 44:5101-5111

Voukantsis D, Karatzas K, Kukkonen J, Rasanen T, Karppinen A, Kolehmainen M (2011) Intercomparison of air quality data using principal component analysis, and forecasting of PM10 and PM2.5 concentrations using artificial neural networks, in Thessaloniki and Helsinki. Sci Total Environ 409:1266-1276

Voukantsis D, Karatzas K, Jaeger S, Berger U, Smith M (2013) Analysis and forecasting of airborne pollen-induced symptoms with the aid of computational intelligence methods. Aerobiologia 29:175-185

Ziska L, Knowlton K, Rogers C, Dalan D, Tierney N, Elder MA, Filley W, Shropshire J, Ford LB, Hedberg C, Fleetwood P, Hovanky KT, Kavanaugh T, Fulford G, Vrtis RF, Patz JA, Portnoy J, Coates F, Bielory L, Frenz D (2011) Recent warming by latitude associated with increased length of ragweed pollen season in central North America. P Natl Acad Sci USA 108:4248-4251

COMPARISON OF THE RESULTS OF TWO MICROCLIMATOLOGICAL MODELS AND MEASUREMENTS

LA ÉGERHÁZI[1], A KOVÁCS[1], Á TAKÁCS[1] and L ÉGERHÁZI[2]

[1]Department of Climatology and Landscape Ecology, University of Szeged, P.O.Box 653, 6701 Szeged, Hungary
[2]Department of Medical Physics and Informatics, University of Szeged, Korányi fasor 9., 6720 Szeged, Hungary
E-mail: egerhazi@geo.u-szeged.hu

Summary: The present paper analyses the thermal comfort conditions of a typical summer day in a popular playground simulated by two micrometeorological models, ENVI-met and RayMan in a Central-European city, Szeged. The thermal comfort conditions of the study area were quantified by the Physiologically Equivalent Temperature (PET). The outputs of the simulations were compared to each other and than they were collated the onsite measurements which were carried out in a sun-exposed and in a shaded point of the investigated area. According to the models, the highest heat load in the selected time intervals occurred in the middle parts of the playground, which were exposed to the sun, while more comfortable conditions could be experienced in the shade of the vegetation and the buildings. Based on the comparison of the measured and modelled data, both models underestimated the real thermal parameters under sun-exposed conditions. However, in the shade RayMan was more accurate, and here the measured and modelled PET values were almost identical. Beside these results, the main positive and negative features of the applied models are also discussed in the paper.

Key words: thermal comfort, ENVI-met, RayMan, Physiologically Equivalent Temperature (PET), playground

1. INTRODUCTION

In urban environments, the use of artificial materials with inappropriate thermal properties, the lack of green spaces, the overcrowding, as well as the accelerated anthropogenic heat and air pollution have an increasing adverse effect on the citizens (Unger 1999). Considering the projected tendency of the global air temperature changes and the heat waves which are expected to occur with an increased frequency and extended durations in the future, this issue will become even more significant (IPCC 2013). To mitigate the impacts of the observed and projected stressful thermal conditions, an effective coordination of multi-disciplinary teams (consisting of climatologists, urban planners, architects, and psychologists among others) is required (Eliasson et al. 2007). Urban planners and architects should seek to support climate-sensitive planning and site-specific design with precise microclimate knowledge. Moreover, they should meet the needs and behavioural attitudes of the citizens and visitors of open spaces under various thermal conditions. However, nowadays the aesthetic aspects of the area design often have priority, while the actual demands of the visitors and the function of the area seem to be disregarded.

In order to foster the climate-sensitive awareness of the planners, micro-bioclimatological simulations can provide an effective support by modelling the various spatial and temporal microclimatic patterns in urban spaces with different designs (Bruse

2004). Application of micro-scale models can represent a valuable tool to create thermal stress maps, which can illustrate the thermal differences in public spaces or even in a small part of the city with relatively high temporal and spatial resolution. Since microclimate modelling can also be performed on fictional situations, the influences of an altered design (e.g. change in land use, vegetation or building density) on the environment and human comfort conditions can be considered and predicted already in the planning phase. Moreover, consequences of future climatic trends may be simulated by changing the meteorological input data, e.g. using projected temperatures based on the climate change scenarios (Huttner et al. 2008).

Over the past years, the number of available microclimate models and simulations has increased rapidly. Although these tools involve many assumptions and simplifications (Ali-Toudert and Mayer 2007), they seem to be the most affordable and cost-effective option for the simulation of the interactions between the complex urban surface and the microclimatic conditions. Due to their simplicity, short computing time and free availability, the most popular and widely applied models in Central-Europe are RayMan (Matzarakis et al. 2007) and ENVI-met (Bruse 2004).

This study examines the applicability of these two models in the urban planning practice by comparing the model results of a typical summer day with onsite microclimate measurements in a popular playground. The study aims to evaluate the effectiveness of the models in different planning phases.

2. MATERIALS AND METHODS

2.1. Description of the study area

The investigated area is located in the centre of Szeged (46°N, 20°E, 82 m above sea level), a medium-sized city in the south-eastern part of Hungary. Szeged belongs to the climatic region Cf according to Köppen's classification (temperate warm climate with uniform annual distribution of precipitation) or to the climatic region D.1 according to Trewartha's classification (continental climate with a long warm season) (Unger et al. 2000, Balázs et al. 2009).
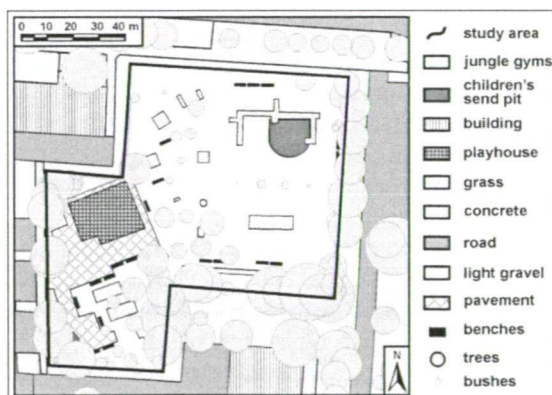

Fig. 1 Map of the investigated playground

The study area is one of the most modern and popular playgrounds in Szeged with an approximate area of 3,300 m². The surface of the playground is primarily covered by light-coloured gravel, while the immediate vicinity of a playhouse is covered by paving stone. A large number of deciduous trees are planted mainly at the boundaries of the playground, but in the middle part of the area there are only a few trees, which are too young to provide relevant shade (Fig. 1). Therefore in the morning and early afternoon hours considerable part of the area is exposed to the direct sunlight. In the playground children can choose from several toys such as jungle gyms, swings and slides, moreover 20 benches offer seating places to the visitors (Fig. 1).

2.2. Methods

The present paper analyses the spatial and temporal patterns of the thermal comfort conditions in the examined playground, which were simulated by two micrometeorological models, ENVI-met and RayMan. The models were run with the input data of a typical hot, cloudless and relatively windless summer day (12th July 2011), since under these conditions the developed thermal and microclimate differences are expected to be clearly observable. From the outputs of both models, two typical dates (11 a.m. and 5 p.m.) were selected to represent the daily course of the comfort parameters. The results obtained from the simulations were compared to each other as well as to the onsite measurements (see Section 2.2.3.).

thermal sensation	very cold	cold	cool	slightly cool	neutral (comfortable)	slightly warm	warm	hot	very hot
PET (°C)	4	8	13	18	23	29	35	41	
physiological stress level	extreme cold	strong cold	moderate cold	sligthly cold	no stress	sligthly heat	moderate heat	strong heat	extreme heat

Fig. 2 PET scale for different human thermal sensation and stress levels (based on Matzarakis and Mayer 1996)

The thermal comfort conditions were quantified by the widely used human bioclimatological index, Physiologically Equivalent Temperature (PET). PET is defined as the air temperature at which, in a typical indoor setting, the heat budget of the body is balanced with the same core and skin temperature as those under the prevailing complex outdoor conditions (Höppe 1999). The PET value ranges were defined according to different Central European thermal sensation and physiological stress levels (Matzarakis and Mayer 1996) (Fig. 2).

The software Surfer 8 was used to interpolate the grid of the modelled PET values and to create the heat stress maps.

2.2.1. Model simulation with ENVI-met

ENVI-met is a three-dimensional microscale climate model, which is capable to simulate the interactions between the urban design and the microclimate with relatively high temporal (10 min) and spatial (0.5–10 m) resolution (Bruse 2004). The simulation requires two groups of model input data. The 'Area input file' includes the morphological elements (buildings, plants, land covers etc.) and the 'Configuration file' contains the basic settings

(such as the durations of the simulated time period and the time steps) as well as the necessary initial meteorological parameters related to the simulation.

In the present study, ENVI-met was run with a spatial resolution of 1.5 m and the results were referred to the bioclimatological reference height of 1.1 m. The required initial meteorological data included the air temperature, the relative humidity (both measured at 12 a.m.), the average wind speed, the most frequent wind direction and the specific humidity (Table 1). These parameters were obtained from the meteorological station of the Hungarian Meteorological Service located at a distance of about 6 km from the playground, except for the specific humidity, which was acquired from Wyoming Weather Web (2013) The model started at midnight and 24 hours were allowed to the modelled parameters to stabilise (time designations in this section refer to the timescale of the model). The simulation finished at 7 p.m. CEST (one hour after the closing time of the playground), therefore the total simulated time was 43 hours (Table 1). The output of the model was saved every 30 minutes to a predefined folder.

Table 1 Basic input parameters of the ENVI-met

Temperature (K)	294
Relative humidity at 2 m (%)	75
Wind speed at 10 m (ms⁻¹)	3.3
Wind direction (°)	10
Spec. humidity at 2500 m (gkg⁻¹)	7
Roughness	0.1
Total simulation time (h)	43
Start of simulation	00:00:00

2.2.2. Model simulation with RayMan

RayMan is a small-scale radiation and bioclimate model which calculates the complex radiation fluxes and the thermal bioclimatic indices, such as PET (Matzarakis et al. 2007). RayMan simulates the short- and long-wave radiation flux densities from the three-dimensional surroundings in both simple and complex urban environments, on the basis of parameters such as air temperature, air humidity, global radiation (or cloud cover), time of day and year, albedo of the surrounding surfaces and their solid-angle proportions. Beside these parameters, the model requires input data on surface structures of the study area (buildings and trees) and on personal parameters. However, this model is not capable of taking into account the different types of land cover.

We used four parameters as input meteorological data for the simulation: the 10-min averages of the air temperature [°C], the relative humidity [%], the wind velocity [ms⁻¹], and the global radiation [Wm⁻²], obtained from the Hungarian Meteorological Service as mentioned above. Wind speed data at 10 m a.g.l., were reduced to 1.1 m a.g.l. using the equation applied by e.g. Gulyás et al. (2006). The global radiation data were modified by the model according to the obstacles (surface structures, such as buildings or trees). The personal input data referred to a typical European male, who is 35 years old, 1.75 m tall, and weights 75 kg. The spatial distributions of the thermal comfort indices were determined through a new interpretation of the RayMan model. From the input parameters 10-min PET values were calculated by the model along a 3 m × 3 m grid network (i.e. the spatial resolution was 3 m), using 764 simulation points (Fig. 3b).

2.2.3. Onsite measurements and comparison of the modelled and measured PETs

During the onsite measurements air temperature [°C], relative humidity [%], wind speed [ms^{-1}], as well as short- and long wave radiation fluxes [Wm^{-2}] were recorded in the studied playground. The data were collected between 10 a.m. and 6 p.m. every minute by two mobile micro-bioclimatological stations at the reference height (1.1 m). One of the stations was always located in the shade (VK1), while the other station was exposed to the sun (VK2). From these onsite data 10-min average PET values were calculated.
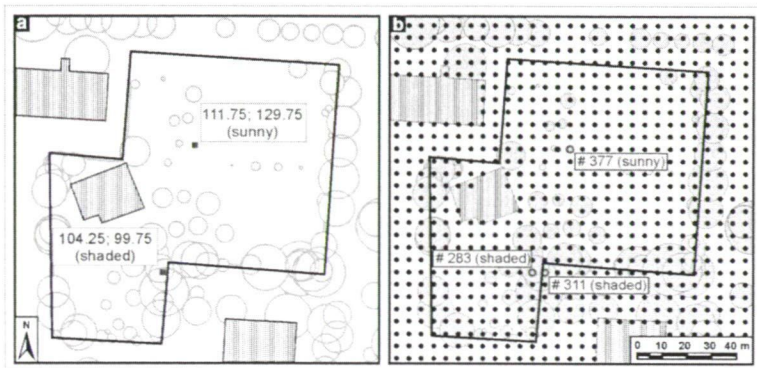

Fig. 3 The two selected cells of the ENVI-met (a) and the three chosen grid points of the RayMan (b) for the comparison to the onsite measurements

The comparison was based on two cells from the 'Area input file' of ENVI-met and three points from the grid network of RayMan, according to the positions of the two mobile stations, one situated in a sun-exposed and one in a shaded location. On the ENVI-met map their positions were identified with the coordinates (111.75; 129.75) and (104.25; 99.75), respectively (Fig. 3a). The first point (sunny condition) was represented on the RayMan map by its equivalent point #377 (Fig. 3b). However, the equivalent position of the second point (#283) in the RayMan model was exposed to the sun from the early afternoon hours. Therefore, by substitution, a nearby point was selected on the RayMan map (#311), which was not exposed to the sun in the afternoon (Fig. 3b).

3. RESULTS AND DISCUSSIONS

3.1. Comparison of the spatial and daily PET patterns simulated by the models

Based on the results of the ENVI-met and RayMan models, at 11 a.m. heat load was dominant almost in the whole area (Fig. 4). According to both heat stress maps, in the northern parts of the playground warm thermal conditions were found with a PET of 29–35°C. Furthermore, the darker patches in the central part of the ENVI-met map indicate PET values of 35–41°C, which corresponds to hot thermal sensation.
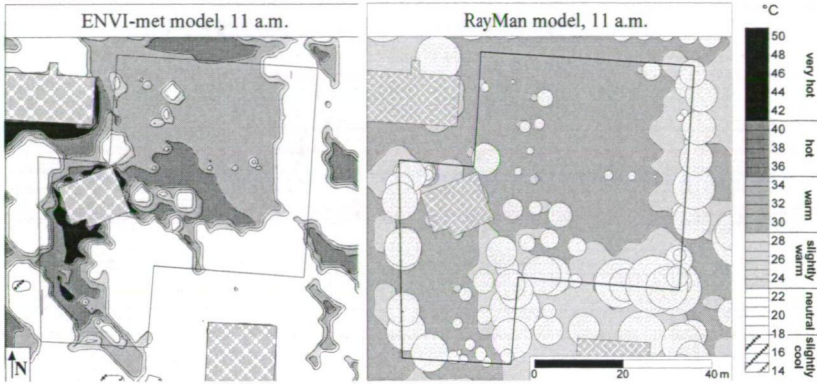
Fig. 4 Thermal stress maps based on ENVI-met and RayMan simulations at 11 a.m. CEST, 12th July 2011 (black line indicates the border of the investigated playground)

The heat stress map of ENVI-met illustrates that the highest heat load appeared around the playhouse, where PET values exceed 41°C denoting extreme heat stress (very hot thermal sensation). This can be explained by the strong heat radiation of the pavement (see Fig.1) warmed up by the direct solar radiation. Since the RayMan model cannot take into account the types of land covers this pattern cannot be observed on this map. Both models suggest that the thermal stress in the immediate vicinity of the single trees was slightly moderate; ENVI-met map shows neutral while RayMan map indicates slightly warm thermal sensation in these areas. Due to the shading effect of the dense foliage, the thermal conditions were much more pleasant near the southern and eastern boundaries of the area. Here neutral thermal conditions (18–23°C) were present on the ENVI-met map, and slightly warm (23–29°C) on the RayMan map.
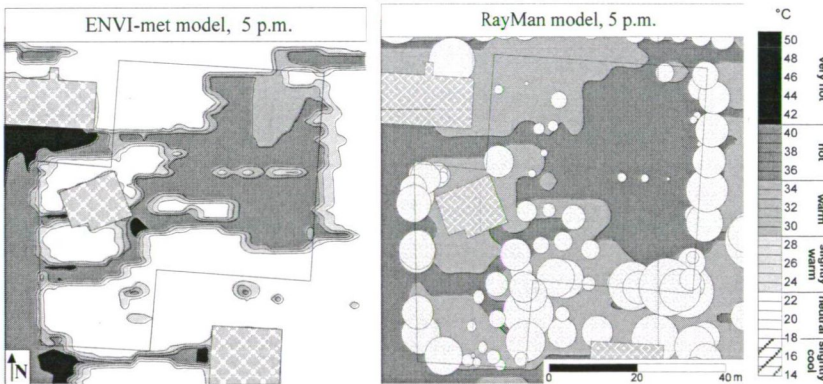

Fig. 5 Thermal stress maps based on ENVI-met and RayMan simulations at 5 p.m. CEST, 12th July 2011

Despite the lower sun elevation at 5 p.m., more stressful thermal conditions occurred in the places exposed to the sunlight than in the forenoon (Fig. 5). Both thermal stress maps show that hot thermal sensation (35–41°C) prevailed in the sun-exposed middle and eastern parts of the area. However, the effects of the single trees can be observed primarily on the ENVI-map. The heat load in the afternoon hours requires special attention, since this is the

period when the playground is usually the most visited (after the end of working hours of the parents). The shading of the trees and the surrounding buildings provides slightly more pleasant thermal conditions in the southern areas and the western part of the playground. This corresponds to neutral thermal sensation (PET of 18–23°C) on the ENVI-met map, but according to the results of RayMan simulation, significant heat stress, namely warm thermal sensation (29–35°C) can be found also in the shaded areas.

3.2. Comparison of the simulation results to the onsite measurements in the sun-exposed and shady point

According to Fig. 6, the outputs of the two applied models show remarkable differences compared to the onsite measured values in the sun-exposed point of the playground. Although the tendencies of the modelled (both RayMan and ENVI-met) and measured PET (VK2) values seem to be similar, both simulations underestimated the real thermal conditions. By the end of the day, the discrepancies became even larger. This can be explained by the fact that these models treat the obstacles (trees and building) in a simplified form (e.g. cuboids, sphere), which overshadowed the area in the investigated point already after 5 p.m. The triangle-shaped markers illustrate the magnitude of the VK2–RayMan and VK2–ENVI-met PET-differences, respectively. Based on these results, the RayMan model approximates the actual thermal conditions somewhat better. The differences were about 5–10°C, apart from the morning and evening hours when the average discrepancy between RayMan and VK2 data was 8.8°C, while in the case of ENVI-met it reached 11.0°C (Table 2). It is not surprising that this latter value is greater, since the ENVI-met simulates all the meteorological parameters (not only the radiations as the RayMan), from which it then creates the most probable weather situtation.
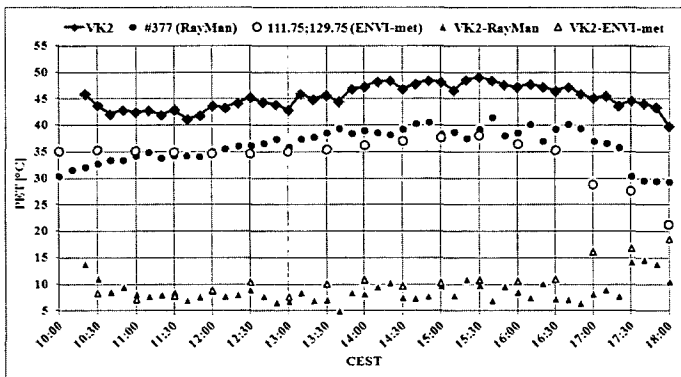

Fig. 6 Modelled and measured PET values and their differences at the sun-exposed point

Table 2 Output of the paired t-test under sun-exposed condition

	Mean (°C)	Std. deviation (°C)	Std. error mean (°C)	95% Confid. interval of the difference (°C)		t	Df	Sig. (2-tailed)
				Lower	Upper			
VK2–RayMan	8.7896	2.0687	0.3017	8.1822	9.3970	29.129	46	0.000
VK2–ENVI-met	11.0408	3.3348	0.8337	9.2638	12.8178	13.243	15	0.000

The relationship between the modelled and measured PET values in the sun-exposed position was evaluated by means of paired t-test, and the differences between the modelled and the measured data were found to be significant at a level of 5% (p < 0.001) (Table 2).

As illustrated in Fig. 7, the ENVI-met model behaved similarly for the shaded and the sun-exposed situations. The thermal comfort conditions in the shaded areas modelled by the ENVI-met were cooler (neutral thermal sensation) than measured in the actual environment (slightly warm and warm sensation). The VK1–ENVI-met difference was consequently above 5°C during the day, and in the late afternoon this difference exceeded 12°C. In the shade, RayMan simulates the thermal comfort conditions much more adequately than ENVI-met; the modelled and measured PET values were almost equal during the forenoon. By the afternoon hours, however, the measured PET values (VK1) slightly increased under the trees compared to the simulated values. This can be explained by the fact that the foliages became warmer during the day due to the incoming solar radiation, thus they emitted more energy toward to the surface. This local temperature increase cannot be observed on the modelled PET map, because the input parameters of the simulation were obtained from the weather station, and furthermore the RayMan model probably did not take into account the increasing temperature of the foliage during the day. The mean discrepancy was only 1.2°C between the modelled and measured PET values (Table 3), and even the maximum difference did not exceed 3.5°C (Fig. 7).
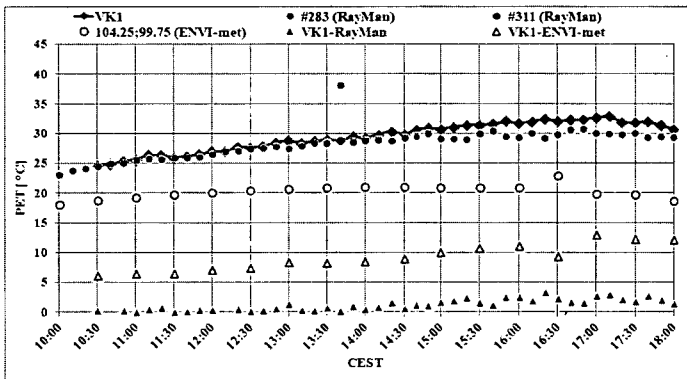

Fig. 7 Modelled and measured PET values and their differences at the shaded point

Table 3 Output of the paired t-test for the shaded condition

	Mean (°C)	Std. deviation (°C)	Std. error mean (°C)	95% Confid. interval of the difference (°C)		t	df	Sig. (2-tailed)
				Lower	Upper			
VK1–RayMan	1.1603	0.9515	0.1403	0.8778	1.4429	8.271	45	0.000
VK1–ENVI-met	9.0502	2.2152	0.5538	7.8698	10.2306	16.342	15	0.000

According to the results of the paired t-test for the shaded point (Table 3), the difference between the modelled and the measured data pairs proved to be significant again (p < 0.001) at a level of significance of 5%.

3.3. Evaluation of ENVI-met and RayMan from practical aspects

In this chapter, the main advantages and disadvantages of ENVI-met and RayMan are summarized regarding their practical applications (Table 4).

Table 4 Main advantages and disadvantages of ENVI-met and RayMan models

	RayMan	ENVI-met
simulation	point-to-point (result: grid network)	an area by default
simulated parameters	only the complex radiation environment	all the meteorological parameters
input data	more input parameters, reduction of the wind speed (1.1 m); real meteorological data	only 1 value for each meteorological data; no wind speed reduction
preparation of input data	complex (larger database)	simplified (only 1 input value for each parameter)
obstacles, land cover	only vegetation and buildings	land cover, vegetation, buildings
shape of the obstacles	foliage: spheriform or cone, buildings: cuboids	all objects are cuboid-shaped (with grid-cell resolution)
output data model duration	even several years/simulation	max. 1–2 weeks/simulation
diurnal resolution	even 1 min	at least 10 min
investigated area	no nesting grids, no size limitation	nesting grids, limited size
duration of simulation	shorter (about 3 days/area, depending on resolution)	longer (even 1 week, depending on resolution)
accuracy	more accurate approximation of the real condition	less accurate
usability	user-friendly, less computing capacity	complex interface, more computing capacity

Table 4 highlights that RayMan models only the complex radiation environment, while ENVI-met simulates all the meteorological parameteres including air temperature, relative humidity, wind speed and solar radiation. ENVI-met requires only one input data for each meteorological parameter in the simulation, from which it creates a most probable weather situation. However, RayMan uses real meteorological parameters during the simulation, therefore its output is more accurate. Unfavourably, in the case of RayMan wind speed must be reduced manually before the simulation. RayMan is able to produce databases of several-year model time duration, while ENVI-met simulates data sets of 1–2 weeks at maximum due to the complexity of the model.

One of the most advantageous feature of ENVI-met is the capability of estimating the thermal effects of vegetation, buildings as well as the land cover. Contrary to this, RayMan takes into account only the vegetation and the buildings during the simulation. Due to the grid-cell resolution, all obstacles are cuboid-shaped in ENVI-met, while in RayMan the foliages are spheriform (deciduous trees) or cone (coniferous trees). Since ENVI-met is a very complex model the evaluation time of the simulation is much longer than that of the RayMan, and it requires more computing capacity at the same time.

4. CONCLUSIONS

The study presented the spatial and diurnal patterns of thermal comfort conditions of a popular playground on a typical summer day simulated by two micrometeorological

models, ENVI-met and RayMan in a Central-European city, Szeged. The results of the simulations were compared to each other and than to the onsite measurements which were carried out in a sun-exposed and in a shaded point of the investigated area.

According to the heat stress maps of both models, more pleasant conditions occurred under the trees at the investigated times (11 a.m. and 5 p.m.), while the highest thermal load was found in the sun-exposed middle part of the area. In the afternoon (5 p.m.), however, despite the lower sun elevation the PET values were slightly increased in the middle of the playground, and the corresponding heat load was observed on the ENVI-met map, too. Based on the comparison of two models for the sun-exposed point, not only the ENVI-met, but also RayMan underestimated the measured PET values. However, in the shade RayMan was more accurate, and the mean difference between the measured and the modelled PET values was only 1.2°C. For both the sun-exposed and the shaded conditions, the difference between the modelled and the measured data was significant at a level of significance of 5%. Finally, the paper listed the main advantages and disadvantages of the simulations based on their practical applications.

REFERENCES

Ali-Toudert F, Mayer H (2007) Effects of asymmetry, galleries, overhanging facades and vegetation on thermal comfort in urban street canyons. Sol Energy 81:742-754

Balázs B, Unger J, Gál T, Sümeghy Z, Geiger J, Szegedi S (2009) Simulation of the mean urban heat island using 2D surface parameters: empirical modeling, verification and extension. Meteorol Appl 16:275-287

Bruse M (2004) ENVI-met website. http://www.envimet.com [accessed January 2014]

Eliasson I, Knez I, Thorsson S, Westerberg U, Lindberg F (2007) Climate and behavior in a Nordic city. Landscape Urban Plan 82:72-84

Gulyás Á, Unger J, Matzarakis A (2006) Assessment of the microclimatic and thermal comfort conditions in a complex urban environment: modelling and measurements. Build Environ 41:1713-1722

Höppe P (1999) The physiological equivalent temperature – an universal index for the biometeorological assessment of the thermal environment. Int J Biometeorol 43:71-75

Huttner S, Bruse M, Dostal P (2008) Using ENVI-met to simulate the impact of global warming on the microclimate in central European cities. Ber Meteor Inst Albert-Ludwigs-Univ Freiburg 18:307-312

IPCC (2013) Climate Change 2013: The Physical Science Basis. Contribution of Working Group I to the Fifth Assessment Report of the Intergovernmental Panel on Climate Change. [Stocker TF et al. (eds)]. Cambridge University Press, Cambridge, United Kingdom and New York, USA

Matzarakis A, Mayer H (1996) Another kind of environmental stress: thermal stress. WHO Newsletter 18:7-10

Matzarakis A, Rutz F, Mayer H (2007) Modelling radiation fluxes in simple and complex environments – application of the RayMan model. Int J Biometeorol 51:323-334

Unger J (1999) Comparisons of urban and rural bioclimatological conditions in the case of a Central-European city. Int J Biometeorol 43:139-144

Unger J, Bottyán Z, Sümeghy Z, Gulyás Á (2000) Urban heat island development affected by urban surface factors. Időjárás 104:253-268

Wyoming Weather Web (2013) Weather information from the University of Wyoming, Department of Atmospheric Science. http://weather.uwyo.edu/upperair/europe.html (WMO station number 12982) [accessed May 2013]

THE INFLUENCE OF BUILT FORM AND VEGETATION ON THE CANOPY LAYER MICROCLIMATE WITHIN URBAN BLOCKS

CV GÁL

College of Architecture, Illinois Institute of Technology, 3360 S. State St., Chicago, IL 60616-3793, USA
E-mail: cgal@hawk.iit.edu

Summary: A numerical simulation study was conducted to reveal the effects of built form on the canopy layer microclimate at the scale of city blocks and to evaluate the role of vegetation in modifying these environments. The study took four metropolitan urban block typologies from Budapest as models and compared their microclimate dynamics with and without vegetation. Microclimate modeling was performed by ENVI-met (Bruse 2011), while MATLAB was utilized for the data analysis. The findings indicate that built form and vegetation are key factors governing the canopy layer microclimate. Their influence is primarily exerted through shading and enclosure.

Key words: urban block, typology, trees, mean radiant temperature (MRT), numerical simulation, ENVI-met

1. INTRODUCTION

Regional climate projections for Hungary indicate a rather sharp increase in summertime temperatures by the end of the next century. While the prognosis for the mid-century is a 1.7–2.6°C rise in temperatures, by the end of the twenty-first century, models signal a 3.5–6.0°C increase in summertime conditions (Horányi 2011). In line with these changes, the frequency of extreme warm temperature events are also expected to rise (Bartholy and Pongrácz 2011).

In light of these projections, the understanding of microclimate modification by means of built form and vegetation is of key importance to architects, planners and other professionals in developing effective mitigation strategies in the future. As part of a larger study, the aim of this paper is to assess the microclimate performance of built form at the scale of city blocks and to evaluate the role of vegetation in influencing the climate of these spaces.

Fig. 1 From left to right: the block of courtyard apartments, the perimeter block, the Zeilenbau configuration and the hybrid block typology (Google Maps 2010)

2. MATERIALS AND METHODS

A numerical simulation study was carried out to assess the impact of built form and vegetation on the microclimate within urban blocks. The study utilized ENVI-met (Version 3.1 BETA V) for microclimate simulation (Bruse 2011) and MATLAB (Version 7.12) for the analysis and visualization of the results. The adopted research methodology consisted of two distinct phases. During the first, the examined cases were developed as well as the baseline case without buildings. In the course of the second, numerical simulations were run and the results analyzed.

2.1. Numerical modelling

The study utilized a typological approach to assess the effect of built form. The cases examined were developed on the basis of Budapest's four metropolitan urban block typologies: the nineteenth-century configuration consisting of attached courtyard apartment buildings, the perimeter block built up at its edges, the Zeilenbau design of parallel rows of buildings, and the hybrid form composed of short towers on a unifying base (see Fig. 1). The corresponding layouts, adapted to ENVI-met, are illustrated in Fig. 2. The buildings are uniformly 24 meters high, except for the hybrid configuration's base, which is set to 6 m. The models have a grid resolution of 6 m horizontally and 3 m vertically.

The influence of vegetation on the microclimate within these typologies was also evaluated numerically. The analysis adopted a rudimentary approach to lay out greenery within the blocks. The guiding principles were as follows. First, 40% of the available open space within the blocks received vegetation. Second, vegetated areas consisted of deciduous trees only with medium dense canopy. Third, trees were primarily arranged in rows along facades (see Fig. 3). Fourth, the top of the tree canopy was set to 21 meters uniformly across typologies. In most cases this resulted in 21 m tall trees, except for the hybrid configuration, where 15 m tall trees were placed on top of the six-meter-high base.
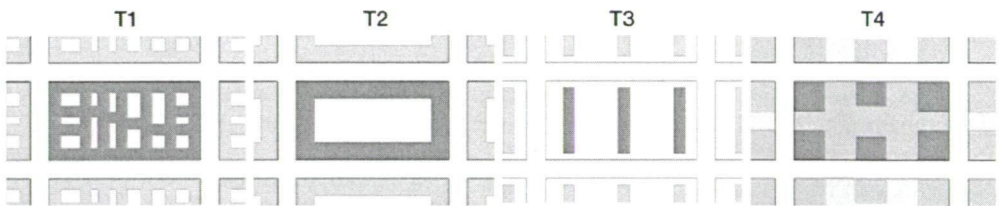

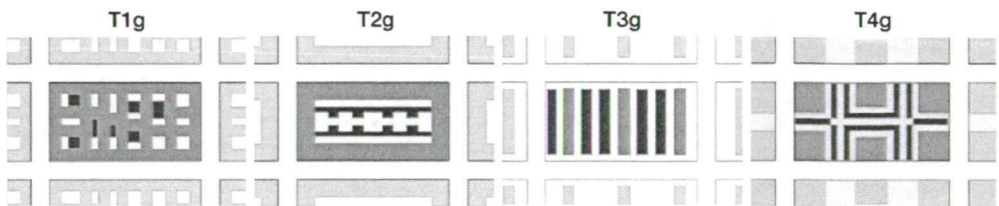Fig. 2 The model equivalents of the four urban block typologies

Fig. 3 The four model with trees (indicated by black patches within the blocks)

The baseline case without buildings was developed to emulate a typical July day in Budapest as described in the literature (Bacsó 1959, Réthly 1947). It both provided the climate parameters needed by the numerical model and the baseline canopy layer conditions applied as a reference. The air temperature and specific humidity cycles reproduced by the baseline configuration are plotted along with the reference data on Fig. 4. Further details on the development of the baseline case are discussed in Gál (2014).

The study follows a well-established procedure in numerical modeling. The digital model of each case consists of nine identical urban block configurations arranged in a three-by-three grid layout. In order to minimize the edge effect and to reduce the influence of bordering streets, the analyses only take the UCL above the central block into consideration. ENVI-met was run for 48 hours from July 7th. Due to the model's long spin-up time, only the results of the second day were evaluated. Additionally, to reduce systematic model errors, results are reported relative to the baseline conditions.
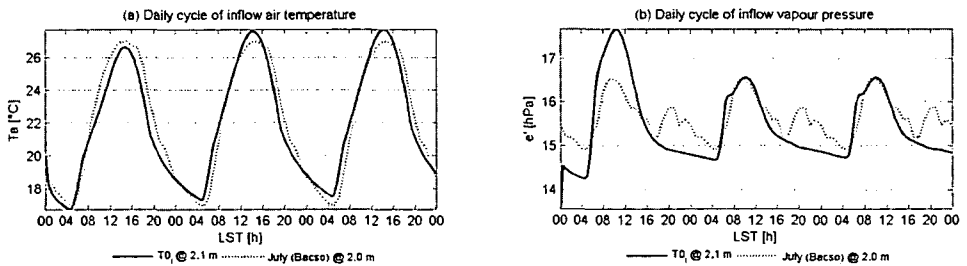

Fig. 4 Comparison of ENVI-met simulated (baseline case) and average July conditions in Budapest, Hungary (Bacsó 1959): (a) potential air temperature, (b) vapor pressure

2.2. Method of analysis

The present paper examines how built form and vegetation modify the microclimate within urban blocks. During clear and calm conditions, the key parameters governing the human thermal comfort and surface temperatures are radiation and air temperatures. Consequently, the study focuses on air temperature and MRT differences, with the latter used as an indicator of radiative conditions within the urban canopy. The presented analysis utilizes volumetric median air temperatures (ΔT_{UCL}) and mean radiant temperatures ($\Delta T_{MRT-UCL}$) calculated for UCL above the central urban block, relative to the baseline condition. For an ease of comparison, characteristic heat island measures calculated for the entire canopy are also reported.

In order to analyze UCL conditions in a concise manner, the study adopted a simple method based on areal average values (Gál 2014). The concept, illustrated in Fig. 5 briefly, consists of areal medians calculated for each elevation in the UCL and for every half hour of a diurnal cycle. Since results are reported relative to baseline conditions, areal values for the baseline model are derived from an identical canopy volume to that of the analyzed configuration. In other words, the volumes contained by buildings in a given model are first extracted from the canopy of the baseline, only then are areal medians calculated. The areal median canopy differences are subsequently assembled into a matrix, with different elevations arranged into columns and results from different times joined into rows. The magnitude of selected climate parameters is indicated by colors. This representation has the

advantage of providing a more detailed overview of the diurnal evolution of UCL conditions, while retaining the relative positions of adjacent air layers.
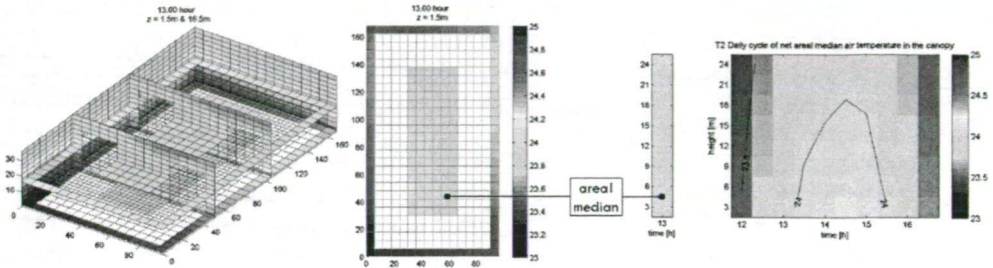

Fig. 5 The method of deriving an areal median matrix, illustrated on air temperature values

3. RESULTS AND DISCUSSIONS

3.1. The influence of form

The diurnal evolution of potential air temperatures relative to the baseline is presented on Fig. 6a. As a result of mutual shading, denser configurations remain about 1.5–2°C cooler than the baseline case during the warmest hours of the day. This phenomenon, called the intra-urban cool island, is characteristic to deep urban canyons where shaded cool surfaces offset the warming of the adjacent air (Johansson 2006). Besides shading, reduced intermixing – as a result of buoyancy difference between the cooler air of the canopy and warmer one above and likewise the consequence of the skimming flow that develops over densely built environments – also contributes to the emergence of this phenomenon (Johansson 2006). Among the denser typologies, lowest daytime temperatures are achieved in courtyard configurations. These results are in line with Berkovic et al. (2012), who found that courtyards without lateral openings have lower air and radiant temperatures. The role of courtyards in mitigating canopy layer temperatures is perhaps best represented by the comparison between the perimeter block configuration (T2) and the hybrid form (T4). While the two has the same building density, the canopy of T2 remains about 0.2°C cooler than T4 through the day.

In case of open configurations, nighttime temperatures confirm the generally reported inverse relationship between a configuration's rate of cooling and building density: the Zeilenbau (T3) with lowest density and building surface fraction cools down the most, while the hybrid form (T4) with the entire block covered remains the warmest configuration. The nighttime temperature difference between these two cases is nearly 1.5°C. According to the results, this correlation does not hold true for courtyard configurations (T1, T2). T1, which is the densest configuration and has the second greatest building surface fraction after T4, remains about 0.5°C cooler than its less dense courtyard counterpart, the perimeter block (T2). T1 also stays about 0.7°C cooler than T4. Ali-Touder and Mayer (2006) reported a similar relationship between nocturnal temperatures and high aspect ratios. According to their findings, deep urban canyons with H/W = 4, remained about 0.5–1°C cooler than comparable shallower configurations at 21:00 LST. These findings indicate that beyond a

certain threshold of density (signaled by sky view factor or aspect ratio), the cooling effect from mutual shading extends into the night.

The diurnal course of mean radiant temperatures is presented in Fig. 6b. According to the results, large open spaces in T2 and T3 provide little to no protection from solar radiation during the day. In contrast, the mutual shading of towers in the case of T4 offers a 5–15°C radiant temperature reduction within the canopy. The greatest cooling is realized in typology T1, where small courtyards decrease MRT by over 25°C. The only time during the day when radiant temperatures in T1 approach baseline conditions is around noon, when the high sun is able to penetrate the small courtyards. Compared to daytime, the variation of nighttime radiant temperatures is much reduced. The microclimate dynamics of configurations are set apart by their openness: typologies with large open spaces (T2, T3) remain about 5°C cooler than the typologies with relatively evenly distributed building masses. While this difference confirms a better nighttime cooling due to greater sky view factors, the considerably reduced range of nocturnal MRT values might also be the sign of ENVI-met's limitation to account for the heat stored in building envelopes.
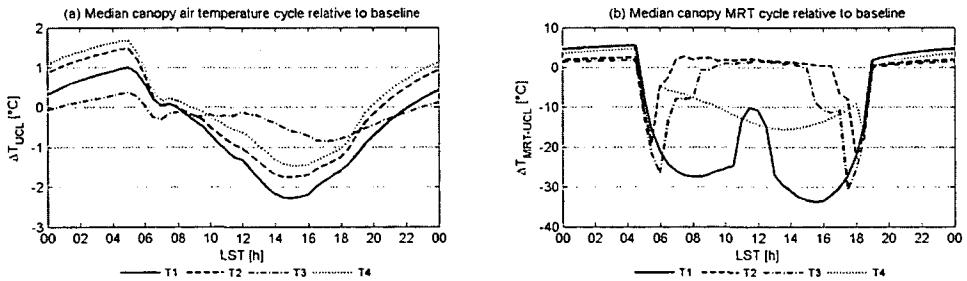

Fig. 6 Diurnal cycles of the UCL relative to the baseline, non-vegetated configurations:
(a) potential air temperatures, (b) mean radiant temperatures

The diurnal spatial and temporal evolution of potential air temperatures within the UCL is shown in Fig. 7a. The presented trends are in line with previous observations: all typologies experience daytime temperature reduction and nighttime temperature excess to a varying degree. The daytime cool island intensity is greatest at configurations with courtyard (T1, T2). Since the heavier cold air of courtyards remains relatively separated from the well-mixed, but warmer air of streets, daytime cooling within these configurations lasts longer and affects the greater part of the canopy. During the hottest hours of the day, cooling intensity exceeds 3°C at the bottom of the small courtyards (T1). Among the typologies T3 interferes the least with the background climate, as both daytime temperature reduction and nighttime temperature excess remain below 1.2°C. Hence, the configuration's low building density and openness not only facilitate radiative and convective cooling at night, but also contribute to higher temperatures during the day: the lack of shading increases both surface and air temperatures, while the lack of enclosure ensures that the warm canopy air remains well-mixed and evenly distributed. In the case of T4, the mutual shading of towers decreases daytime, but increases nighttime temperatures.

The effects of built form on the radiation fluxes within the canopy are shown in Fig. 7b with deeper colors indicating greater radiation reductions. The dark tapered areas during early and late hours of the day, around 6:00 and 18:00 LST respectively, are the results of shortwave radiation obstructions at low sun angles. With increasing sun angles, the effect of

mutual shading decreases. During high sun hours, shading completely ceases in configurations with large open spaces (T2, T3). At T4, the interference between the towers decreases radiant temperatures by over 10°C from approximately 10:00 to 18:00 LST. Solar obstruction is greatest at configuration with small courtyards (T1). Here, the icicle shape pattern around noon indicates the average depth that solar radiation infiltrates the courtyards. The relatively symmetrical MRT patterns in Fig. 7b are the outcome of spatial symmetries in configurations, as well as the alignment of typologies with cardinal directions.
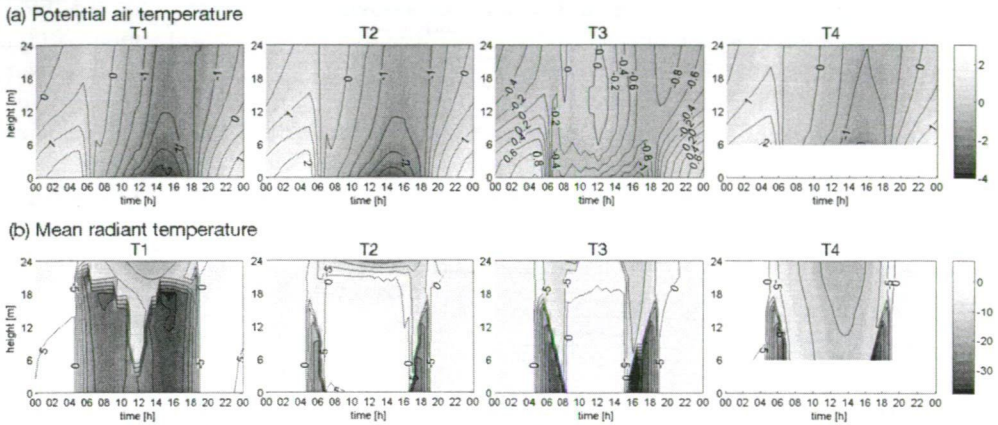

Fig. 7 Diurnal cycles of the UCL relative to the baseline, non-vegetated configurations:
(a) potential air temperatures, (b) mean radiant temperatures

3.2. The effect of vegetation

The influence of greenery on the potential temperature cycle of typologies is shown in Fig. 8a. A comparison with non-vegetated conditions in Fig. 6a reveals that trees are most effective in configurations with large open spaces (T2, T3). At night, the Zeilenbau (T3) remains about 1°C cooler than the denser configurations. Except for a brief period between 12:00 to 16:00 LST, T3 also stays the coolest typology during the day. The likely reasons behind these cool conditions are the configuration's high green area ratio and low building surface fraction. In case of typologies with evenly distributed building masses, the effect of trees is largely limited to nocturnal temperatures. The nighttime temperature reduction is about 0.3°C and 1°C in the case of T1 and T3, respectively. Since ENVI-met cannot account for the heat stored in building envelopes, this difference is likely the result of the reduced heat stored in the ground due to shading. According to the new thermal dynamics of typologies, the temperature cycles of courtyards configurations (T1, T2) stand apart. They are characterized by a nearly 1°C smaller diurnal range. The perimeter block (T2), characterized by a larger green area ratio and a smaller building surface fraction than T1, remains about 0.2–0.4°C cooler through the day. In contrast, while the temperature cycles of open configurations are likewise nearly identical, their canopy temperatures remain about 1°C apart over the day.

The effect of vegetation on the evolution of relative MRT cycles is presented in Fig. 8b. With its well-distributed building mass and lowest amount of greenery, T1 is the typology least affected by trees. In this case, the only noticeable outcome of shading is the disappearance of extreme radiant temperatures around noon (see Fig. 6b). With regard to

other typologies, vegetation resulted a MRT cycle similar to that of T1. The irregularities and minor differences between the four typologies are due to the directionalities present in the combined layout of buildings and vegetation.
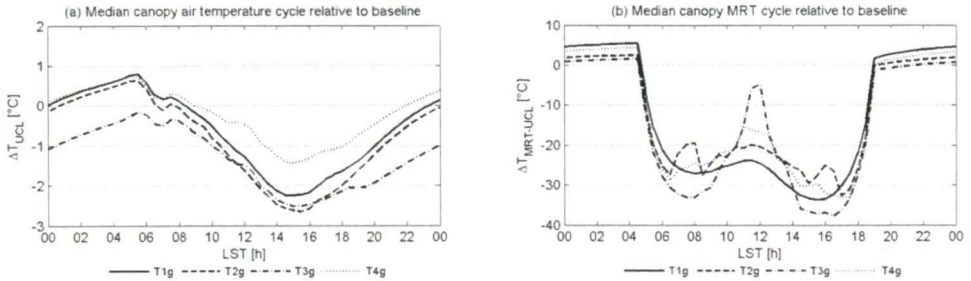

Fig. 8 Diurnal cycles of the UCL relative to the baseline, vegetated configurations: (a) potential air temperatures, (b) mean radiant temperatures

Fig. 9a presents the influence of vegetation on the distribution of relative potential air temperatures within the UCL. With the introduction of trees, the configurations with large open spaces (T2, T3) became the coolest ones. During the day, the greatest absolute cooling is achieved by T2 with over 3.5°C reduction near the ground, while the most prolonged and spatially extensive cooling within the canopy is realized by T3. In contrast, at configurations where mutual shading was already present (T1, T4) vegetation increased median canopy temperatures by 0.1–0.2°C during the day. This increase is likely the result of decreased turbulence, an effect that was also reported experimentally by Park et al. (2012). Similarly to the non-vegetated state, T3 cools down the most at night, while T4 remains the warmest configuration.

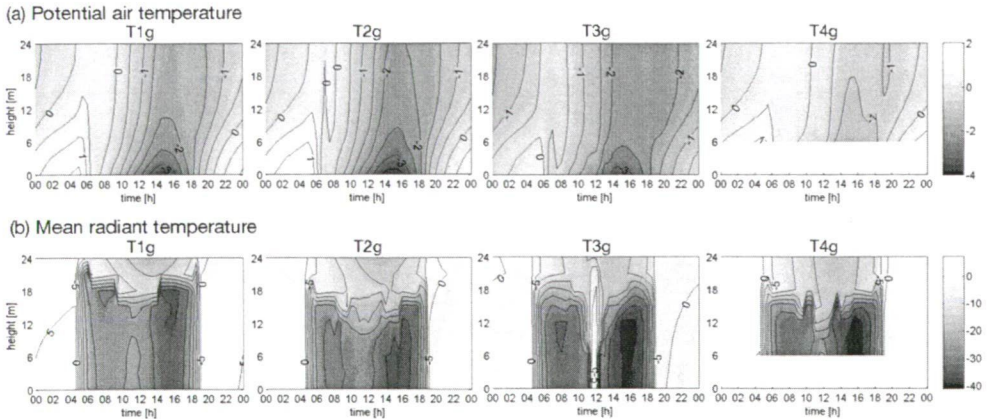Fig. 9 Diurnal cycles of the UCL relative to the baseline, vegetated configurations: (a) potential air temperatures, (b) mean radiant temperatures

The relative MRT patterns within the canopy are shown in Fig. 9b. At 3 m vertical grid resolution, the introduced trees with medium canopy density result in a transitory MRT zone between the elevations of 15 to 21 meters. Only below this zone does the shading effect

of vegetation come into full force. As already noticed above, the introduction of greenery results in radiant temperature patterns akin to the initial T1 configuration (see Fig. 7). The minor differences and apparent irregularities are the results of combined directionalities in models. The interference between building and tree layouts is best illustrated with the MRT patterns of T2 and T3. In the case of the latter, the lack of radiation reduction at noon is the outcome of the parallel north-south oriented paths between the rows of trees and buildings. When aligned with the solar azimuth angle, these spaces became fully irradiated. At T2, the slight decrease of shading during the morning and afternoon hours, around 9:00 and 15:00 respectively, are the result of the east-west oriented paths along the facades. These places became irradiated when the sun is aligned with the cardinal east-west direction. Since T4 has both north-south and east-west oriented paths, it carries the MRT pattern characteristics of both previous cases, although with smaller differences.

Fig. 10 summarizes the influence of built form and vegetation on canopy layer temperatures. Typologies without vegetation (black bars) can be divided into two groups by their microclimate dynamics. In contrast to T3, dense configurations are characterized by greater temperature range reductions, nighttime heat island magnitudes and daytime cooling (see Fig. 10a, 10b and 10c respectively). With the introduction of trees (white bars), the division between the thermal behaviors of typologies becomes more nuanced. While nighttime heat island magnitudes remained to be governed by building densities (Fig. 10b), the diurnal temperature reduction on Fig. 10a indicates a new division along the openness of typologies. In case of courtyard configurations, the diurnal temperature range of the canopy is about 1°C smaller. With regard to heat island magnitudes, the presence of vegetation decreased nocturnal values in all cases and increased daytime cool island intensities in configurations with large open spaces (T2, T3). As noted above, daytime cooling decreases slightly with the addition of vegetation to typologies where mutual shading is already present (T1, T4). These results are in line with other studies that found the ability of trees to reduce daytime temperatures limited or controversial (Ali-Toudet and Mayer 2007, Emmanuel and Fernando 2007, Spangenberg et al. 2008, Park et al. 2012).
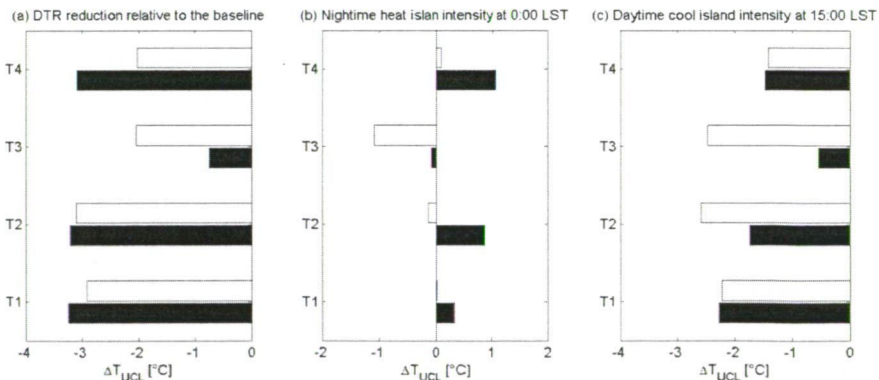

Fig. 10 UCL temperature characteristics for non-vegetated (black) and vegetated (white) configurations: (a) DTR reduction, (b) daytime UHI, (c) nighttime UHI

4. CONCLUSIONS

This paper presented the result of a numerical simulation study performed to reveal the influence of built form and vegetation on the canopy layer microclimate. The boundaries of the study were set by the identified metropolitan blocks of Budapest and by the characteristic summer climate of the city. The analysis on the role of built forms indicated the importance of building density, which, given uniform building heights, is interchangeable with building surface faction within the confines of this study. While low building density is generally associated with low nocturnal heat island intensity, if left unprotected, these areas warm up the most during the day. In reducing daytime air and radiant temperatures, shading and semi-enclosure (i.e. the effect of courtyards) were found to be effective strategies. Out of the two, shading is of primary importance in dense urban environments, since its effect may extend into the evening. According to the findings, canopy layer mean radiant temperatures are more responsive to the influences of built form. During the day, configurations with large open spaces (T2, T3) had the highest radiant temperatures, while the effect of mutual shading decreased default values by 10 to 30°C in the case of T1 and T4.

The rudimentary approach adopted to evaluate the role of vegetation confirmed that microclimate improvements by way of trees are primarily achieved through surface shading. The greatest reduction in daytime air and radiative temperatures were achieved in configurations with large open spaces (T2, T3). Although the introduction of trees slightly increased daytime temperatures at typologies where mutual shading was already present (T1, T4), it nevertheless reduced nighttime temperatures by offsetting the amount of energy intercepted by and stored in the urban texture. The controversies around the use of trees, on one hand, signal the limits of the vegetative approach to daytime temperature mitigation. The results, on the other hand, show that trees are beneficial in situations where shading is scant.

Finally, some remarks on the results and the adopted approach in evaluating the role of greenery. The effectiveness of trees to mitigate heat stresses in the built environment depends not only on the amount of vegetation (the green area ratio), but also on the plant characteristics of the adopted species (i.e. canopy geometry, height, LAD, LAI) and on the layout and distribution of greenery (e.g. Ali-Toudert and Mayer 2005, 2007, Spangenberg et al. 2008, Park et al. 2012). Although important, these parameters were not addressed by the current study. Nevertheless, the author believes that the main issues surrounding the urban use of greenery for microclimate mitigation were illustrated by this concise study. The initial assumption of 40% vegetation over the unbuilt areas of urban blocks, consisting of fully-grown trees, is certainly an optimistic one. First, 21-meter tall trees are less common in cities primarily due to the conflicts with above- and underground infrastructures, and also due to the extreme heat and drought conditions that often characterizes urban environments. Second, green roofs are rarely built with adequate supporting structures to accommodate large trees. As a consequence, the obtained results likely overestimate the effects of greenery, and point towards the decisive role of built form in shaping daytime temperatures within the UCL. These findings are in line with the results of Middler et al. (2014).

To conclude, built form and vegetation are principal factors in governing UCL microclimates. They act by means of shading and enclosure. At uniform building height, the key spatial parameters are influencing the climate between buildings are: building density (or in this special case, the building surface fraction), the openness of the configuration (i.e. the presence or absence of courtyards), and the distribution of building masses (which is signaled by the range of sky view factors calculated for the lowest points of the canopy). Given ENVI-

met's limitation to account for the heat stored in building envelopes and the assumptions made in MRT calculation by the model (Ali-Toudert 2005, Huttner 2012, Kántor and Unger 2011), further investigations are needed to refine and validate the findings of this study.

REFERENCES

Ali-Toudert F (2005) Dependence of outdoor thermal comfort on street design in hot and dry climate. Doctoral dissertation, Meteorologischen Instituts der Albert-Ludwigs-Universität Freiburg, Freiburg, Germany

Ali-Toudert F, Mayer H (2005) Thermal comfort in urban streets with trees under hot summer conditions. In: Raydan DK, Melki Habib (eds) Proc. 22th Int. Conf. PLEA 2005 – passive and low energy architecture, Vol. 2. Notre Dame University, Beirut, Lebanon. 699-704

Ali-Toudert F, Mayer H (2006) Numerical study on the effects of aspect ratio and orientation of an urban street canyon on outdoor thermal comfort in hot and dry climate. Building and Environment 41:94-108

Ali-Toudert F, Mayer H (2007) Effects of asymmetry, galleries, overhanging façades and vegetation on thermal comfort in urban street canyons. Sol Energy 81:742-754

Bacsó N (1959) Magyarország éghajlata [The climate of Hungary. (in Hungarian)] Akadémiai Kiadó, Budapest

Bartholy J, Pongrácz R (2011) A szélsőségek várható változásai és bizonytalanságai Magyarországon [Anticipated changes in extrem events and uncertainties. (in Hungarian)]. In: Bartholy J, Bozó L, Haszpra L (eds), Klímaváltozás 2011. MTA-ELTE Meteorológia Tanszék, Budapest. 223-234

Berkovic S, Yezioro A, Bitan A (2012) Study of thermal comfort in courtyards in a hot arid climate. Sol Energy 86:1173-1186

Bruse M (2011) ENVI-met (Version 3.1 BETA V)

Emmanuel R, Fernando H (2007) Urban heat islands in humid and arid climates: Role of urban form and thermal properties in Colombo, Sri Lanka and Phoenix, USA. Climate Res 34:241-251

Gál CV (2014) The impact of built form on the urban microclimate at the scale of city blocks. In: Proc. 94th AMS Annual Meeting and 11th Symposium on the Urban Environment. Atlanta, GA

Google Maps (2010) Urban blocks from Budapest, Hungary

Horányi A (2011) A hőmérséklet Magyarországra várható változásai és bizonytalanságai [Anticipated temperature change and uncertainty in Hungary (in Hungarian)]. In: Bartholy J, Bozó L, Haszpra L (eds), Klímaváltozás 2011. MTA-ELTE Meteorológia Tanszék, Budapest. 198-208

Huttner S (2012) Further development and application of the 3D microclimate simulation ENVI-met. Doctoral dissertation, Johannes Gutenberg-Universität Mainz, Mainz, Germany

Johansson E (2006) Influence of urban geometry on outdoor thermal comfort in a hot dry climate: A study in Fez, Morocco. Build Environ 41:1326-1338

Kántor N, Unger J (2011) The most problematic variable in the course of human-biometeorological comfort assessment – the mean radiant temperature. Centr Eur J Geosci 3:90-100

Middel A, Häb K, Brazel AJ, Martin CA, Guhathakurta S (2014) Impact of urban form and design on mid-afternoon microclimate in Phoenix Local Climate Zones. Landscape Urban Plan 122:16-28

Park M, Hagishima A, Tanimoto J, Narita K-i (2012) Effect of urban vegetation on outdoor thermal environment: Field measurement at a scale model site. Build Environ 56:38-46

Réthly A (1947) Budapest éghajlata [The climate of Budapest. (in Hungarian)] Budapesti Központi Gyógy és Üdülőhelyi Bizottság, Budapest

Spangenberg J, Shinzato P, Johansson E, Duarte D (2008) Simulation of the influence of vegetation on microclimate and thermal comfort in the city of São Paulo. Revista SBAU, Piracicaba 3:1-19

DIFFERENT ASPECTS IN THE QUANTIFICATION OF THE SKY VIEW FACTOR IN COMPLEX ENVIRONMENTS

M HÄMMERLE[1], T GÁL[2] J UNGER[2] and A MATZARAKIS[1]

[1]Department of Meteorology and Climatology, Albert-Ludwigs-University, Werthmannstraße 10, 79085 Freiburg, Germany
[2]Department of Climatology and Landscape Ecology, University of Szeged, P.O.Box 653, 6701 Szeged, Hungary
E-mail: m.haemmerle@stud.uni-heidelberg.de

Summary: This paper examines potential applications of the sky view factor (SVF) regarding two- or three-dimensional sites. First, the concepts of the radiation budget, Lambert's cosine law and hemispherical description of radiating of environments are introduced and connected to the sky view factor. Based on a comparison between different models and methods which calculate the SVF, the paper then focuses on two different kinds of SVF-calculation depending on the type of analyzed site. It is assumed that in case the point of interest represents a flat, two-dimensional area, it makes sense to include the cosine law whereas in case the point of interest represents a solid three-dimensional object the application of Lambert's law could have to be applied in another way. It is shown that the inclusion or exclusion of the cosine law results in different SVF values. It is concluded that depending on the type of surveyed area, the application of a 2D- or 3D-sky view factor should be considered in order to get a better approximation of the radiation fluxes.

Key words: sky view factor, Lambert's cosine law, radiation budget, complex environment, fish eye picture

1. INTRODUCTION

The sky view factor (SVF or ψ_s) is commonly defined as a dimensionless parameter which represents the fraction of visible sky on a hemisphere centred over the analyzed location (Oke 1981). The maximum SVF-value is 1, which occurs when the observer stands e.g. on a vast plain area or on the highest peak of a mountain range. On the opposite side, the SVF can reach a minimum value of zero which means that no sky is visible, as may be the case for a person standing in a metro station or in a very dense forest.

As the SVF changes, so do the radiation fluxes at the observed location and thus the radiation budget (Fig. 1).

Each flux-describing term of the surface radiation budget (Fig. 1) can be influenced by different settings of surface geometry when short and long wave radiation coming from the sky is replaced by radiation emitted by or radiation reflected from objects which obscure the sky (Fig. 2).

Because of the relation of sky view factor and energy balance of a surface, the SVF is widely used in studies in urban climatology (Oke 1987), biometeorology (Watson and Johnson 1988), forest climatology (Chen et al. 1991, Hale and Edwards 2002), archaeology (Kokalj et al. 2011), transport meteorology (Chapman and Thornes 2006), research on renewable energy sources (Rakovec and Zakžek 2013), urban planning (Lin et al. 2010), etc.
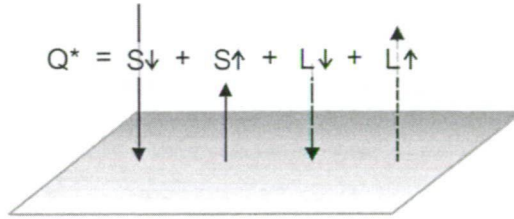
Fig. 1 Radiation budget of an "ideal" site. $Q*$ = net radiation budget, $S\downarrow$ = incoming short wave radiation (direct solar and diffuse), $S\uparrow$ = outgoing short wave radiation (reflection), $L\downarrow$ = incoming long wave radiation (atmospheric downward-radiation), $L\uparrow$ =outgoing long wave radiation (emission of solid surfaces)
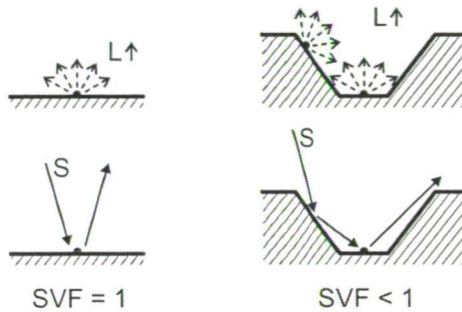

Fig. 2 Influence of horizontal (left) and convoluted (right) surfaces with accordingly different SVF values on radiation fluxes. L = long wave radiation, S = short wave radiation. (after Oke 1987)

Another definition of the sky view factor is based on radiation geometry: A view factor in general is "a geometric ratio that expresses the fraction of the radiation output from one surface that is intercepted by another. It is a dimensionless number between zero and unity" (Oke 1987). Thus the sky view factor is the geometric ratio that expresses the fraction of the radiation output from the sky that is intercepted by a surface. In this way of defining the SVF, the radiation fluxes between two-dimensional surfaces are crucial parts and thus the cosine law of Lambert has to be taken into account:

$$I = I_0 \cos(\Theta) \qquad (1)$$

where I is the energy actually received at the observed location, I_0 is the energy of the original beam and Θ is the angle between the surface's normal (n, see Fig. 3) and the incoming beam. Depending on Θ, the area of interest receives thus more or less of the incoming radiation. Fig. 3 illustrates three exemplary cases and indicates the corresponding factor $\cos(\Theta)$.

The application of Lambert's cosine law can also be interpreted as a weighting factor for radiation emitted by the surroundings of a certain location. If e.g. in the middle picture of Fig. 3 radiation is emitted by an object situated 30° above ground, half of the radiation flux is received at the point of interest. The extreme case would be that radiation emitted from an object which is at the same level as the point of interest, the radiation passes by and no radiation at all is received (Fig. 3 right).
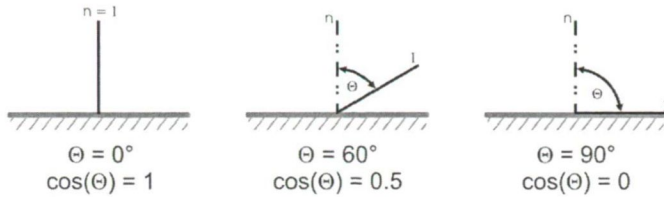
Fig. 3 Zenith angle (Θ) and the corresponding factor $\cos(\Theta)$. n = surface normal, I = beam of incoming radiation

In order to get a basis for calculating the total radiation received at a certain point, the surrounding radiation sources are commonly projected onto a hemisphere which is centred at the analyzed area (Fig. 4). The angle Θ can now be described as zenith angle.
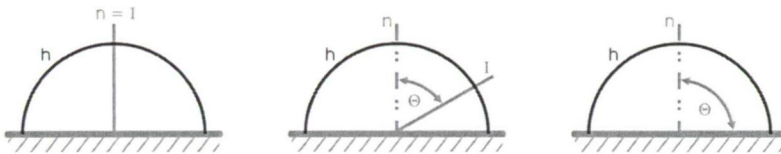

Fig. 4 Same as Fig. 3 but with a hemisphere (h) placed over the analyzed area
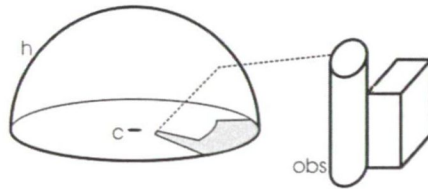
Fig. 5 Principle of projecting surroundings onto a hemisphere's (h) underlying circle. c = analyzed location in the center of the hemisphere's great circle, obs = obstacles in the perimeter obstructing the sky, grey = projection of the obstacle onto the great circle

When the radiating environment's shapes on the hemisphere are further projected onto the hemisphere's underlying circle, the result is a circular image. Fig. 5 shows a draft of a hypothetic set of buildings and their projection onto a circular picture. The analyzed location is marked with a "c", the overlying hemisphere with "h", obstacles with "obs" (Fig. 5). The path of the projection, first onto the hemisphere and then onto the hemisphere's great circle, is represented by the dashed line. As Fig. 5 is only intended to show the principle, the projection path, the shape of the projection etc. are not geometrically correct. It can be seen that the projection path breaks on the hemisphere. This break depends on and changes with the projection (e.g. equidistant, orthographic, equisolid angle) and will be ignored in the following text in order to keep the focus on the zenith angle. As the following deals with a geometrically distorted zenith angle, it will be shown as Θ'.

If one changes from an inclined view of Fig. 5 to a view vertically above the same scene, the result is (again not geometrically correct and only illustrating the principle) shown in Fig. 6.
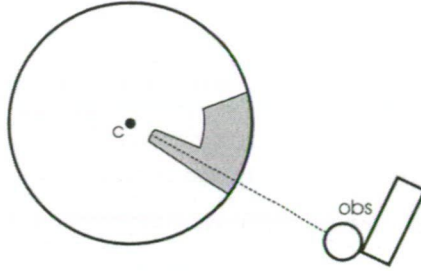
Fig. 6 Same as Fig. 5 but with a view hovering over the scene

An example image is shown in Fig 7. It was taken with fish eye lens (Nikon FC-E8) mounted on a Nikon Coolpix 4500 digital camera facing upwards.
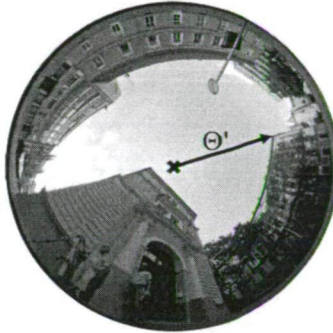
Fig. 7 Example of a fish eye photograph. x = center of the image, arrow and Θ' = distance between image's center and obstacle

Regarding this depiction of the radiating environment, the angle Θ' basically represents the distance between the image centre (in Fig. 7 marked with a black cross) and an emitting object (in Fig. 7 exemplarily the roof's corner at which the black arrow points). Integrating the edges of radiating objects, i.e. integrating the sky line both around the circle and all over the zenith finally leads to the sky view factor as a parameter representing the radiating environment.

The objectives of this paper are to show connections between the sky view factor and Lambert's cosine law as well as to point at potential biases coming with the application of the cosine law in SVF-related calculations depending on the geometry of the analyzed point or area of interest.

2. METHODS

While evaluating the SVF for a set of pictures like the one shown in Fig. 7 as well as calculating the corresponding SVF with models using 3D databases, it was found that the SVF values differ significantly between two groups of methods and models (Hämmerle et al. 2011a). In the present study, the fish eye images were evaluated using the following methods.

Manual method according to Steyn (1980): The fish eye images were printed with an overlaying polar grid. On the print, the obstructed areas were manually delineated. Based on the delineation, the obstructed angle of each annulus was estimated and then used to calculate the sky view factor according to the formula given in Steyn (1980).

Steyn-method implemented in an ArcView Avenue-Script. The workflow is basically the same as above but the tasks are completely done on screen. The pictures do not have to be printed and delineation of the obstacles is done by digitizing the obstacle's shapes in a GIS (Hämmerle et al. 2011b).

RayMan-model (Matzarkis et al. 2007): This model includes the "Edit free sky view factor"-tool which calculates the SVF from fish eye pictures or any other circular images with distinct obstacles. In order to determine the SVF on the basis of a fish eye picture, the image is loaded into the "Edit free sky view factor"-tool. After that, the obstacles are digitized on screen. The tool then counts the sky pixels and relates them to the overall number of pixels in the image. As an alternative to fish eye images taken with a digital camera, obstacle files can be loaded into the tool. A fish eye image is then produced which can also be used for deriving the sky view factor of the scenery modelled in the obstacle file.

BMSkyView (Rzepa and Gromek 2006): This software selects sky pixels according to their similarity in color. Sky pixels are selected manually and then, depending on the chosen threshold, all similar pixels in the image are classified also as sky. Misclassifications (caused e.g. by reflecting windows) are corrected manually. The selected sky pixels finally form the basis for calculating the SVF via the formula in Steyn (1980).

The SVF values presented in the results of this study were calculated by the following software methods. For the input of these software we used a 3D building data base of Szeged, southern Hungary, as described in Unger (2006).

SkyHelios (Matzarakis and Matuschek 2010): This model calculates the SVF for a whole area. In SkyHelios, obstacle-files as well as shape-files can be loaded. Using the computer's video card, fish eye images are produced for each point in the area of interest. Based on the fish eye images, the SVF is calculated for each point. The result is a set of equally distant points with an SVF-value generated for each point.

ArcView SVF-Extension (Gál et al. 2009): This script was developed in the proprietary Avenue script language which is implemented in ESRI ArcView. The script works with a shape file containing the footprints and heights of buildings. From each point of interest, the horizon is scanned for obstacles, i.e. buildings. If an obstacle is hit, its elevation angle is calculated based on the height data read from the data base. The SVF is calculated for the same points based on the highest elevation angle in each direction. The highest obstacle in the scanned direction is taken for SVF-calculation. The scanning range and angular step width can be selected depending on the available computing power and time.

The SOLWEIG-model (Lindberg et al. 2008) based on a shadow casting algorithm as described in Ratti and Richens (1999). A virtual hemisphere, equipped with light sources, is placed over each point of interest. A DSM containing the obstacles is loaded into the model, partially obstructing the hemisphere. The value of the SVF is calculated based on the number of obstructed light sources.

As the original shape files of the 3D building data base cannot be processed directly with RayMan, the shape file had to be converted to the obstacle file format of RayMan before calculating. The footprints of the buildings in the obstacle file have to be convex quadrilateral.

For the conversion a script is developed using ArcView GIS system's built-in object-oriented script language (Avenue). The script uses the fact that all of the polygons can be split into triangles using the rule that triangles have to be convex. The script divides the buildings' polygons within a user defined distance from a selected centre point iterative into triangles. The result is stored in a text file which satisfies the criteria of the obstacle file format. The maximum number of iterations can be changed before the calculation, because the conversion of the more complex polygon shapes in some cases needs a higher number of runs. After splitting the polygons, a new vertex is inserted into the longest side of each triangle in order to meet the expectations of the obstacle file format. The building's relative height is calculated using the elevation of the top of the building and the elevation of the center point of the area. The output of the script can be used directly as input for the RayMan model. Vegetation can also be converted by this script. This Avenue-script and additionally, a Python plug-in for QGIS are freely available and is available from the authors on request.

Fig. 8 shows a resulting obstacle file loaded in RayMan. The obstacle file shown in Fig. 8 contains all buildings within an area of 400 x 400 m and the point of interest as centre point. The centre of the scene in Fig. 8, where the line S-N and E-W cross, corresponds to point 3033 of the transect through an urban neighbourhood that is analysed in this study.
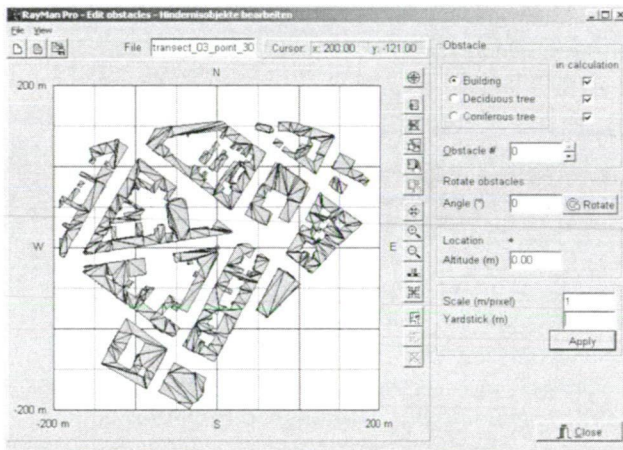
Fig. 8 RayMan Pro-interface showing an obstacle-file derived from a shape-file.
Red point: analyzed point, grey: surrounding buildings in obs-format

3. EXEMPLARY RESULTS

Fig. 9 gives as an example the development of the SVF-values along a straight transect of 19 equidistant points (0.5 m) within an urban setting (for more details see Hämmerle et al. 2011a). The images were taken from ground level on a y-shaped intersection of three streets with a Nikon Coolpix 4500 digital camera and a Nikon Fisheye Converter FC-E8 0.21x mounted on a Gorillapod original tripod supplementary equipped with a bubble level. The surrounding buildings are up to 15 meters high except one building of some 30 meters north-east of the transect. Vegetation in leaf-on phase was covering the sky only to a very small

part and was manually eliminated in the models using fish-eye pictures. Fig. 7 corresponds to point 3033 in the given diagram.

Sky view factor values with / without Lambert's cosine law
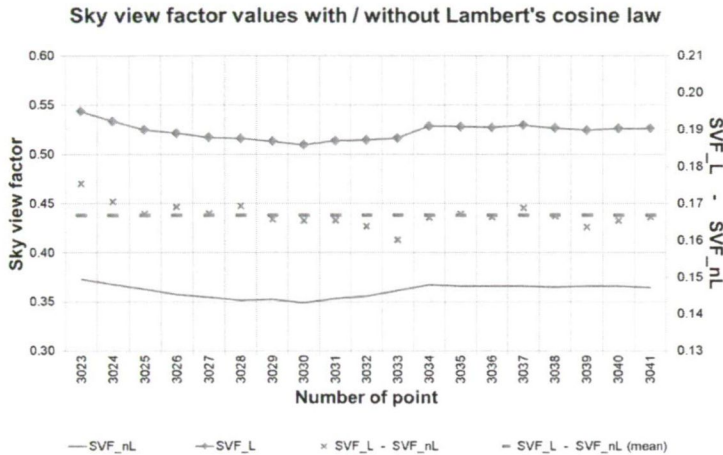
Fig. 9 SVF-values along an urban canyon, calculated with different methods. X-axis: single points of transect, left y-axis: SVF for each point, right y-axis: difference between SVF-values derived from models with applied cosine-law (SVF_L-line) and SVF-values derived from models without Lambert's law (SVF_nL-line). Crosses: Difference SVF_L - SVF_nL for each point, dashed line: mean of all differences

The different SVF-values turned out to be influenced by taking into account Lambert's cosine-law or not (Hämmerle et al. 2011a). In Fig. 9, the lower line (SVF_nL, for "SVF no Lambert") shows the mean SVF-value coming from three methods: RayMan, SkyHelios with vector input, SkyHelios with raster input. The upper line (SVF_L) includes all seven used methods and shows again the mean SVF of the seven values. This time, Lambert's cosine law was applied by RayMan and SkyHelios. The difference between the lower and upper line (i. e. SVF_L – SVF_nL) for each point is marked with an "x" in the diagram. The dashed line shows the average of all differences.

The reason for the higher SVF-values when applying Lambert's cosine law is to be found in the strong emphasis of the area around the zenith or respectively the lower weight of objects obstructing the sky at the horizon. Illustrating this dependence, fig. 10 shows the sky view factor for different heights over point 3033 (corresponding fish eye picture in Fig. 7). On the basis of the 3D building data base as described in Gál et al. (2009) the SVF was calculated in steps of 0.25 Meters from ground level to 25 Meters above ground. One calculation was done in ArcView using the ArcView SVF-Extension (Gál et al. 2009), two other runs were made with RayMan (Matzarakis et al. 2007).

The results of the three SVF-calculations for different heights on and above point 3033 are shown in Fig. 10.

The left curve in Fig. 10 (RayMan-weight) shows the SVF-values for the RayMan-calculation without the weight according to Lambert's cosine-law. The other two curves (RayMan+weight, ArcView+weight) result from SVF-calculations which apply the cosine-weighting. In all the three cases, especially in the first 15 meters of the vertical transect, the sky view factor is lower. At the height of about 15 meters the sky starts to open and

accordingly the SVF increases. After emerging from the street canyon only a few higher buildings obstruct the sky but they appear very low on the horizon. Fig. 11 shows a sequence of 5 fish eye images generated with RayMan for five different heights. The sun path in the fish eye images is inserted automatically by RayMan but are not of interest for this study.
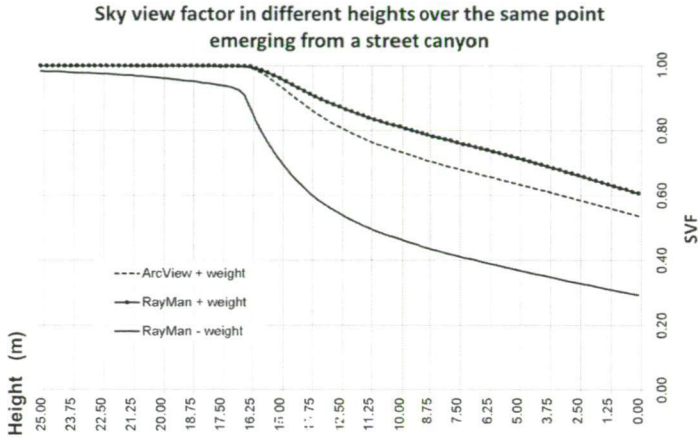
Fig. 10 SVF-values for successive heights above a fixed point, calculated with different methods. Y-axis: height of SVF-calculation, x-axis: SVF-range, solid line: SVF-value at different heights calculated with RayMan not applying the cosine-law, dashed line and solid line with points: SVF-value at different heights calculated with RayMan and ArcView with applied cosine-law
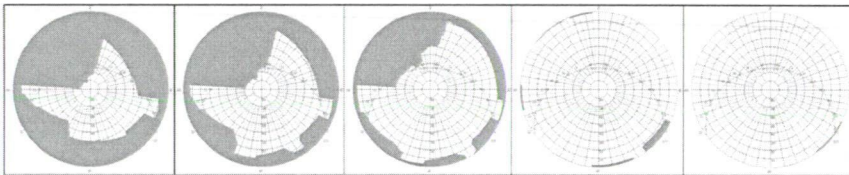
Fig. 11 RayMan-generated fish eye pictures for the same position but with different heights (left to right: 0.00 m, 6.25 m, 12.50 m, 18.75 m, 25.00 m). Grey: surrounding buildings, polar diagram: indicating open sky, red line: sun path

The SVF-values for the heights above 15 meters emphasize the different weighting of objects obstructing the lower parts of the horizon (Figs. 10 and 11). If Lambert's cosine law is not applied (left curve in Fig. 10), the still obstructing buildings are taken into account and a SVF of 1 is not reached. On the other hand, weighting the objects according to Lambert's Law leads to a sky view factor of 1 starting from about 16 meters height (central and right curves in Fig. 10).

3. DISCUSSION

The question comes up why in some models the cosine-law was included and why not in others. The reason most likely lies in the way of defining the area of interest: As long as a point or a two-dimensional area like a square is regarded, Lambert's law can be applied

without restrains. But what happens if a 3D object like a person is placed in a radiating environment and the radiation received by this object is of central interest? Fig. 12 illustrates this case by simply putting a cylinder (representing approximately the shape of e.g. a person as proposed in Johnson and Watson 1984, Höppe 1984) into Fig 4.
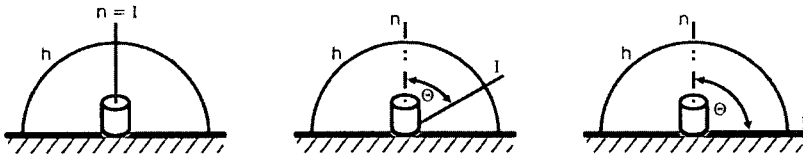
Fig. 12 Cosine-weighting and its influence on radiation received by a solid object (same as fig. 4 but with an object placed in the hemisphere's center)

If Lambert's cosine law is applied here in the standard way, all fluxes received by non-horizontal areas are calculated as too low. In case of radiation parallel to the horizon (right part of Fig. 3) the object would not receive any radiation at all if the cosine-weighting is applied because of $\Theta = 90°$.

Thus it seems necessary to discuss the definition of the sky view factor depending on the aim of an analysis: Is the point of interest a flat area or is it an object whose radiation fluxes are of central concern? Should there accordingly be defined a SVF_{2D} which includes Lambert's cosine-law and on the other hand a SVF_{3D} with an adaption of the weighting appropriate for solid objects? How could a comprehensive implementation be found of the extremely complex matter of how to weight all radiation fluxes received by a 3D object and the surfaces it consists of? How to deal with different wave-lengths, the distinction between direct and diffuse short wave radiation and the different components of the radiation budget? How to include the sun path in connection with the date and latitude of the point or object of interest?

3. CONCLUSION

In this paper the cosine law according to Lambert was introduced and connected to hemispherical photography and the sky view factor. It was found that with different settings the application of Lambert's cosine law can lead to different results. The question came up whether Lambert's cosine law should be applied or not depending on the type of the analyzed area or object. In case a study deals with a flat area, the cosine law seems according to our results straightforward and offers an established way of taking angle-dependent radiation fluxes into account. On the other hand in case the study deals with solid three-dimensional objects, the application of Lambert's cosine law may lead to biased results. The question of introducing two types of SVF, one for a 2D-setting, the other for a 3D-setting, should be discussed intensively in order to improve the quality and reliability of studies in all concerned research in e.g. urban climatology and in the various branches of biometeorology.

REFERENCES

Chapman L, Thornes JE (2006) A geomatics based road surface temperature prediction model. Sci Total Environ 360:68-80

Chen JM, Black AT, Adams RS (1991) Evaluation of hemispherical photography for determining plant area index and geometry of a forest stand. Agr Forest and Meteorol 56:129-143

Gál T, Lindberg F, Unger J (2009) Computing continuous sky view factors using 3D urban raster and vector databases: comparison and application to urban climate. Theor Appl Climatol 95:111-123

Hala SE, Edwards C (2011) Comparison of film and digital hemispherical photography aross a wide range of canopy densities. Agr Forest and Meteorol 112:51-56

Hämmerle M, Gál T, Unger J, Matzarakis A (2011a) Comparison of models calculating the sky view factor for urban climate investigations. Theor Appl Climatol, 105:521-527

Hämmerle M, Gál T, Unger J, Matzarakis A (2011b) Introducing a script for calculating the sky view factor used for urban climate investigations. Acta Climatologica et Chorologica Univ Szegediensis, 44-45:83-92

Höppe P (1984) Die Energiebilanz des Menschen. Wiss Mitt Met Inst Univ München, München

Johnson GT, Watson ID (1984) Person view-factors in the urban environment. Arch Meteor Geophy B 34:273-285

Kokalj Ž, Zakšek K, Oštir K (2011) Application of sky-view factor for the visualisation of historic landscape features in lidar-derived relief models. Antiquity 85:263-273

Lin TP, Matzarakis A, Hwang RL (2010) Shading effect on long-term outdoor thermal comfort. Build Environ, 45:213-221

Lindberg F, Thorsson S, Holmer B (2008) SOLWEIG 1.0 - Modelling spatial variations of 3D radiant fluxes and mean radiant temperature in complex urban settings. Int J Biometeorol 52:697-713

Matzarakis A, Matuschek O (2010) Sky view factor as a parameter in applied climatology – rapid estimation by the SkyHelios model. Meteorol Z 20:39-45

Matzarakis A, Rutz F, Mayer H (2007) Modeling radiation fluxes in simple and complex environments - application of the RayMan model. Int J Biometeorol 51:323-334

Oke TR (1981) Canyon geometry and the nocturnal urban heat island. Comparison of scale model and field observations. J Climatol 1:237-254

Oke TR (1987) Boundary layer climates. Methuen, London

Rakovec J, Zakžek K (2013) On the proper analytical expression for the sky-view factor and the diffuse irradiation of a slope for an isotropic sky. Renew Energ 37:440-444

Ratti C, Richens P (1999) Urban texture analysis with image processing techniques. In: Augenbroe G, Eastman Ch (eds) Proceed 8th Int Confon Computer Aided Architectural Design Futures held in Atlanta, Georgia

Rzepa M, Gromek B (2006) Variability of sky view factor in the main street canyon in the center of Łódź. Preprints Sixth Int Conf on Urban Climate, Göteborg, Sweden. 854-857

Steyn DG (1980) The calculation of view factors from fisheye-lens photographs. Atmos Ocean 18:245-258

Unger J (2004) Intra-urban relationship between surface geometry and urban heat island: review and new approach. Climate Res 27:253-264

Watson ID, Johnson GT (1988) Estimating person view-factors from fish-eye lens photographs. Int J Biometeorol 32:123-128

INVESTIGATION OF CARBON SEQUESTRATION PROCESSES OF RECONSTRUCTED GRASSLANDS AND WETLANDS TO AID ECOSYSTEM SERVICE-BASED DECISION MAKING

M KISS[1], Z NÉMETH[2], I BÁRÁNY-KEVEI[1] and S CZÓBEL[2]

[1]Department of Climatology and Landscape Ecology, University of Szeged, P.O.Box 653, 6701 Szeged, Hungary
[2]Department of Nature Conservation and Landscape Ecology, Szent István University, Páter K. str 1, 2100 Gödöllő, Hungary
E-mail: kiss.marton@geo.u-szeged.hu

Summary: In this paper, we analysed the effect of habitat reconstructions on some parameters characterizing the carbon exchange processes of ecosystems. Besides extending our knowledge on the ecophysiological functioning of different plant communities, our work was motivated by international policy goals as well: a considerable amount of degraded ecosystems and their services was declared in the European Union to be reconstructed in the next few years. These kinds of projects need detailed impact analyses and a methodological grounding. We would like to contribute to these goals with the results of field measurements carried out in an extensive habitat reconstruction area in the Egyek-Pusztakócs habitat complex (Hortobágy National Park, Eastern Hungary). In this paper, we analysed the results of carbon and nitrogen contents of soils and biomass samples and the average net ecosystem exchange values of the investigated ecosystem types. Our results show that natural or near-natural, well-structured grasslands have an outstanding carbon sequestration and storing potential in the studied landscape type, the restored grasslands lag behind in every parameters. In the process of secondary succession, the carbon exchange characteristics of the restored grasslands seem to follow mainly the species composition, and the effects of land management can modify the effects of regeneration from the point of view of ecophysiological functioning.

Key words: wetland, grassland, arable land, carbon sequestration, habitat reconstruction

1. INTRODUCTION

Mapping ecosystem services and related spatial assessments may be prerequisites of land use decisions on different spatial scales. Maps of ecosystem funcions and service supply give an overview of the general state of the natural capital of the different sites, while the bundles and tradeoffs between them make the evaluation of land use management alternatives possible. Owing to the many contributions of the recent years, the number of spatial assessment approaches is growing rapidly in this field. These works are necessary also for the methodological grounding of the fulfilment of international policy objectives (implementing the targets of the EU Biodiversity Strategy 2020 on mapping ecosystem services on a national scale and developing Green Infrastructure).

The sequestration and storage of greenhouse gases (mainly of carbon) is one of the most widely recognized and studied regulating ecosystem services. As it has a global relevance, it does not affect the people's well-being directly, but in the context of climate change, it has a clear importance and it can be quantified relatively easily. Thus, there are many experiences of the mapping, modelling and sometimes monetary evaluation of this

service (Nelson et al. 2009, Crossman et al. 2011). According to the general groups of ecosystem service mapping methods, mapping approaches of carbon sequestration and storage can also be classified as land cover-based assessments, indicator mapping and spatial modelling.

In the next years and decades, huge territories with degraded habitats will be reconstructed for nature protection reasons. This is a consequence partly of the abandonment of cultivated lands following changes in agricultural policy, of the strengthening of the nature conservation sector, and of direct policy goals (restoration of 15% of degraded ecosystems is prescribed in the EU Biodiversity Strategy 2020). In many cases, the declared aim of habitat reconstruction projects is restoring and increasing the amount of ecosystem services of the study area. It means that it is supposed that there is a clear positive correlation between biodiversity (of which the increase is the direct target of habitat reconstruction projects) and ecosystem services. However these connections (which were discussed as biodiversity-ecosystem function relationships in the literature previously) are not that straightforward, and they should be clarified in some aspects (and it should be investigated and evaluated differentially for the different functions/services). The different ecosystem functions may be connected to certain species or species groups, and the relationships highly depend on the spatial and temporal extent of the investigations (Isbell et al. 2011). Grasslands of different structure and species composition can be studied relatively easily from the point of view of carbon sequestration (which was the main issue in our work) through biomass production and changes in the carbon content of soils (Tilman et al. 2001, Steinbeiss et al. 2008). Another important aspect that should be taken into consideration if we evaluate effects of habitat reconstructions on ecosystem functions and services is the fact that reconstructed communities achieve the targeted state concerning species composition and other important ecological attributes only in the long run. In the case of some weakly regenerating communities, total regeneration cannot be achieved at all. There are a number of studies on the effects of habitat and landscape reconstruction projects on ecosystem functions and services, on different spatial scales (Benayas et al. 2009, Feng et al. 2013). Among these, we can also find investigations of greenhouse gas exchange processes of planted grasslands (Nelson et al. 2008, De Deyn et al. 2011), and budgets dealing with more than one GHG, based on complex flux measurements (Merbold et al. 2014). In most of these works, detailed investigation of the regeneration process was not among the targets. Thus, our field measurements were carried out in order to answer this central problem.

These results, besides providing a valuable input for more detailed ecological-ecophysiological impact assessment of habitat reconstructions, may help in adequately parameterizing different parts of the complex system of sequestering carbon (or other greenhouse gases) in integrated ecosystem service evaluation systems (Kiss et al. 2013) or spatial models. If we derive indicators or proxy values for mapping ecosystem services, it should be taken into consideration that the service supply is highly dependent on the variability of several natural factors (e.g. weather) and on land management intensity (Cseh et al. 2014). Some of the spatial models for ecosystem service assessments developed in recent years were made with the explicit inclusion of land management intensity, on different spatial scales (Petz and van Oudenhoven 2012, Schulp et al. 2012). Greenhouse gas exchange processes of grasslands, arable lands and wetlands are a good example of that, as different abiotic parameters and different forms of agricultural land use, which can be distinguished from the point of view of management intensity (intensive or extensive arable farming, different forms of grazing) affect the greenhouse gas budget heavily. Referring investigations

were carried in Hungary as well, in the frame of Greengrass project (Czóbel et al. 2008b, 2012, 2013, Horváth et al. 2008, 2010). Based on that, the aim of our work was to study the intra-annual variability of some important attributes of carbon exchange processes in the investigated habitats. We also give some proposals on the usability of these results and those of previous related Hungarian projects in evaluating the effects of large-scale land use change projects with targeted indicators and evaluation systems.

2. MATERIAL AND METHODS

2.1. Description of the study area

The study area of our work was the Egyek-Pusztakócs habitat complex in Hortobágy National Park (situated in Eastern Hungary), on the borderline region of two landscapes, the Hortobágy and the Tiszafüred-Kunhegyes plain. A large-scale wetland rehabilitation was carried out there during a long-term programme from 1976 to 1997, while between 2004 and 2007, the largest grassland reconstruction project of Europe was implemented (Vida et al. 2010, Török et al. 2011, Lengyel et al. 2012), financed by the LIFE programme of the European Union (on 760 hectares in total). The targeted habitat types of the reconstructions were mainly loess and alkali grasslands, for which reference undisturbed stands are also available in the Egyek-Pusztakócs unit and in the wider area. Besides these, arable lands with different management intensity and wetlands (rehabilitated mainly in the frame of the previously mentioned landscape reconstruction programme) can also be found in the study area. These habitats formed the measurement units of our work, which were compared from the point of view of greenhouse gas exchange processes. The study area is part of the floodplain of the Tisza River. This fact determines the morphological characteristics and, through that, the natural vegetation patterns. As this area is situated west from the „classical" Hortobágy region (a part of it is in another landscape), the morphological variability is higher than in most parts of the National Park. In deeper areas (in former riverbanks and floodplain marshes), wetlands with different inundation lengths can be found, while on positive morphological forms (alluvial plateus), the main natural habitats are dry grasslands. These were intended to be reconstructed in the frame of the LIFE project, with low-diversity seed mixtures. Our measurement points were situated in different-aged reconstructed grasslands (planted in 2005 and 2008), one almost undisturbed natural grassland site, one extensively and one intensively managed arable land as reference stands to characterize the former land use of the reconstructed habitats, and 3 points from a lakeside zonation of a rehabilitated marsh system (Fig. 1).

2.2. Methods

In this paper, we examine net ecosystem CO_2 exchange (NEE), carbon and nitrogen content of soil and vegetation from the attributes describing the ecosystems' carbon budget. Our measurements were carried out monthly in the vegetation period of the year 2011. CO_2 fluxes were measured from grassland (natural grassland, restored in 2005 and 2008), wetland (*Lemna, Juncus* and *Eleocharis* dominated stands) and arable land (extensively and intensively managed) sites. Stand level CO_2 flux measurements (NEE) were performed at monthly intervals during the growing period using chamber technique and ADC LCA2 (ADC Bioscientific, UK) portable infrared gas-analyser operated in open system mode. The

photosynthetic system was connected to a water clean, portable, non-destructive, self-developed chamber (d=60 cm, made from plexiglass) taking air samples from the connecting (inner and outer) tubes (Czóbel et al. 2004). Carbon dioxide exchange rate has been calculated from the differences or changes in CO_2 concentrations (for more details, see Czóbel et al. 2004, 2005). Stand level chamber measurements were carried out in clear and sunny days between 10:00 and 16:00 in order to avoid the unsteady meteorological paramereters affecting the NEE values. On a peculiar NEE measurement day the carbon flux of each site were measured alternately for an average of 60 min per plot. The mean and standard deviation of the data collected were calculated for each plot. The C and N contents of the soils were measured in two samples (from layers of 0-10 and 10-30 cm) in every measurement points. Soil and water samples were measured once in the first intensive growing phase of the vegetation period, while the biomass was sampled at the end of the vegetation period as well. The C and N content measurements were carried out, after drying till a constant mass state, with Elementar Vario Max CN device, using methods developed for the specific sample types, the positive control was glutamic acid. Water samples were collected from *Eleocharis* and *Juncus* stands measured with Apollo 9000 TOC analysator, by 5 point calibration, using potassium nitrate and calcium carbonate as positive control.
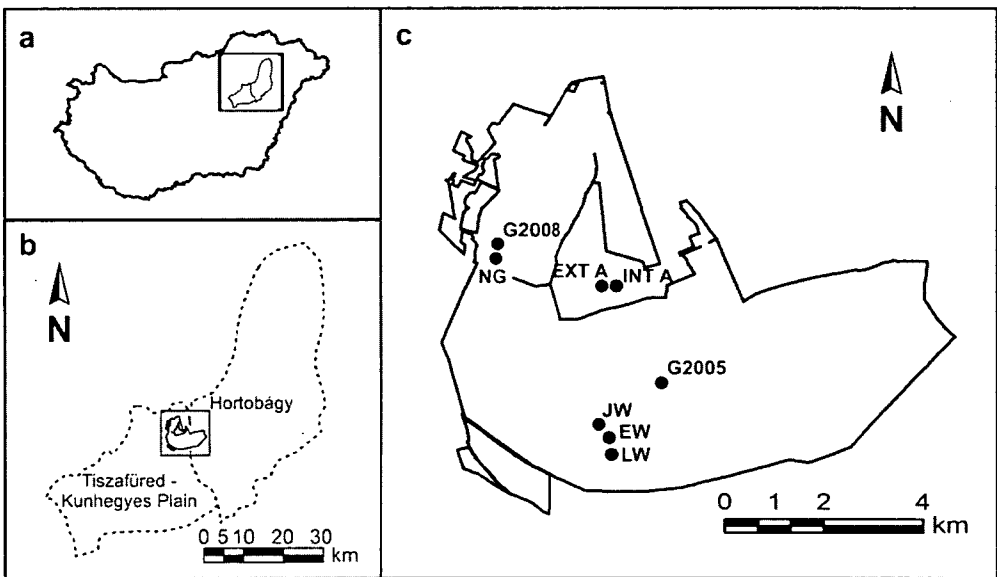
Fig. 1 Location of the two landscapes containing the Egyek-Pusztakócs unit of the Hortobágy National Park in Hungary (a), the habitat complex (b) and the sampling points (c) (G2005: grassland reconstructed in 2005, G2008: grassland reconstructed in 2008, NG: natural grassland, INT A: intensively managed arable land, EXT A: extensively managed arable land, LW: *Lemna*-dominated wetland, EW: *Eleocharis*-dominated wetland, JW: *Juncus*-dominated wetland)

3. RESULTS AND DISCUSSION

The total carbon contents of the two soil layers were considerably low, and the upper layers were observed to be higher at all of the samples (Fig. 2). From the grassland points,

the highest C content was measured in the upper layer of the natural grassland, the earlier restored grassland's value was a bit lower (5.4%), and the later restored grassland was much lower (56.7%). The intensive arable land was characterized with higher values in both layers than the extensive arable land (lower layer. 23.5%, upper layer: 13.7%), this is certainly due to fertilizer application. Concerning the total N content of the soils, the ratios between the investigated habitat types are similar, we measured higher N content in the lower layer in two cases (in the grassland restored later and in the extensive arable land). The high C content of the natural grassland calls attention to the high carbon storing potential of these well-structured grasslands with low anthropogenic disturbance. The high C and N content in the soils of the earlier restored grassland can be probably explained by the fact that this is under a considerably intensive grazing, which causes notable increase in these parameters according to the results of previous Hungarian measurements as well (Czóbel et al. 2008a). Another cause can be that the carbon content of the biomass is lower there than in the case of the other grasslands. The plants can affect the soil carbon content through the nitrogen exchange: under vegetation types providing litter with lower C/N ratio the microbial activity can be stronger and the amount of the available nitrogen can increase. This can enhance productivity and the amount of carbon as an input to the soil (Ogle et al. 2004). However the regeneration process that can be characterized with constant organic material input and the exclusion of tillage operations probably contributes to the high soil carbon content of the grassland restored earlier. It should be stated that in the case of most grassland types, to achieve a soil carbon content equal or close to the reference natural grassland, several decades are needed (McLauchlan et al. 2006). In element contents, the values of *Eleocharis* stands were observed to be many times higher (C: 114.08 g l^{-1}), N: 70.24 g l^{-1}) than those of *Juncus* stands (C: 4.78 g l^{-1}, N: 2.22 g l^{-1}).
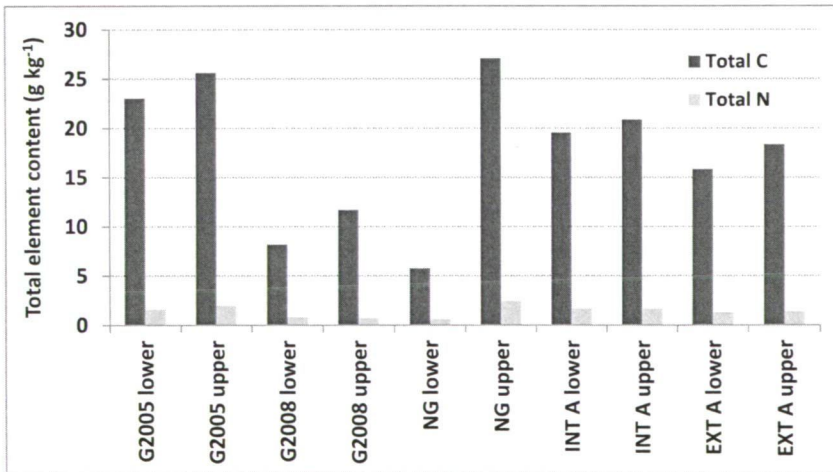
Fig. 2 Carbon content of soils in the grassland and arable land sampling points

We observed lower variability in the element contents of the biomass samples during the year. The value measured in autumn was higher than that measured in spring in the case of the natural grassland. The C content was almost the same at the two arable lands, and clearly higher element contents were measured in autumn in the wetland's samples. A possible explanation can be that in the extremely dry year of 2011, the plants survived the

summer period with strong precipitation deficit by allocating C to the above-ground parts. In the case of N content, the ratios between the investigated types were almost the same in the samples collected in spring and autumn, but the intra-annual variability was higher. The increased N content of the grassland restored earlier (compared to the other grasslands) is probably partly a consequence of grazing, which caused the higher N content of the aboveground biomass (Czóbel 2008a).

Table 1 Carbon contents of aboveground biomass samples

	Spring			Autumn		
	TC (g kg^{-1})	TN (g kg^{-1})	C/N ratio	TC (g kg^{-1})	TN (g kg^{-1})	C/N ratio
G 2005	415.9	16.8	24.8	402.9	20.7	19.5
G 2008	436.1	7.8	55.7	431.5	15.8	27.3
NG	427.9	13.9	30.9	440.8	16.4	26.8
INT A	407.7	15.7	26.0	408.5	32.7	12.5
EXT A	406.7	6.4	63.3	412.5	24.8	16.6
LW	289.9	21.6	13.4	416.3	36.3	11.5
EW	386.2	24.4	15.8	398.0	24.0	16.6
JW	407.3	18.9	21.6	428.5	13.4	31.9

We measured the lowest CO_2 uptake values on the arable lands, and the highest ones on wetland points. The three investigated grasslands' average carbon fixation was higher (with 10.6%) than the average value of the two arable lands. The wetlands sequester more than grasslands with one fifth (18.6%) and than arable lands with one third (31.1%) on average. The CO_2 uptake value was lower on the grassland restored in 2005 than that of the one restored in 2008. The higher CO_2 fixation value (with 21.2%) of the latter one is presumably caused by the greater amount of biomass of r-strategist weed species that are present in a high density after the restoration activities (in the first phase of the secondary succession). This is underlined by our aboveground biomass measurements as well. The natural grassland that was not affected by the habitat reconstruction, sequestered more C (with 14.8%) than the regenerating grassland type characterized with the highest CO_2 uptake values among the restored grasslands. The measurements carried out in the different grassland types show that the natural or near-natural grassland community has a very high carbon storing potential, which is above the potential of habitats in different stages of the succession.

The extensively managed arable land sequestered more (with 5.7%) carbon in the measurement period than the intensively managed type. All of the wetlands had higher CO_2 fixation values than the arable lands' values and also than the value of the grassland of 2005. The lowest sequestration values were measured in the *Juncus*-dominated stands, the *Lemna* stand was above it with 10,8%. The *Eleocharis*-dominated habitat's value was higher than it (with 40.6%), this had the highest CO_2 fixation of all of the investigated ecosystem types. The *Eleocharis* stand's potential was around twice as much (181%) as the grassland restored in 2005, which had the lowest values among the studied habitats.

3. CONCLUSIONS

From our results regarding the ecophysiological characteristics of the habitats, we highlight the following: the natural or semi-natural, well-structured grassland types have an

outstanding role in the stand-level CO_2 sequestration and in soil carbon storage as well. In the restored habitats, no clear tendency could be observed concerning the carbon budget in the short interval of some years after the reconstruction. The carbon content of the soil is highly affected by grazing intensity after the end of arable farming, and the net sequestration values do not change linearly after the restoration activities. In the first years after seed sowing, the spreading of weed-type species temporarily increase NEE values. This can be observed in the case of other ecosystem services too: Szabó (2012) provided results also from the monitoring of the Egyek-Pusztakócs LIFE project and pointed out that wild bees providing the service of crop pollination appear with highest diversity in new fallows characterized by a high number of plant species. The effects of secondary succession on carbon exchange clearly need further observations, possibly in more landscape types. Some of the models developed for mapping ecosystem services (Petz and van Oudenhoven 2012, Tallis et al. 2013) are suitable for incorporating land management intensity, though it is carried out by changing the parameterization of the carbon pools. Theoretically, it enables differentiating between land management alternatives (at the same land use form). It could be important in the light of the results above and our former studies (Czóbel et al. 2008a, 2008b, 2012, 2013) about the effects of land management on the ecophysiological characteristics of grasslands and other habitats. There are clear differences in element contents of different carbon pools as a consequence of management intensity, which can be considered in indicator-based assessments or modelling works. In impact assessments of the effects of habitat reconstructions on carbon sequestration or other ecosystem services with synbotanical-synphysiological aspects, the indicators or proxy values should be given based on measurements carried out possibly in a similar area, with regard on succession state, land management and its intensity.

REFERENCES

Benayas JMR, Newton AC, Diaz A, Bullock JM (2009) Enhancement of Biodiversity and Ecosystem Services by Ecological Restoration: A Meta-Analysis. Science 325:1121-1124

Crossman ND, Bryan BA, Summers DM (2011) Carbon payments and low-cost conservation. Conserv Biol 25:835-845

Cseh V, Kiss M, Tanács E (2014) Carbon sequestration of floodplain forests: a case study from Hungary, Maros river valley. Tiscia 40:3-10

Czóbel S, Balogh J, Fóti S, Péli ER, Szerdahelyi T, Szirmai O, Nagy Z, Tuba Z (2004) Long-term effects of irrigation and fertilization on stand CO_2 fluxes and soil biochemical processes in a Hungarian loess grassland. In: Hidvégi Sz, Gyuricza Cs (eds) Proc. III. Alps-Adria Scientific Workshop, Dubrovnik, Croatia. 130-134

Czóbel S, Fóti S, Balogh J, Nagy Z, Bartha S, Tuba Z (2005) Chamber series and space-scale analysis of CO_2 gas-exchange in grassland vegetation: A novel approach. Photosynthetica 43:267-272

Czóbel S, Balogh J, Fóti S, Szirmai O, Nagy Z (2008a) Temporal changes in biomass and soil element contents under different manipulations of temperate grasslands. Cereal Res Commun 36:1963-1966

Czóbel S, Szirmai O, Nagy J, Balogh J, Ürmös Z, Péli ER, Tuba Z (2008b) Effects of irrigation on the community composition, and carbon uptake in Pannonian loess grassland monoliths. Commun Ecol 9:91-96

Czóbel S, Szirmai O, Németh Z, Gyuricza Cs, Házi J, Tóth A, Schellemberger J, Vasa L, Penksza K (2012) Short-term effects of grazing exclusion on net ecosystem CO_2 exchange and net primary production in a Pannonian sandy grassland. Notulae Botanicae Horti Agrobotanici Cluj-Napoca 40:67-72

Czóbel S, Németh Z, Szirmai O, Gyuricza Cs, Tóth A, Házi J, Vikár D, Penksza K (2013) Short-term effects of extensive fertilization on community composition and carbon uptake in a Pannonian loess grassland. Photosynthetica 51:490-496

De Deyn GB, Shiel RS, Ostle NS, McNamara NP, Oakley S, Young I, Freeman C, Fenner M, Quirk H, Bardgett RD (2011) Additional carbon sequestration benefits of grassland diversity restoration. Journal of Appl Ecol 48:600-608

Feng X, Fu B, Lu N, Zeng Y, Wu B (2013) How ecological restoration alters ecosystem services: an analyis of carbon sequestration in China's Loess Plateau. Sci Rep 3:2846

Horváth L, Grosz B, Machon A, Balogh J, Pintér K, Czóbel S (2008) Influence of soil type on N_2O and CH_4 soil fluxes in Hungarian grasslands. Commun Ecol 9:75-80

Horváth L, Grosz B, Machon A, Tuba Z, Nagy Z, Czóbel S, Balogh J, Péli E, Fóti S, Weidinger T, Pintér K, Führer E (2010) Estimation of nitrous oxide emission from Hungarian semi-arid sandy and loess grasslands; effect of soil parameters, grazing, irrigation and use of fertilizer. Agr Ecosyst Environ 139:255-263

Isbell F, Calcagno V, Hector A, Connolly J, Harpole WS, Reich PB, Scherer-Lorenzen M, Schmid B, Tilman D, van Ruijven J, Weigelt A, Wilsey BJ, Zavaleta ES, Loreau M (2011) High plant diversity is needed to maintain ecosystem services. Nature 477:199–202

Kiss M, Gere C, Kiss M (2013) Basics of an integrated ecosystem service evaluation system for the Tisza River Basin. Rev Agr Rural Dev 2:314-319

Lengyel S, Varga K, Kosztyi B, Lontay L, Déri E, Török P, Tóthmérész B (2012) Grassland restoration to conserve landscape-level biodiversity: a synthesis of early results from a large-scale project. Appl Veg Sci 15:264-276

McLauchan KK, Hobbie SE, Post WM (2006) Conversion from agriculture to grassland builds soil organic matter on decadal timescales. Ecol Appl 16:143-153

Merbold L, Eugster W, Stieger J, Zahniser M, Nelson D, Buchmann N (2014) Greenhouse gas budget (CO_2, CH_4 and N_2O) of intensively managed grassland following restoration. Glob Change Biol, 10.1111/gcb.12518

Nelson JDJ, Schoenau JJ, Malhi SS (2008) Soil organic carbon changes and distribution in cultivated and restored grassland soils in Saskatchewan. Nutr Cycl Agroecosys 82:137-148

Nelson E, Mendoza G, Regetz J, Polasky S, Tallis H, Cameron DR, Chan KMA, Daily GC, Goldstein J, Kareiva PM, Lonsdorf E, Naidoo R, Ricketts TH, Shaw MR (2009) Modeling multiple ecosystem services, biodiversity conservation, commodity production, and tradeoffs at landscape scales. Front Ecol Environ 7:4-11

Ogle SM, Ojima D, Reiners WA .(2004) Modeling the impact of exotic annual brome grasses on soil organic carbon storage in a northern mixed-grass prairie. Biol Invas 6:365-377

Petz K, van Oudenhoven APE (2012) Modelling land management effect on ecosystem functions and services: a study in the Netherlands. Int J Biodivers Sci, Ecosyst Serv Manage 8:135-155

Schulp CJE, Alkemade R, Goldewijk KK, Petz K (2012) Mapping ecosystem functions and services in Eastern Europe using global-scale data sets. Int J Biodivers Sci, Ecosyst Serv Manage 8:156-168

Steinbeiss S, Bessler H, Engels C, Temperton VM, Buchmann N, Roscher C, Kreutziger Y, Baade J, Habekost M, Gleixner G (2008) Plant diversity positively affects short-term soil carbon storage in experimental grasslands. Glob Change Biol 14:2937-2949

Szabó G (2012) Az egyek-pusztakócsi gyeprekonstrukció hatása vadméhekre (Hymenoptera: Apoidea). [The effect of grassland reconstruction in Egyek-Pusztakócs on wild bee populations (Hymenotera: Apoidea) (in Hungarian)]. Természetvédelmi Közlemények 18:456-466

Tallis HT, Ricketts T, Guerry, AD, Wood SA, Sharp R, Nelson E, Ennaanay D, Wolny S, Olwero N, Vigerstol K, Pennington D, Mendoza G, Aukema J, Foster J, Forrest J, Cameron D, Arkema K, Lonsdorf E, Kennedy C, Verutes G, Kim CK, Guannel G, Papenfus M, Toft J, Marsik M, Bernhardt J, Griffin R, Glowinski K, Chaumont N, Perelman A, Lacayo M, Mandle L, Griffin R, Hamel P, Chaplin-Kramer R (2013) InVEST 2.6.0 User's Guide. The Natural Capital Project, Stanford

Tilman D, Reich PB, Knops J, Mielke T, Lehman C (2001) Diversity and productivity in a long-term grassland experiment. Science 294:843-845

Török P, Kelemen A, Valkó O, Deák B, Lukács B, Tóthmérész B. (2011) Lucerne-dominated fields recover native grass diversity without intensive management actions. J Appl Ecol 48:257-264

Vida E, Valkó O, Kelemen A, Török P, Deák B, Miglécz T, Lengyel S, Tóthmérész B. (2010) Early vegetation development after grassland restoration by sowing low-diversity seed mixtures in former sunflower and cereal fields. Acta Biologica Hungarica 61:246-255

FIRST RESULTS OF THE RADON CONCENTRATION MONITORING IN ABALIGET AND KISPAPLIKA CAVES

G KOLTAI[1,2,3], Z TEGZES[3] and E HÜLBER[4]

[1]*Department of Climatology and Landscape Ecology, University of Szeged, P.O.Box 653, 6701 Szeged, Hungary*
[2]*Current address: Department of Geology and Paleontology, University of Innsbruck, Innrain 54, 6020 Innsbruck, Austria*
[3]*Pro Natura Karst and Cave Research Group, 7634 Pécs, Magyarürögi út 8/4, Hungary*
[4]*Radosys Ktf, 1116 Budapest, Vegyész utca 17-25*
E-mail: Gabriella.Koltai@uibk.ac.at

Summary: Radon concentration has been investigated in Abaliget and Kispaplika caves, Mecsek Mountains, Hungary for 9 month. Track-etched detectors were used to measure the radon levels of cave air inside the passages. Our primary aim was to gain information about both the radon concentration levels and the convectional characteristics of these caves. Meteorological data provided by the Public Limited Company for Radioactive Waste Management was used to analyse the possible direction of airflow inside the caves. Both caves were characterized by higher summer and lower winter values and the changes of radon concentration were governed by the inside and outside temperature difference induced ventilation of the caves.

Key words: radon, track-etched detector, cave air circulation, Mecsek Mts.

1. INTRODUCTION

Radon (^{222}Rn) is usually present in the natural environment, since most natural materials contain uranium. Soils usually have 2-3 g t^{-1} of ^{238}U, therefore the radon level of pore-air varies from 7 to 220 kBq m^{-3} having a mean at 27 kBq m^{-3} (Hakl 1992). Due to the continuous mixing in the air column, the radon concentration of free air has a much lower range (0.001-0.1 kBq m^{-3}). In enclosed places radon can be significantly enriched due to the limited ventilation. The radon concentration of cave air ranges from 0.1 to 20 kBq m^{-3} around the world (Hakl et al. 1997). In Mecsek Mts. generally high radon values have been reported, exceeding the mean levels recorded in other Hungarian caves (Koltai et al. 2010).

As radon is an inert gas that has a 3.8-day half-life, it can easily diverge from its parent substance and therefore it can be used as an excellent tracer of underground airflow (Hakl 1997, Dezső and Molnár 2001). Since carbonate rocks are highly fractured radon transport measurements can be particularly useful in the microclimate studies of limestone caves (Hakl et al. 1997). The primary factors governing the migration of radon are temperature, humidity and rock porosity whereas air movements caused by temperature differences or rapid atmospheric pressure changes can have a secondary influence on it, as well (Papp et al. 2004).

The radon concentration of cave air was monitored in several small caves in Western Mecsek Mts. with the aim of studying the characteristics of cave air flow between 1992 and 2007 (Zalán 1998, Koltai et al. 2010, Koltai et al. 2012). Microclimate measurements in Abaliget Cave started in 1992 and were carried out for several years (Zalán 1995, Hakl et al.

1996, Várhegyi 1996). The temperature, relative humidity and radon concentration of cave air was continuously monitored at three different sites inside the cave. In Kispaplika Cave no radon measurement has been carried out before.

In the present paper we would like to summarize the preliminary results of the 9-month-long radon concentration monitoring done in Abaliget and Kispaplika caves.

2. MATERIALS AND METHODS

2.1. The study area

The geological structure of Western Mecsek is characterized by an anticlinal with an eastern-western line of strike. The rocks of the anticlinal are particularly stressed, fragmented and moved by faults (Barta and Tarnai 1999). In Western Mecsek karstic rocks geologically belong to one single block, however, on the surface they can be found in three different zones. The Abaliget and Kispaplika caves are located in the Abaliget-Mecsekrákos fracture and Misina in a 40 km^2 territory. The area is divided by the drainage basins of eight efflux caves.

The catchment areas of Abaliget and Kispaplika caves are 15.25 km^2 and 0.85 km^2, respectively (Ország 2003). Both caves were formed in the Lapis Limestone Formation, a thin-bedded, well-karstifiable Anisian limestone (Ország 2003).

Abaliget Cave is the longest cave in Mecsek Mts. with its 1.7 km horizontal and 52 m vertical dimensions. The main passage is 450 m long and ends in a sump. A large room (Large Chamber), which has a 22x12x10 m extension, can be found approximately 20 m above the sump (Fig. 1). Kispaplika Cave is rather small: 52.6 m long and 26 m deep. Apart from the three shafts the passages are quite narrow (Fig. 2).

Fig. 1 The map and the longitudinal profile of Abaliget Cave

2.2. Methods

Radosys RSFV track-etch detectors were used for measuring radon concentration for a 9-month-long period in 2012-2013. In both caves, instruments were deployed at three different locations (Figs. 1, 2) and were changed within 1-3 month intervals. The underground data were comprehensively analysed in relation to mean ambient air temperature and atmospheric pressure. Meteorological data was collected at the closest weather station, located approximately 5 km from the research area. Both parameters were recorded at 10 minutes frequency. The weather station is run by Public Limited Company for Radioactive Waste Management.
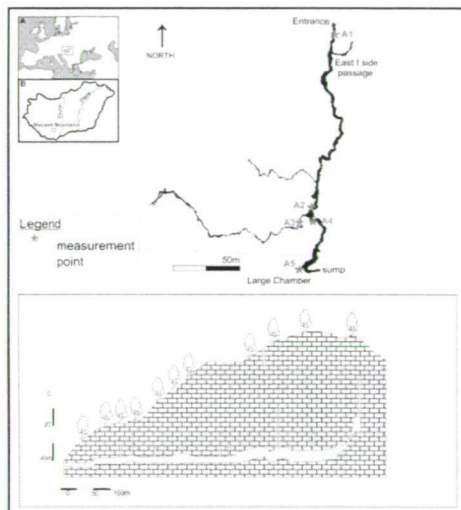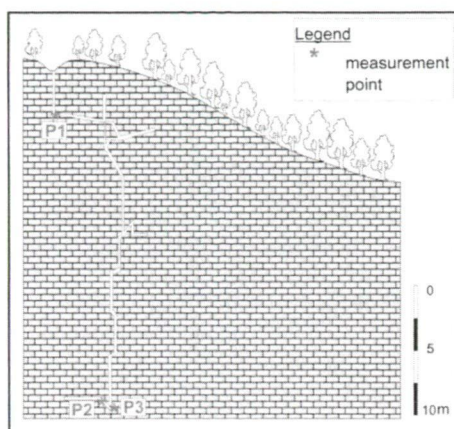
Fig. 2 The longitudinal profile of Kispaplika Cave with the measurement sites

3. RESULTS AND DISCUSSION

3.1. Radon concentration in the caves

The radon concentration of cave air shows a clear seasonal pattern. During the warm summer period the cave was characterized by radon levels varying between 6 and 16 kBq m^{-3}, while in winter much lower values (0.1-1.3 kBq m^{-3}) were recorded. Similar seasonal changes were reported during the previous monitoring (Zalán 1995, Hakl et al. 1996, Várhegyi, 1996). Furthermore, as Table 1 shows radon concentration significantly increased with the distance from the cave entrance except for elevated radon level periods when the detectors placed at A1 recorded higher values than the ones at A2. This might be the consequence of a radon-rich air contribution coming from the East I side passage.

Table 1 Mean radon levels (Bq m^{-3}) measured in Abaliget and Kispaplika caves, Mecsek Mts., Hungary

Place	Measurement period					
Abaliget Cave						
	26.08.12 - 30.09.12	30.09.12 - 29.10.12	29.10.12 - 02.01.13	02.01.13 - 17.02.13	17.02.13 - 24.03.13	24.03.13 - 03.06.13
A1	7.2**	3.6*	0.2*	0.1*	0.3*	2.8**
A2	5.1**	3.4*	0.4*	0.2*	0.6*	2.4**
A3	5.8**	4*	0.4*	0.2*	0.7*	4.9**
A4	7.9**	5**	0.5*	0.2*	1.0*	4.3**
A5	10.3**	16.7**	0.7*	0.6*	1.3*	6.3**
Kispaplika Cave						
	01.09.12 - 30.09.12	30.09.12 - 28.10.12	28.10.12 - 04.01.13	04.01.13 - 15.02.13	15.02.13 - 24.03.13	24.03.13 - 03.06.13
K1	4.2*	2.7*	0.1*	0.1*	4.3*	2.4**
K2	19.3**	17.2**	5.3**	0.3*	8*	5.1**
K3	21.0**	16.7**	5.1**	0.3*	8.2*	4.6**

* 1 sigma uncertainty is 15%, ** 1 sigma uncertainty is 40%

In horizontal caves with one entrance, like Abaliget Cave, there is usually a continuous inward airflow in winter and an outward one in summer. The direction of airflow is governed by the temperature difference inside and outside the cave. The direction of airflow turns when the surface temperature exceeds or falls below the cave air temperature. Consequently, high summer concentrations are driven by the outward cave airflow that brings the radon accumulated in the fractures of the rock matrix. On the contrary, in winter radon-poor air enters the cave from the surface while diluting the radon concentration of the passages. During transitional periods, when the surface and the cave air temperature are nearly identical, winter and summer flow regimes are following each other and therefore radon concentration fluctuates between two stable levels. Hakl et al. (1996) found the width of this transition phase to be 10°C, owing to the existence of a well-developed vertical fracture system in Abaliget Cave.
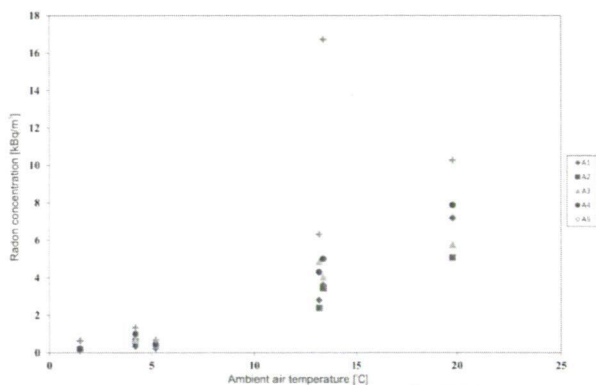
Fig. 3 Mean radon concentration as a function of mean surface air temperature

Table 2 Characteristic radon concentration of cave air in Mecsek Mts, during summer and winter periods (Koltai et al. 2010)

Name of the cave	Place of the detector	Period	Mean ^{222}Rn concentration [kBq m^{-3}]	
			Summer	Winter
Aktív	entrance zone	2000 – 2001	26.5	4.05
Sózó	entrance zone	1999 – 2002	19-20	1-2
Szuadó	entrance zone	2007 – 2008	-	25.35
Trió	end zones	2006 – 2007	7.6	10.5
Upper Szajha	entrance zone	2003 – 2004	1.1	0.4
Vadetetős	entrance zone	2003 – 2004	3.6	15
		2007 – 2008	2.71	2
	end zone	2007 – 2008	11.8	17.4
Pietró	entrance zone	1995 – 2005	2.5-3	7-8
Tüskés	entrance zone	2002 – 2005	2	6-7
Abaliget	entrance zone	2012 – 2013	7	0.1-0.2
	end zone		10	0.6
Kispaplika	entrance zone	2012 – 2013	4.2	0.1
	end zone		21	0.2

Similarly to Abaliget Cave, Kispaplika Cave was also characterized by higher summer and lower winter values. High and low radon concentration periods are mainly driven by air

circulation changes inside the cave, induced by the temperature difference of the air inside and outside the cave. In winter the cold surface air sinks into the cave, it warms up inside and rises and comes out, creating an auto-circulation inside the cave. Even though in the case of narrow entrance vertical caves radon concentration changes are mainly controlled by atmospheric pressure (Géczy et al. 1988), these signals, if present, are masked by temperature induced changes of cave airflow owing to the used method.

On account of the preliminary results of the 9-month monitoring, both Abaliget and Kispaplika caves are characterized by similar values to the other caves monitored previously in the area. Winter values are slightly lower than in the other caves. The radon concentration of the caves located in Mecsek Mts. is particularly high, the source of which is still unrevealed. Several factors, for instance the poor ventilation of small and narrow passages or sediments acting as high radon sources can significantly contribute to the high radon concentrations measured over the years. In a previous study of a narrow entrance vertical cave (Vadetetős Cave), both rock and clayey sediment samples were collected in order to mark off the possible sources of radon. The analysed samples showed usual levels of [226]Ra and [232]Th (Koltai et al. 2012). Further investigation is needed as to locate the exact sources of elevated radon levels measured in some these caves.

3.2. Correlation coefficient among the variables

In both caves large correlation coefficients were found between outside air temperature and radon concentrations at the different measurement points (Table 2). The relationship is less strong in the case of Kispaplika Cave. In the first cave correlation coefficients become slightly higher with increasing distance from the entrance. In both caves the last measurement points at the end zones are characterized by the weakest relationships.

Table 3 Correlation coefficients between the radon concentration of cave air and the meteorological parameters at the different measurement points.

Measurement point	Correlation coefficient with mean ambient temperature	Correlation coefficient with mean ambient pressure
Abaliget Cave		
A1	0.92	0.43
A2	0.95	0.42
A3	0.95	0.25
A4	0.97	0.37
A5	0.60	0.29
Kispaplika Cave		
K1	0.97	0.31
K2	0.77	0.62
K3	0.77	0.61

4. CONCLUSIONS

During the 9-month monitoring both Abaliget and Kispaplika showed elevated summer and low winter radon levels. On the basis of statistical analyses the changes of cave air radon concentration are primarily governed by temperature difference induced cave air circulation. Although in Kispaplika cave air pressure changes might contribute to significant

short term increases, the used method was not suitable to study the influence of atmospheric pressure variations. Moreover, with one exception (A1) radon concentration gradually rose with increasing distance from the entrance. During the elevated period, the detector at A1 measurement point recorded higher values than at A2 which might be a consequence of radon rich air coming from East I side passage.

REFERENCES

Barta K, Tarnai T (1999) Karstmorphological research in the Mecsek Mountains, Southern Hungary. Acta Carsologica 28:13-26

Hakl J, Csige I, Hunyadi I (1996). Radon transport in fractured porous media – experimental study in caves. Environ Int 22:433-437

Hakl J (1997) Application of Radon-222 as a Natural Tracer in Environmental Studies. PhD thesis. Lajos Kossuth University Debrecen

Hakl J, Hunyadi I, Csige I, Géczy G, Lénárt L, Várhegyi A (1997) Radon Transport Phenomena Studied in Karst Caves - International Experiences on Radon Levels and Exposures. Radiat Meas, 28:675-684

Dezső Z, Molnár L (2001) Barlangkutatás radonnal [Doing cave research with radon (in Hungarian)] In: Sásdi L. (ed.) Professional Meeting of Hungarian Speleologists, Pécs. Hungary. 84-90

Géczy G, Csige I, Somogyi G (1988) Air circulation in caves traced by natural radon. In: Kósa A (ed) Proceedings of the 10th International congress of Speleology, Vol. 2. Hungarian Speleological Society, Budapest, Hungary. 615-617

Koltai G, Ország J, Tegzes Z, Bárány-Kevei I (2010) Comprehensive radon concentration measurements in caves located in the area of Mecsek Mountains. Acta Carsologica 39:513-522

Koltai G, Tegzes Z, Dezső Z, Bárány-Kevei I (2012) Radon measurements in Vadetetös Cave, Mecsek Mts, Hungary. In: Stuenzi, H. (ed): Proceedings of the 13th International Congress of Speleology, Muotathal, Switzerland. 121-127

Ország J (2003): Az Abaligeti-barlang és a felszín kapcsolatának vizsgálata [Studying the relationship between Abaliget Cave and the surface (in Hungarian)] MSc thesis, University of Szeged, Szeged, Hungary

Papp B, Deák F, Horvát Á, Kiss Á, Vid G (2004) A barlangi agyagos kitöltés radon viszonyainak vizsgálata a Baradla-barlang egy pontján. [Radon measurement of clay that fills in cave passages, at one point of Baradla Cave (in Hungarian)] IX. Karstdevelopment Conference (ed. Veress, M.) Szombathely. 321-328

Várhegyi A (1996) Monitoring jellegű vizsgálatok az Abaligeti-cseppkőbarlangban [Monitoring of Abaliget Cave (in Hungarian)] Pro Natura Karst- and Cave Research Group's Report of the Research Year 1995, Pécs, Hungary. 42-49

Zalán B (1995) Beszámoló a mecseki karsztterületen végzett monitoring eredményeiről. The results the monitoring activity done on the karst areas of Mecsek Mts. (in Hungarian)] Pro Natura Karst- and Cave Research Group's Report of the Research Year 1995, Pécs. 40-45

Zalán B (1998) Radonmérések néhány mecseki barlang bejáratánál. [Radon measurements at the entrances of some caves in Mecsek Mountains (in Hungarian)] Pro Natura Karst- and Cave Research Group's Report of the Research Year 1997, Pécs, Hungary. 20-26

Zalán B (2004) Radon-transzport mérések négy mecseki barlangban. [Radontransport measurements of four caves in Mecsek Mountains (in Hungarian)] Pro Natura Karst- and Cave Research Group's Report of its Research Activity in 2004, Pécs, Hungary. 30-37

ANALYSIS OF TOURISM CLIMATIC CONDITIONS IN HUNGARY CONSIDERING THE SUBJECTIVE THERMAL SENSATION CHARACTERISTICS OF THE SOUTH-HUNGARIAN RESIDENTS

A KOVÁCS and J UNGER

Department of Climatology and Landscape Ecology, University of Szeged, P.O.Box 653, 6701 Szeged, Hungary
E-mail: kovacsattila@geo.u-szeged.hu

Summary: People living in different regions adapt physiologically and psychologically to the background climatic conditions of their place of origin. This may influence their decisions in the planning phase when travelling for holidays by determining their climatic preferences and the importance of individual climatic parameters. Due to the different levels of adaptation and acclimatization the subjective thermal assessments (e.g. the thermal perceptions) of the tourists in response to a thermal environment might be extremely varied, which should be considered in the climate potential studies. This paper analyses the tourism climatic potential of some Hungarian tourist destinations, assuming that people visiting these places have adapted to the climatic conditions prevailing in the Southern Great Hungarian Plain. We characterize the tourism climatic conditions using the Tourism Climatic Index (TCI) modified in a way which enables to include the real thermal perception characteristics of the people living in this region. To achieve this goal, we integrate a thermal sensation scale of the Physiologically Equivalent Temperature (PET) into the TCI which was modified to reflect the thermal sensation properties of the South-Hungarian citizens. Moreover, we compare the results with those referring to people living under the Western-Central-European climatic conditions by applying also the widely known conventional PET thermal sensation scale in the TCI. The preliminary results indicate that the most favourable tourism climatic conditions in terms of TCI occur in the shoulder seasons in each investigated area. The annual course of TCI is similar in the case of both methods with different PET scales, however the South-Hungarian residents seem to perceive the tourism climatic conditions less stressful throughout the year compared to the Europeans, which can be very unfavourable and dangerous in extreme warm conditions.

Key words: thermal adaptation, tourism climate potential, modified Tourism Climatic Index, Physiologically Equivalent Temperature, thermal sensation classes, Southern Great Hungarian Plain

1. INTRODUCTION

Climate and weather play a key role in the travel decisions of tourists by designating areas that offer suitable climatic conditions or by determining the best time to travel. However, visitors coming from different countries or even from distinct regions of a country may have differences in climatic preferences and in priorities for climate conditions, and thus in their choice of destination. For example, Morgan et al. (2000) found considerable differences in the preferences and the relative rankings of weather parameters between beach users of North and Mediterranean European origin using questionnaire data. Also, on the basis of questionnaire surveys conducted in Canada, New Zealand and Sweden Scott et al. (2008) pointed out that the background climatic conditions prevailing in the place of origin may explain some of the features of climatic preferences and the relative importance of the

parameters, e.g. low mean summer temperatures experienced in the home country may create a desire for higher temperature when travelling for beach holidays.

These significant differences between the residents may be attributed to the various levels of physiological adaptation of the local residents to the special climatic background in their home country. Moreover, expectations, thermal experiences, as well as the different cultures and attitudes may influence their climatic preferences psychologically (Nikolopoulou and Steemers 2003, Knez and Thorsson 2006, Knez et al. 2009).

In the climate potential analyses of tourist areas it should be taken into account that travellers visiting these places have adapted both physiologically and psychologically to the thermal conditions of their place of origin and therefore their subjective evaluations might be different. This study aims to analyse and compare the annual variations of the tourism climatic potential of a few Hungarian popular tourist areas with a modified version of the Tourism Climatic Index (TCI), considering the thermal perception characteristics of the Western-Central-European people and the residents who live under the climatic conditions of the Southern Great Hungarian Plain.

2. METHODS AND MATERIALS

2.1. The original Tourism Climatic Index

In the climatic potential analysis the Tourism Climatic Index is applied which is a widely used metric for the suitability of climate for outdoor light activities (e.g. sightseeing, shopping) (Mieczkowski 1985). The TCI integrates monthly averages of seven climatic parameters relevant for tourism into five sub-indices which are then rated on different scales ranging from 'unfavourable' (0) to 'optimal' (5). After summing the weighted individual sub-indices the index takes on the following expression:

Table 1 Rating categories of the Tourism Climatic Index (Mieczkowski 1985)

TCI scores	Categories
90–100	Ideal
80–89	Excellent
70–79	Very good
60–69	Good
50–59	Acceptable
40–49	Marginal
30–39	Unfavourable
20–29	Very unfavourable
10–19	Extremely unfavourable
<10	Impossible

$$TCI = 2 \cdot (4 \cdot CId + CIa + 2 \cdot R + 2 \cdot S + W) \qquad (1)$$

where CId = daytime comfort index (consisting of the combination of daily maximum temperature and minimum relative humidity), CIa = daily comfort index (daily mean temperature and mean relative humidity), R = monthly amount of precipitation, S = daily sunshine duration, and W = daily mean wind speed. With an optimal rating of 5 for each sub-index, the maximum value of the TCI is 100. Mieczkowski (1985) proposed a classification of TCI scores, with values exceeding 40, 60 and 80 representing at least 'marginal', 'good' and 'excellent' conditions, respectively (Table 1).

A schematic framework of possible types of annual TCI distributions introduced by Scott and McBoyle (2001) is indicated in Fig. 1.

2.2. Applied modifications in the Tourism Climatic Index

In recent years a number of studies have revealed limitations in relation to the structure and applicability of the TCI. Some of them have suggested to update its daytime and daily

comfort sub-indices (CId and CIa) to reflect a more current state of human bioclimatological knowledge (Scott et al. 2004, Amelung and Viner 2006, Perch-Nielsen et al. 2010); others have emphasized the coarse temporal scale of TCI (i.e. monthly averages) and suggested refinements (de Freitas et al. 2008, Yu et al. 2009, Perch-Nielsen et al. 2010).
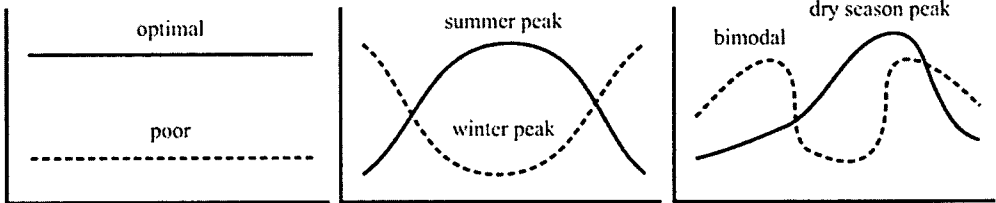

Fig. 1 Conceptual framework of annual TCI distribution (based on Scott and McBoyle 2001)

In this study we use a TCI modified in two steps. First, we used ten-day averages of each sub-index (CId, CIa, R, S as well as W) instead of monthly ones, which suits better to the tourists' interests. Ultimately, these ten-day averages were rated with scores in the TCI. Otherwise, the rating systems of wind speed, precipitation, sunshine duration, as well as the weightings of all sub-indices remained unchanged, holding the concept of Mieczkowski (1985).

Table 2 PET thermal sensation scale (°C) for the Western-Central-European residents (Matzarakis and Mayer 1996) and the modified thermal sensation class boundaries for people living in the Southern Great Hungarian Plain (Kovács et al. 2014)

Thermal sensation classes	European PET scale (°C)	South-Hungarian PET scale (°C)
Very hot	>41	–
Hot	35–41	>45.5
Warm	29–35	31.5–45.5
Slightly warm	23–29	21.9–31.5
Neutral	18–23	14.1–21.9
Slightly cool	13–18	7.4–14.1
Cool	8–13	1.3–7.4
Cold	4–8	<1.3
Very cold	<4	–

A further modification of TCI was to integrate the most widely applied thermal comfort index, namely the Physiologically Equivalent Temperature [PET (°C)] (Matzarakis and Mayer 1996, Höppe 1999) into the daytime (CId) and daily comfort (CIa) sub-indices. Notably, in the modified TCI the new CId and CIa sub-indices consist of the calculated daily maximum and daily average PET. However, for this integration process a rating system of both sub-indices has to be developed. Such a method was presented in Kovács and Unger (2014) based on the conventional relationship between the Predicted Mean Vote (PMV) and the Predicted Percentage of Dissatisfied (PPD). Since our aim is to reflect the real thermal perception characteristics of the residents in the Southern Great Hungarian Plain in the TCI, in this study we present a preliminary method in which their thermal sensation properties can be included. To achieve this goal, we have modified the thermal sensation boundaries of the PET classes recently (Kovács et al. 2014), which were derived originally for the Western-Central-European climatic conditions (Matzarakis and Mayer 1996). This new scale was

developed on the basis of a quadratic regression function between the PET index derived from microclimate measurements as well as the mean thermal sensation votes of visitors (TSV) collected in simultaneous questionnaire surveys (Kovács et al. 2014). In the questionnaires the interviewees were asked to indicate their TSV on a semantic differential scale with 9 main thermal sensation classes ranging from very cold (-3) to very hot (+3). The measurements and the questionnaire surveys took place in a few outdoor public spaces in Szeged, the centre of the Southern Great Hungarian Plain Region. Table 2 illustrates the Western-Central-European PET scale (hereinafter referred to as European) and the modified thermal sensation class boundaries (hereinafter as South-Hungarian).

In the modified TCI the rating scores of the PET sub-indices were derived in two steps, with interposing the thermal sensation votes of the visitors (PET → TSV → rating scores). We gained scores for each PET value by applying at first the PET–TSV quadratic regression function mentioned above where the PET class boundaries were derived originally by substituting TSV=-2.5, -1.5 etc. values into the fitted quadratic equation (e.g. TSV between -2.5 and -1.5 designated the cool category 7.4–14.1°C) (Kovács et al. 2014). In fact, we gave rating scores not directly to the PET values but to the selected TSV thresholds (e.g.

TSV=-2.5, -1.5, -0.5, 0.5 etc.), and then we fitted a function to these values, resulting in continuous scores (Fig. 2). According to this relationship, the neutral thermal sensation vote (TSV=0) gave the possible maximum score 5 and the scores then decrease continuously in line with the decline of the thermal sensation (Fig. 2).

Utilizing the TSV–rating score relationship we could already rate each PET value continuously considering the PET–TSV function. Since we derived scores continuously we could rate each PET value with different scores and not only the discrete class boundaries. Fig. 3a illustrates

Fig. 2 Rating scores of the thermal sensation vote (TSV)

the derived PET–rating score relationship where we indicated the boundaries of the PET classes. The connections between the applied function relationships can be illustrated simply as follows:

$$\text{score} = f(TSV) \rightarrow TSV = f(PET) \rightarrow \text{score} = f(PET) \qquad (2)$$

We can include also other thermal sensation classes in the method described above, by associating the same TSV value to the adequate class boundaries (with the example given above TSV between -2.5 and -1.5 designates the cool category boundaries). In this study we also derived scores for the conventional European PET scale (Matzarakis and Mayer 1996), by applying this new PET–TSV function as well as the original TSV–rating score relationship (Fig. 3b). Since the boundaries of the corresponding classes have always the same scores the shifts in the boundaries between the two scales are reflected in the resulting scores, and thus we have the possibility to compare the influence of the two methods with different scales on the overall TCI.

Fig. 3 Rating scores of the PET in the cases of the South-Hungarian (a) and the European scales (b). Vertical lines designate the boundaries of the PET classes, while dashed lines indicate the neutral temperatures (i.e. when TSV=0) which have the maximum score 5.
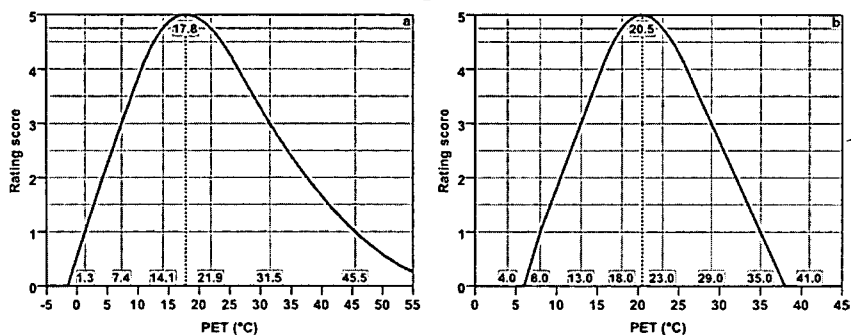
2.3. Study areas and applied data

By means of the modified TCI described above we analyse the annual variations of the tourism climatic conditions on the examples of Szeged (as our reference site) and other three popular Hungarian tourist areas (Budapest, Siófok, Pécs) which have slightly different climates (Table 3). For the calculation of PET and TCI hourly air temperature, relative humidity, wind speed and cloudiness data, as well as daily sunshine duration and precipitation data were used for the periods 1996–2010 (and 2000–2010 in the case of Pécs). We applied the measurement data of stations of the Hungarian Meteorological Service (Table 3). The selected stations are located on grass surface in the suburbs or outside the settlements and do not have considerable horizon limitation (the sky view factor is near to 1), therefore they can provide a good representation of climate on regional scale. The PET values were calculated with the bioclimate model RayMan (Matzarakis et al. 2007, 2010).

Table 3 Meteorological stations included in the analyses with their names and geographical positions

Station	Latitude	Longitude	Altitude (m)
Szeged	46°15'N	20°05'E	82
Budapest-Pestszentlőrinc	47°25'N	19°10'E	139.1
Siófok	46°54'N	18°02'E	108.2
Pécs-Pogány	45°59'N	18°14'E	200.2

3. RESULTS

Using the modified TCI the annual courses of the ten-day rating scores using both methods with different PET scales are illustrated in Fig. 4. In all selected cities a bimodal type of distribution was obtained (see Fig. 1), i.e. the most pleasant climate in terms of sightseeing activities occurs in spring and autumn (TCI>70 and especially in the middle spring it is greater than 80), while in summer the climatic conditions are less favourable (mostly under 70). The most unpleasant conditions occur at the end of July and in early August with the most significant declines in TCI in Szeged and Budapest, though they reflect still good conditions (60<TCI<70). During the winter season there are unpleasant climatic conditions with TCI scores below 50 (Fig. 4).
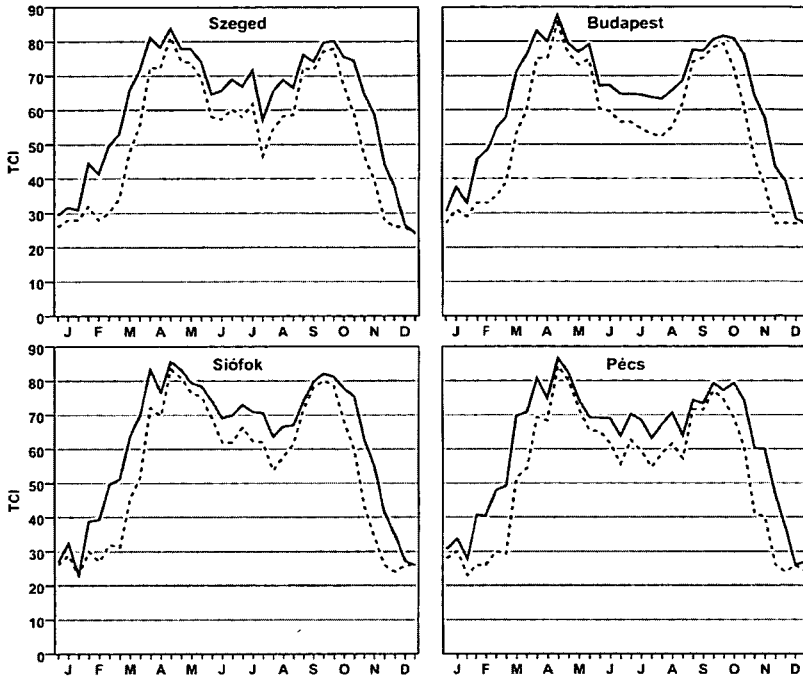
Fig. 4 Annual course of the ten-day TCI rating scores for the selected tourist areas. Solid and dashed lines indicate the results considering the South-Hungarian and European PET rating scales, respectively

The scores are almost always higher in all areas when the South-Hungarian rating scores are used, with the highest average annual difference in Budapest (9.0) and the smallest in Siófok (8.3) (Fig. 3a). The highest differences occur in February, March and November (nearly 20), as well as in the summer months (about 10), which indicate an improvement in the perceived tourism climatic conditions by 1–2 categories of TCI (Fig. 4). This can be explained by the fact that the South-Hungarian residents perceive the extreme conditions less stressful, which is reflected in the broader and less extreme PET classes and thus in the higher rating scores. For example, PET=36°C (corresponding to hot category in the original scale and only to the warm class in the South-Hungarian scale) gave more score (2.24) than in the former case (0.66), indicating rightly the perception characteristics of the South-Hungarian people (Table 2, Fig. 3).

In order to analyse the differences between the two methods with distinct scales in details, it is worth examining the contribution of each sub-index to the overall value of TCI. The results are only presented for Szeged (Fig. 5), since the other areas have similar annual courses. It is clearly shown that the daytime comfort index (CId) is mainly responsible for the bimodal structure of the TCI, since the prevailing heat stress greatly reduces the rating scores in the afternoon hours of summer when usually the daily maximum PET occurs. Moreover, precipitation amount (R) which is the highest on average in summer also contributes to the significant TCI drops according to its rating system. However, the sunshine duration and the daily mean PET sub-indices compensate the declines in the summer months (Fig. 5).
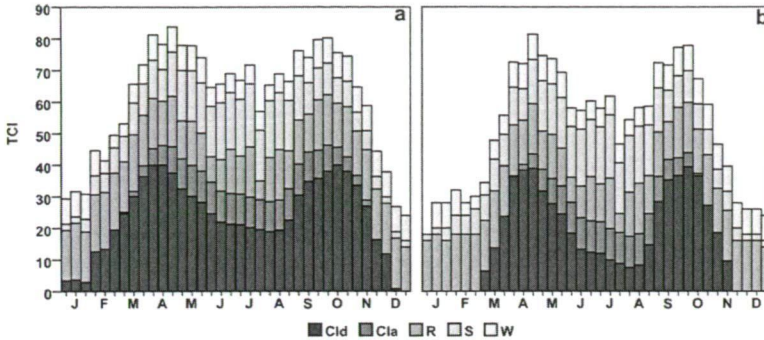
Fig. 5 Ten-day scores of the TCI sub-indices for Szeged considering the South-Hungarian (a) and the European PET scales (b). Note: the scores of R, S and W sub-indices are identical, since their rating systems remained unchanged. (CId = daily maximum PET, CIa = daily mean PET, R = monthly amount of precipitation, S = daily sunshine duration, W = daily mean wind speed sub-index)

Considering the differences in the two rating methods the CId sub-index does not correspond to the TCI value in winter in the case of the European scale (it is equal to zero, i.e. PET is below 6°C), and it has significantly less score from May to August compared to the other case, indicating the altered perceptions of the South-Hungarian residents (Fig. 5). Furthermore, it is obvious that the differences detected in the overall TCI values are due to the CId sub-index because of its high weight in TCI (Table 4). The TCI increases by the CIa sub-index from March to middle November according to the South-Hungarian scores and only from April to middle October in the case of the original scale (Fig. 5). The highest differences in CIa occur in spring and autumn, while in summer the scores are almost identical (Table 4).

Table 4 Mean monthly differences of CId and CIa sub-index scores for Szeged between the methods considering the South-Hungarian and the European PET scales. (CId = daily maximum PET, CIa = daily mean PET sub-index)

Sub-index	J	F	M	A	M	J	J	A	S	O	N	D
ΔCId	3.3	15.2	15.8	1.3	2.3	8.0	10.0	10.0	0.2	4.3	16.2	4.2
ΔCIa	0.0	0.0	1.8	4.4	1.8	-0.1	-0.3	-0.2	2.7	4.4	1.7	0.0

4. CONCLUSIONS

The study analysed the tourism climatic potential of a few Hungarian tourist destinations in terms of the Southern-Hungarian people using a modified Tourism Climatic Index. We integrated the most complex thermal comfort index PET into the TCI and provided a preliminary method to derive rating scores of PET values, which takes the thermal sensation characteristics of the Europeans as well as the residents in the Southern Hungarian Great Plain into account. We applied the conventional European PET thermal sensation classes (Matzarakis and Mayer 1996) as well as a recently developed new scale (Kovács et al. 2014) which reflects more properly the thermal perceptions of the South-Hungarian citizens outdoors. In the rating systems the shifts in the class boundaries of the two scales are reflected in the derived scores.

The results indicated a bimodal annual course of TCI in all cities with the most pleasant tourism climatic conditons for sightseeing tours occuring in the shoulder seasons.

The summer months are less applicable for outdoor activities, which can be attributed to the intense heat load in the afternoon hours (expressed by the daily maximum PET sub-index).

The course of the two TCI scores based on the different PET scales seem to be similar but the South-Hungarian people perceive the tourism climatic conditions better throughout the year. The differences often exceed 10–15 scores, denoting considerable changes. The differences can be attributed to the fact that the South-Hungarian citizens tend to perceive the extreme conditions less stressful, which is reflected in the broader and less extreme South-Hungarian PET classes and thus in the derived rating scores. It should be noted that the perception characteristics of the South-Hungarians can be very unfavourable and dangerous in extreme warm conditions, though the TCI differences are usually do not exceed 10 in summer. Much more significant differences can be found in early spring and late autumn (usually close to 20) which seems to be rather advantageous in those periods.

REFERENCES

Amelung B, Viner D (2006) Mediterranean tourism: exploring the future with the tourism climatic index. J Sustain Tour 14:349-366

De Freitas CR, Scott D, McBoyle G (2008) A second generation climate index for tourism (CIT): specification and verification. Int J Biometeorol 52:399-407

Höppe P (1999) The physiological equivalent temperature – an universal index for the biometeorological assessment of the thermal environment. Int J Biometeorol 43:71-75

Knez I, Thorsson S (2006) Influences of culture and environmental attitude on thermal, emotional and perceptual evaluations of a public square. Int J Biometeorol 50:258-268

Knez I, Thorsson S, Eliasson I, Lindberg F (2009) Psychological mechanisms in outdoor place and weather assessment: towards a conceptual model. Int J Biometeorol 53:101-111

Kovács A, Unger J (2014) A modification of Tourism Climatic Index to Central European climatic conditions – examples. Időjárás 118:147-166

Kovács A, Kántor N, Égerházi LA (2014) Assessment of thermal sensation of residents in the Southern Great Plain, Hungary. In: Pandi G, Moldovan F (eds) Air and Water Components of The Environment, Babeş-Bolyai University, Cluj-Napoca, Romania. 354-361

Matzarakis A, Mayer H (1996) Another kind of environmental stress: thermal stress. WHO Newsletter 18:7–10

Matzarakis A, Rutz F, Mayer H (2007) Modelling radiation fluxes in simple and complex environments – application of the RayMan model. Int J Biometeorol 51:323-334

Matzarakis A, Rutz F, Mayer H (2010) Modelling radiation fluxes in simple and complex environments: basics of the RayMan model. Int J Biometeorol 54:131-139

Mieczkowski ZT (1985) The tourism climatic index: a method of evaluating world climates for tourism. Can Geogr 29:220-233

Morgan R, Gatell E, Junyent R, Micallef A, Williams AT (2000) An improved user-based beach climate index. J Coast Conserv 6:41-50

Nikolopoulou M, Steemers K (2003) Thermal comfort and psychological adaptation as a guide for designing urban spaces. Energ Buildings 35:95-101

Perch-Nielsen SL, Amelung B, Knutti R (2010) Future climate resources for tourism in Europe based on the daily Tourism Climatic Index. Climatic Change 103:363-381

Scott D, McBoyle G (2001) Using a 'tourism climate index' to examine the implications of climate change for climate as a natural resource for tourism. In: Matzarakis A, de Freitas CR (eds) Proc. First Int. Workshop on Climate, Tourism and Recreation. International Society of Biometeorology, Commission on Climate, Tourism and Recreation, Halkidi, Greece. 69-88

Scott D, McBoyle G, Schwartzentruber M (2004) Climate change and the distribution of climatic resources for tourism in North America. Climate Res 27:105-117

Scott D, Gössling S, de Freitas CR (2008) Preferred climates for tourism: case studies from Canada, New Zealand and Sweden. Climate Res 38:61-73

Yu G, Schwartz Z, Walsh JE (2009) A weather-resolving index for assessing the impact of climate change on tourism related climate resources. Climatic Change 95:551-573

SEPARATION OF THE CURRENT AND PAST METEOROLOGICAL PARAMETERS IN INFLUENCING THE CURRENT POLLEN CONCENTRATIONS

L MAKRA[1], Z CSÉPE[1], I MATYASOVSZKY[2], G TUSNÁDY[3] and ÁJ DEÁK[4]

[1]*Department of Climatology and Landscape Ecology, University of Szeged, 6701 Szeged, P.O.B. 653, Hungary*
[2]*Department of Meteorology, Eötvös Loránd University, 1117 Budapest, Pázmány Péter Street 1/A, Hungary*
[3]*Mathematical Institute of the Hungarian Academy of Sciences, 1364 Budapest, P.O.B 127, Hungary*
[4]*Department of Physical Geography and Geoinformatics, University of Szeged 6701 Szeged, P.O.B. 653, Hungary*
E-mail: makra@geo.u-szeged.hu

Summary: A new procedure is introduced in order to separate the effects of the current and past meteorological elements influencing the current pollen concentration for different taxa. The data set covers an 11-year period (1997-2007) including daily pollen counts of 19 taxa and 4 climate variables (mean temperature, precipitation total, global solar flux and relative humidity). Results are evaluated with special interest to the interactions between the phyto-physiological processes and the meteorological elements for each taxon. The taxa examined can be classified into three groups, namely arboreal deciduous (AD), arboreal evergreen (AE) and herbaceous (H) taxa. It was found that a better comparison can be established if the taxa are separated within each group according to the starting month of their pollination season. Within the group of AD taxa, *Alnus, Populus* and *Ulmus* are marked by a late summer – early autumn peak of the role of past meteorological elements exceeding the role of the current ones almost all over the pollen-free period. For *Juglans, Morus, Platanus* and *Quercus*, the major weights of the current meteorological elements in the spring and early summer show the most characteristic contribution to the pollen production. For AE taxa, the picture is not clear. For H taxa, the curves of *Cannabis, Plantago, Rumex* and *Urtica* indicate the most equalized course of weights. *Ambrosia, Artemisia* and Chenopodiaceae comprise the highest weights of the past weather conditions of all taxa until at least three months before the start of the pollination.

Key words: pollen season, climate change, respiratory allergy, factor analysis with special transformation

1. INTRODUCTION

Recently, the earth's ecosystem has been experiencing a global warming. Projections of future climate change suggest further global warming, sea level rise and an increase in the frequency of some extreme weather events (Parry et al. 2007). By the late 21st century, distributions of European plant species are projected to have shifted several hundred kilometres to the north (Parry et al. 2007, Lindner et al. 2010). The rate of change will exceed the ability of many species to adapt. As for plant phenology, the timing of seasonal events in plants is changing across Europe due to changes in the climate conditions. Between 1971 and 2000, the average advance of spring and summer was 2.5 days per decade. The pollen season starts on average 10 days earlier and is longer than it was 50 years ago (Feehan et al. 2009).

Climate change in association with an extended urbanization, with high levels of vehicle emissions in urban areas, and living in an artificial environment with little

movement exert negative impact on individuals in most industrialized countries. Hence, these factors may contribute to explaining the increasing frequency of respiratory allergy and asthma (D'Amato 2011). Pollen is an important trigger of respiratory diseases. Both quantity related (total annual pollen counts, annual peak pollen counts) and phenological (start, end and duration of the pollen season) characteristics of different taxa are functions of the meteorological variables. Greater concentrations of carbon dioxide and, consequently, higher temperatures may increase pollen quantity and induce longer pollen seasons (Ziska et al. 2003, Clot 2008). Pollen allergenicity can also increase as a result of these changes in climate. Furthermore, there is evidence that high levels of traffic-derived air pollutants may interact with pollen and bring about more intense respiratory allergy symptoms (Hjelmroos et al. 1999, Motta et al. 2006). Accordingly, global warming may induce a wide pollen-related public health problem; for which the societies should be prepared in time.

The main aim of this paper is to study an extended spectrum of airborne pollen characteristics (19 plant taxa) for the Szeged region in Southern Hungary. A novel procedure is introduced in order to separate the effect of the past and current weather conditions in influencing current pollen production of the different taxa. This kind of separation has not been demonstrated in the literature. Results are evaluated with special attention to the interactions between the phyto-physiological processes and the climate elements; furthermore, they are compared for each taxon based on different aspects.

Predicting the pollen season characteristics (e.g. the start of the pollen season) as early as possible is of basic importance in order to prepare sensitive people in time for the days of pollen dispersion. Our analysis helps to identify those key periods and meteorological variables which most affect the daily pollen counts of the given taxon. Changing climate involves different changes in the weather elements of each season. A potential importance of the procedure is that a period with a changing climate that may have a major impact on the current pollen counts can be detected by the past of climate elements.

2. MATERIALS

2.1 Location and data

Szeged (46.25°N; 20.10°E), the largest settlement in South-eastern Hungary is located at the confluence of the rivers Tisza and Maros. The area is characterised by an extensive flat landscape of the Great Hungarian Plain with an elevation of 79 m above sea level. The city is the centre of the Szeged region with 203,000 inhabitants.

The pollen content of the air was measured by a 7-day recording Hirst type volumetric spore trap (Hirst 1952). The air sampler is located on top of the building of the Faculty of Arts at the University of Szeged, approximately 20 m above the ground surface (Makra et al. 2010). Meteorological variables include daily values of mean temperature (T, °C), relative humidity (RH, %), global solar flux (GSF, W m^{-2}) and precipitation total (P, mm), respectively. They were collected in a meteorological station located in the inner city area of Szeged. The data set consists of daily pollen counts (daily pollen count m^{-3} of air) of 19 taxa taken over the 11-year period 1997-2007. With their Latin (English) names they are: *Alnus* (alder), *Ambrosia* (ragweed), *Artemisia* (mugwort), *Betula* (birch), *Cannabis* (hemp), Chenopodiaceae (goosefoots), *Juglans* (walnut), *Morus* (mulberry), *Pinus* (pine), *Plantago*

(plantain), *Platanus* (plane), Poaceae (grasses), *Populus* (poplar), *Quercus* (oak), *Rumex* (dock), *Taxus* (yew), *Tilia* (linden), *Ulmus* (elm) and *Urtica* (nettle). These 19 taxa produce 93.2% of the total pollen amount for the given period. Taxa with the highest pollen levels include *Ambrosia* (32.3%), Poaceae (10.5%), *Populus* (9.6%) and *Urtica* (9.1%) that together account for 61.5% of the total pollen production.

The pollen season is defined by its start and end dates. For the start (end) of the season we used the first (last) date on which 1 pollen grain m^{-3} of air is recorded and at least 5 consecutive (preceding) days also show 1 or more pollen grains m^{-3} (Galán et al. 2001). For a pollen type, the longest pollen season in the 11-year period was considered.

2.2 Factor analysis with special transformation

Factor analysis identifies any linear relationships among subsets of examined variables and this helps to reduce the dimensionality of the initial database without substantial loss of information. First, a factor analysis was applied to the initial datasets consisting of 9 variables (8 explanatory variables including 4 climatic variables in the past and the same 4 climatic variables on the actual day, and 1 resultant variable defined by the daily pollen concentration of the given taxa) transforming the original variables to fewer variables. These new variables (called factors) can be viewed as latent variables explaining the joint behaviour of past and current meteorological elements as well as current pollen concentration variables. The number of retained factors can be determined by different criteria. The most common and widely accepted one is to specify a least percentage (80%) of the total variance in the original variables that has to be achieved (Jolliffe 1993, Liu 2009). After performing a factor analysis, a special transformation of the retained factors was made to discover to what degree the above-mentioned explanatory variables affect the resultant variable and to give a rank of their influence (Jahn and Vahle 1968). When performing factor analysis on the standardized variables, factor loadings received are correlation coefficients between the original variables and, after rotation, the coordinate values belonging to the turned axes (namely, factor values). Consequently, if the resultant variable is strongly correlated with the factor (the factor has high factor loading at the place of the resultant variable) and - within the same factor - an explanatory variable is highly correlated with the factor, then the explanatory variable is also highly correlated with the resultant variable. Hence, it is advisable to combine all the weights of the factors together with the resultant variable into one factor. Namely, it is effective to rotate so that only one factor has a large weight with the resultant variable. The remaining factors are uncorrelated (are of 0 weights) with the resultant variable (Jahn and Vahle 1968). This latter procedure is called special transformation.

3. RESULTS

Airborne pollen concentrations can be influenced not only by the current values of the meteorological elements, but also by their past values. As it is hard to distinguish between the effect of the current and past values of the meteorological variables no attempt has been made so far to determine the relative weight of these two components in influencing the measured current pollen concentration. In our present approach the current meteorological elements (daily mean temperature, daily relative humidity, daily global solar flux and daily

precipitation total) were characterised by their actual values, while past meteorological elements were described by their cumulative values. These elements were considered since they indicate the highest impact on pollen production (Galán et al. 2000, Bartková-Ščevková 2003, Štefanič et al. 2005, Kasprzyk 2008, Makra and Matyasovszky 2011).

The calculation procedure and main results are presented in detail for Poaceae, because this species group has the longest pollen season in Hungary and significantly contributes to the total annual pollen production. In order to assess the effect of the antecedent and current meteorological conditions on the current Poaceae pollen concentration, the 1st-day, 2nd-day, ..., 180th-day values of both the pollen concentration and the four meteorological elements of the current pollen season were taken. (The duration of the Poaceae pollen season in Szeged lasts from April 16 until October 12, namely 180 days. (Table 1).). The values of these meteorological variables were then cumulated for 186-day, 185-day, ..., 1-day periods starting 186 days, 185 days, ..., 1 day before the actual day of the actual pollen season. This is because there are 186 days between the end of the previous-year pollen season and the beginning of the actual pollen season. Hence, 186 9-dimensional data sets were produced and a factor analysis with special transformation was performed for each of them (Figs. 1-3). The altogether 5496 factor analyses carried out for all the 19 taxa resulted in 3 and 4 factors, except for *Artemisia* (2 factors).

The main findings for Poaceae are as follows (Fig. 2, 2nd panel from above, right). The total weights (summarized absolute values) of the factor loadings for the past meteorological variables are decreasing from day 186 until day 58 (disturbed by a sudden local maximum on day 90). Then, a strong increase can be observed reaching a local maximum on day 20, which is followed by a steep decrease until present. The total weights of the factor loadings for the current climate parameters are below those of the past climate variables between days 186 and 128, as well as between days 42 and 10. However, between days 128 and 42, as well as between day 10 and the present the effect of the current climate is stronger.

Table 1 Plant habits and phenological pollen season characteristics

Taxa	[1]Plant habit	Pollen season		
		Start	End	Duration, day
Alnus	AD	Feb 3	Apr 8	65
Betula	AD	Mar 22	May 8	48
Juglans	AD	Apr 12	May 19	38
Morus	AD	Apr 18	May 22	35
Platanus	AD	Apr 8	May 20	43
[2]*Populus*	AD	Feb 27	Apr 20	53
Quercus	AD	Apr 2	May 11	40
Tilia	AD	May 16	Jul 1	47
Ulmus	AD	Feb 6	Apr 8	62
Pinus	AE	Apr 25	Jun 8	45
Taxus	AE	Feb 13	Apr 15	62
[2]*Ambrosia*	H	Jul 15	Oct 15	93
Artemisia	H	Jul 18	Oct 9	84
Cannabis	H	Jun 6	Sep 3	90
Chenopodiaceae	H	Jun 22	Oct 11	112
Plantago	H	May 12	Aug 29	110
[2]**Poaceae**	**H**	Apr 16	Oct 11	180
Rumex	H	May 13	Aug 12	92
[2]*Urtica*	H	May 4	Sep 26	146

[1]AD: arboreal deciduous, AE: arboreal evergreen, H: herbaceous;
[2]**Bold**: taxa with the highest pollen levels in Szeged region

climate variables between days 186 and 128, as well as between days 42 and 10. However, between days 128 and 42, as well as between day 10 and the present the effect of the current climate is stronger.

From day 15 until present the total weights sharply decrease. In general, this is in agreement with our preliminary expectation that current climate has a higher importance close to the current pollen release; while back in time the role of both the past and current

climate varies depending on periods. The effect of the current climate begins to increase on day 90 (i.e. 90 days preceding April 16 (Table 1) corresponding to the date January 16).

It can be concluded after a further analysis of the curves in Figs. 1-3 and 4 that from mid-October to mid-January temperature and global solar flux can determine the future pollen production, whereas from mid-January the role of precipitation increases as the water-storage of the soil must be restored before the start of the vegetation. Current effects of global solar flux, precipitation and relative humidity indicate peak values a few days before the pollination season and exceed their past effects in this period. Water and light are required to start photosynthesis, namely vegetative and generative processes that are essential for the pollen production. Even if the past meteorological conditions were optimal for grasses the current precipitation and global solar flux can overwrite the past effects, and early April weather conditions are essential for the pollen production. Although the weight of relative humidity also increases by early April this is only a consequence of the beginning photosynthesis facilitated by an increased global solar flux and precipitation. As a result, these latter two meteorological parameters are the most essential factors of pollen production for grasses and temperature has only a regulating effect.

Poaceae contains lots of species and the start of their pollen season differs notably. Therefore, any changes in precipitation, temperature or global solar flux may change the species composition significantly. The change in dominant grass species was observed in several landscape types in Hungary during the recent years (Deák 2010, 2011, 2012).

For *Alnus,* the weights of the past meteorological parameters are somewhat higher compared to those of the current ones with only small variability in most of the pollen-free season (Fig. 1, 1ˢᵗ panel from above, left). This is because *Alnus* requires stable weather conditions for a longer period. *Alnus* can be found in wetlands – in marsh forests or alongside streams in hilly and montane areas that ensure an equalized microclimate. In late September and early October the water-level is the lowest in the wetlands and the soil surface often dries out.

For *Ambrosia*, the total weights of the factor loadings for the past meteorological variables are gradually increasing from the first pollen-free day following the last *Ambrosia* pollen season until the middle of March (Fig. 1, 1ˢᵗ panel from above, right). Then, until present, the importance of the past climate parameters is decreasing. The total weights of the factor loadings for the current climate parameters (solid line) are very low from day 272 until day 138. Then they are increasing steeply, reaching their top values between the days 62 and 50. During the last 50 days until the start of the current *Ambrosia* pollen season the total weights are sharply decreasing. The effect of the past climate is greater on the current *Ambrosia* pollen concentration from day 272 until day 77, while from this day until present the current climate has higher weight in influencing the current *Ambrosia* pollen level. The effect of the current climate begins to increase on day 138 (i.e. 138 days preceding July 15, corresponding to the date February 28) (Fig. 4).

For *Artemisia,* the past meteorological elements have a much more important effect on pollen production, especially between mid-April and mid-June. The past climate conditions can thus compensate the possible negative effects of the current meteorological conditions. The effect of the current weather conditions becomes more important just 1-2 weeks before the pollination season in early July, whereas the weight of the past ones suddenly drops down.
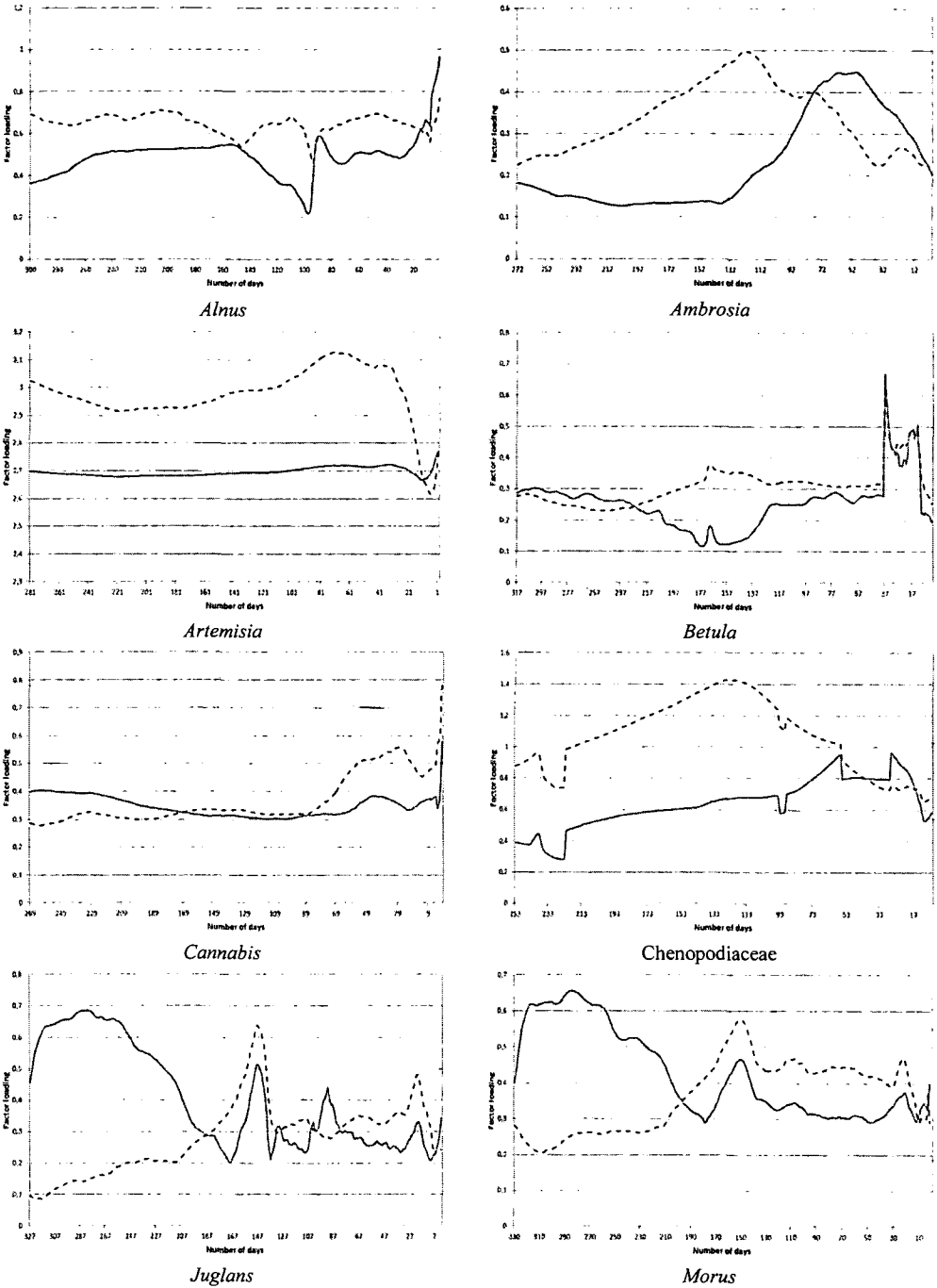
Fig. 1 Total weights of the factor loadings for the current (solid line) and past (dashed line) meteorological elements influencing the current pollen concentrations for the different taxa

Pinus

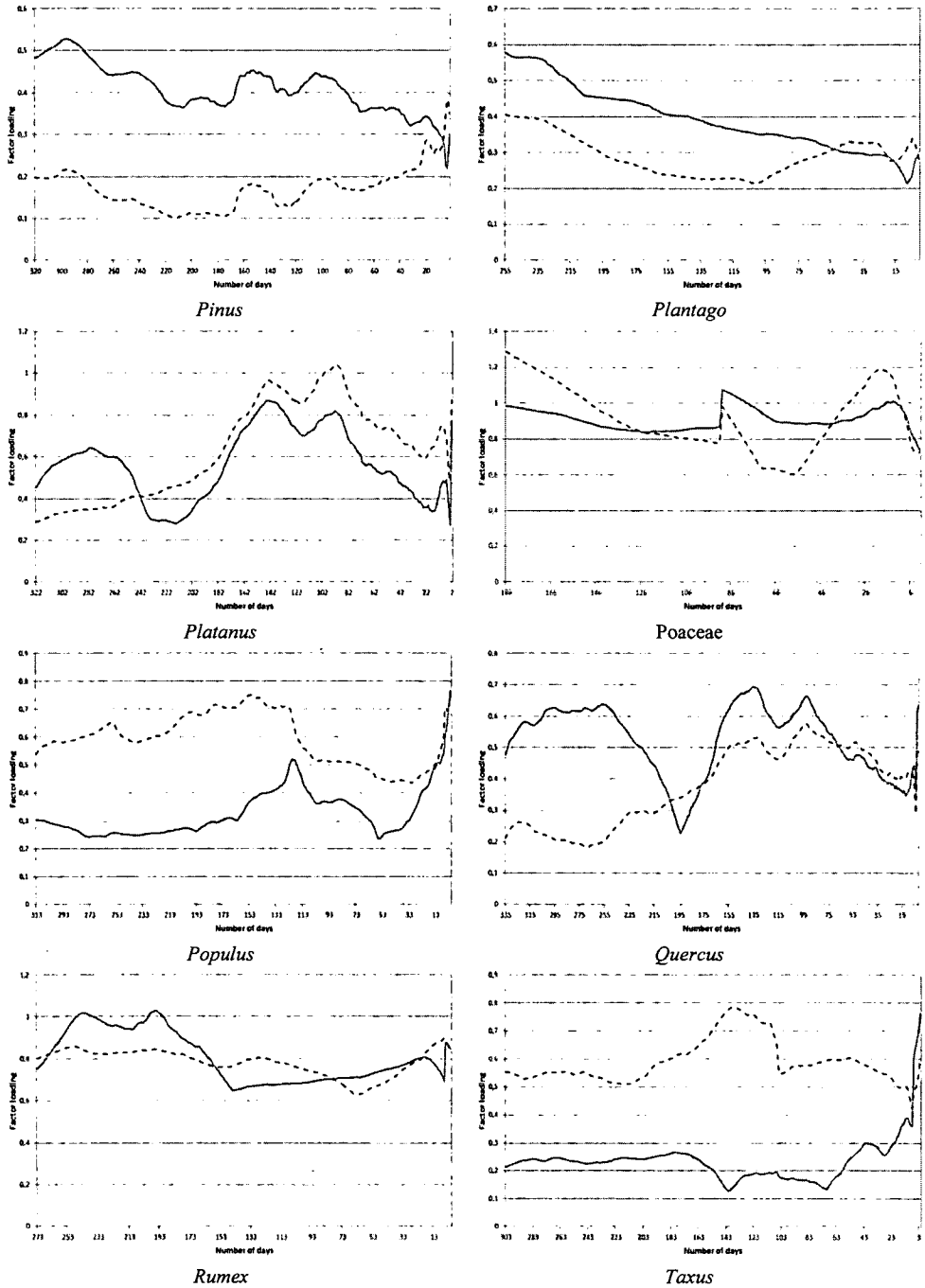Plantago

Platanus

Poaceae

Populus

Quercus

Rumex

Taxus

Fig. 2 Total weights of the factor loadings for the current (solid line) and past (dashed line) meteorological elements influencing the current pollen concentrations for the different taxa

For *Betula,* the effect of the past and current meteorological elements is very similar in the pollen-free season, except the period from August until the end of the autumn when the difference between the weights of the past and current meteorological parameters is the highest with the bigger weights of the past elements (Fig. 1, 2nd panel from above, right). This is because by the end of the summer and during the autumn the water-storage of the soil becomes an important factor for the species of this genus that originally occurs in pioneer montane forests and marsh forests in areas with cooler and humid microclimate (Horváth et al. 1995). From the second half of October, due to the lower temperatures and increasing precipitation, the role of the current meteorological elements increases. Their weight suddenly exceeds the past effects after mid-February.
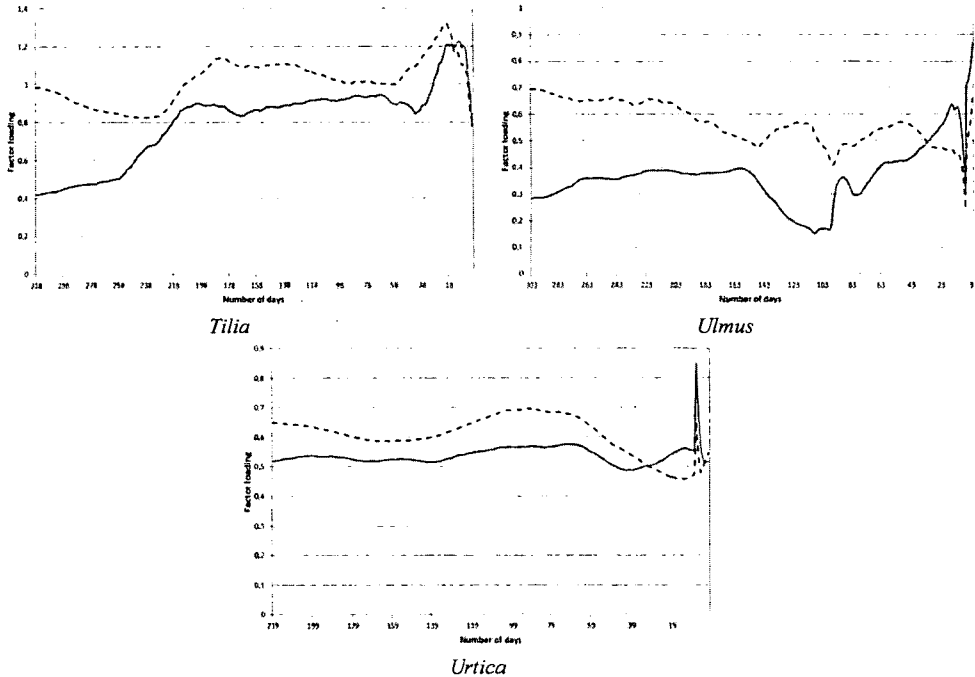

Fig. 3 Total weights of the factor loadings for the current (solid line) and past (dashed line) meteorological elements influencing the current pollen concentrations for the different taxa

For *Cannabis,* the past and current weather conditions have a balanced role after the end of the previous pollination period (Fig. 1, 3rd panel from above, left). The weights of current meteorological elements are slightly higher from early September until the middle of December. Afterwards, there is no significant difference between the effects of the past and current weather conditions. But from early March the effect of the past weather conditions increases reaching its maximum after a little drop by the beginning of the pollen season.

For the Chenopodiaceae family, after the end of the previous pollen season (October 11), the weights of the past meteorological elements are higher than those of the current ones (Fig. 1, 3rd panel from above, right). The effects of both the current and past meteorological elements show a slight increase until March with two small parallel drops. These drops occur in early November and in the second half of March.

global solar flux

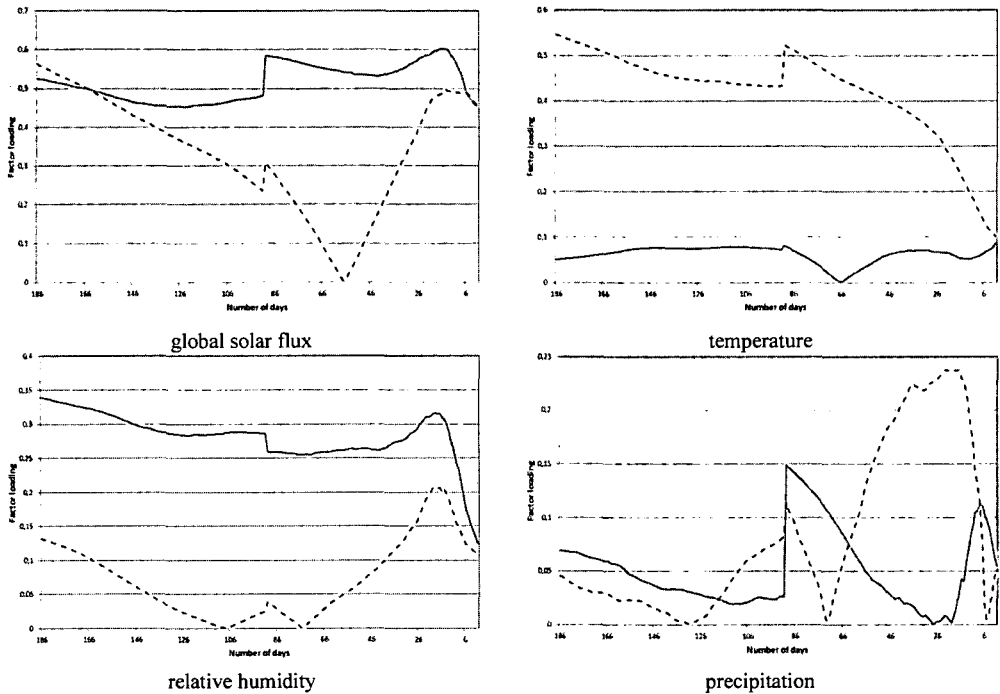temperature

relative humidity

precipitation

Fig.4 Weights of the factor loadings for the current (solid line) and past (dashed line) meteorological elements influencing the current pollen concentrations for Poaceae

For *Juglans,* water income and higher temperatures could be the major factors influencing the run of the curves (Fig. 1, 4th panel from above, left). After the end of the previous pollen season, the weight of current meteorological elements is higher reaching the maximum weight in early July when the lack of water can be a major influencing factor. Following July, the role of the current meteorological elements suddenly decreases and from the middle of October the weight of the past meteorological elements exceeds that of the current ones and they are dominant until early April (start of the pollen season). Two major peaks (in early November and at the turn of March and April (two weeks before the pollen season)) can be identified. Both can be associated with high precipitation events or possible milder periods.

The shape of the curves for *Morus* (Fig. 1, 4th panel from above, right) is similar to those for *Juglans* but with a few differences. The role of the current meteorological elements highly dominates after the previous pollen season: its maximum weights occur in the mid-May – mid-August period. From mid-August, the weight of current meteorological elements begins to drop sharply and the importance of the past meteorological elements starts to grow from late September. Whilst from mid-November the weight of the past weather elements exceed that of the current ones until the preceding week of the pollen season.

Pinus and *Plantago* genera are sensitive especially to the current weather conditions (Fig. 2, 1st panel from above). The past meteorological elements seem to have the smallest effect on these taxa of all analyzed in the study. The current weather conditions have the largest effect on these genera with gradually decreasing weights from the end of the previous

pollen season (late May for *Pinus* and late September for *Plantago*). For *Plantago,* this decrease is continuous, while for *Pinus* two smaller peaks (in mid-November and mid-January) can be observed.

For *Platanus,* the weights of the current meteorological elements exceed those of the past climate in the summer period (late May – early August) (Fig. 2, 2nd panel from above, left). The effect of current climate elements is the highest in June and July. After mid-August, the weights of the past climate elements slightly exceed those of the current ones. Both show an increasing trend in the autumn and winter period. The shape of the curves of both the past and current meteorological variables is nearly parallel for the period between mid-August and the beginning of the new pollen season.

For *Populus,* the past meteorological elements have higher weights compared to the current climate parameters except 2-3 days before the start of the pollen season (Fig. 2, 3rd panel from above, left). This is due to the fact that representatives of these species are mainly found on floodplains or in areas influenced by groundwater-flow, like the sand lands of the Danube-Tisza Interfluve. In floodplain areas the floods of former years lay fresh deposits on which new stands of poplars can germinate. Floodplains always reflect to past meteorological elements via the water-level of the rivers as the increase and decrease of water-level – which is followed also by groundwater – occurs with a delay after a dry or wet period. In the sand lands of the Danube-Tisza Interfluve the Poplar forests are fed by precipitation and stands situated in the blow-outs of the groundwater-flows are supplied by water with a delay of even several days or weeks (Herke 1934, Miháltz 1966, Rónai 1975, Margóczi et al 2008). Due to hydrogeographical reasons *Populus* stocks are mainly influenced by past weather events.

For *Quercus,* the weight of the current meteorological elements is much higher than that of the past climate parameters from mid-May until mid-August (Fig. 2, 3rd panel from above, right). At the beginning of August, the weights of the current meteorological factors begin to decrease sharply and reach their minimum at the middle of September, whereas the role of the past climate parameters shows a moderately increasing trend until the end of December.

For *Rumex,* only small differences can be observed in the weights of the current and past meteorological elements between the previous and the new pollen seasons (Fig. 2, 4th panel from above, left). The current meteorological elements have the largest weights with major peaks in early September and at the end of October which seems favourable for the optimal seed production as well (especially on dry and warm days).

For *Taxus,* the past meteorological elements have a prominent role between the previous and the new pollen seasons except the few days before the beginning of the new pollination period in early February when the current meteorological elements become dominant (Fig. 2, 4th panel from above, right). The weight of the current climate elements definitely increases from the beginning of December comprising two local minima.

Tilia seems to be sensitive to the past weather conditions as the weights of the past meteorological elements are higher than those of the current ones except for several days before the start of the pollen season when the current weather conditions become a bit more important (Fig. 3, 1st panel from above, left). The difference between the roles of current and past weather elements is the highest at mid-May after the end of the previous pollen season. The smallest differences occur at the beginning of September and mid-March.

For *Ulmus,* also the major role of the past weather conditions can be identified except for a few days before the start of the new pollen season when the weights of the current meteorological parameters exceed those of the past ones (Fig. 3, 1st panel from above, right).

The difference between the effect of the past and current weather conditions is the highest after the end of the previous pollen season (early April). The effect of the past meteorological elements is dominant; however, their weights moderately decrease from the start of the pollen-free period involving two local maxima in mid-October and mid-December.

The shape of the curves for *Urtica* is the most equalized of all taxa (Fig. 3, 2nd panel from above, left). After finishing the previous pollen season, the past meteorological elements have slightly larger weights against the current ones and their slight temporal changes are parallel until the beginning of April. For the pollen production the period of early January – early March seems dominant.

4. DISCUSSION AND CONCLUSIONS

Climate change can modify the pollen season characteristics of different allergenic taxa in diverse ways and can exert a substantial influence on habitat regions. To our knowledge, a comprehensive spectrum of the regional pollen flora was only analysed in three studies, namely in Clot (2003) 25 plant taxa, Damialis et al. (2007) 16 plant taxa and Cristofori et al. (2010) 63 plant taxa, respectively. Though these studies provided a broad survey and a detailed analysis on the pollen season characteristics and trends of a large number of taxa, they did not examine the effect of the temporal distribution of the values of the meteorological parameters on the current pollen levels. The present study analyses one of the largest spectra with 19 taxa. Our study can be considered unique in the sense that it separates the effects of the current and past meteorological elements that influence the current pollen concentrations.

Changing climate involves different changes in the weather elements of the individual seasons. A potential importance of our procedure is that a period with a changing climate that may have a major impact on the current pollen counts can be detected by the past of meteorological elements.

As regards the taxa with the highest pollen concentrations, *Ambrosia* genus has only one species, namely *Ambrosia artemisiifolia* (Common Ragweed) in the Szeged region that appears both in the urban environment and in the countryside. Ragweed occurs especially frequently west of the city. The ruling north-western winds can easily transport pollen into the city. Since in the sandy region, northwest of Szeged, stubble stripping is not necessary for ground-clearance due to the mechanical properties of sandy soils *Ambrosia* can spread unchecked. Owing to newly-built motorways around Szeged, several farmland areas have been left untouched for a long time that also favour the expansion of *Ambrosia*. Several species of the Poaceae family, namely *Agropyron repens* (Common Couch), *Poa trivialis* (Rough Meadow-grass), as well as *Poa bulbosa* (Bulbous Meadow-grass) over untouched areas, furthermore *Poa angustifolia* (Narrow-leaved Meadow-grass) and *Alopecurus pratensis* (Meadow Foxtail) in the floodplain and along the dyke surrounding the Szeged region represent a substantial proportion of pollen in the city. Along the urban lakesides *Phragmites australis* (Common Reed) is the most frequent Poaceae. Furthermore, on short grass steppes of sand, loess and saline areas *Festuca pseudovina* and *Festuca rupicola* also occur. For the *Populus* genus, natural species of *Populus alba* (White Poplar) and *Populus canescens* (Grey Poplar) are the most frequent in the city and are characteristic in floodplain forests along the Tisza and Maros Rivers. In addition, cultivated poplars such as I-273 Poplar and *Populus x euramericana* (Canadian Poplar) and its variants are frequently planted in

urban parklands, public places, as well as along roads in peripheries. The *Urtica* genus with its only species of *Urtica dioica* (Common Nettle) in the Szeged region is prevailing in the floodplain forest underwood of the Tisza and Maros Rivers, road- and channel-sides and in locust-tree plantations around the city. *Urtica* also occurs in the neglected grassy lands of the city area (Deák 2010).

The remaining species seldom occur here. *Alnus* species are only found in the Botanical Garden of Szeged. Pollen of *Artemisia, Cannabis,* Chenopodiaceae and *Rumex* can come from neglected areas of both the city and its surroundings, as well as from stubble pastures. *Betula, Juglans, Pinus, Platanus, Taxus* and *Tilia* species have been planted exclusively in public places and gardens; they have no natural habitats in the Szeged region. However, since the 1960s *Pinus* (*Pinus sylvestris* and *Pinus nigra*) species have been extensively planted in the sandy regions north-west of Szeged within the framework of an afforestation programme. Their pollen can easily reach Szeged with the north-western winds. *Morus* is planted along avenues and in public places. *Plantago* species occur in natural grassy areas of both the city and its surroundings. *Quercus* species are planted along the embankment surrounding the city, as well as north of the city. *Ulmus* is planted in the city too; however it is not very common. *Ulmus minor* is quite frequent in all landscape types around Szeged on boundaries, road-sides and channel-sides. Its scattered mono-dominant plantations can appear in loess landscapes and saved-side floodplains, as well as rarely in sand landscapes. In the above-mentioned places the formerly planted *Ulmus pumila,* as an adventive species, also occurs, but its spread is not characteristic. Large natural stands of *Ulmus minor* together with *Ulmus laevis* live in the oak-elm-ash alluvial forests alongside the River Maros where planted and spontaneous stands both appear. They can be found spontaneously even in the willow-poplar alluvial forests thanks to the mature stands of the Pécska forest on the Romanian side (Deák 2010).

The taxa examined can be classified into three groups, namely arboreal deciduous (AD), arboreal evergreen (AE) and herbaceous (H) taxa. It was found that a better comparison can be established if the taxa are separated within each group according to the starting month of their pollination season. Within the group of AD taxa, *Alnus, Populus* and *Ulmus* are marked by a late summer – early autumn peak of their past meteorological elements exceeding those of the current ones almost all over the pollen-free period. For *Juglans, Morus, Platanus* and *Quercus,* the major weights of the current meteorological elements in the spring and early summer involve the most characteristic contribution to the pollen production. A few days before the start of the new pollen season the current weather conditions are predominant for all AD taxa (Figs. 1-2, Table 1). AE taxa comprise only *Pinus* and *Taxus,* but their curves are totally reverse without any similarity (Figs. 1-2; Table 1). For H taxa, Poaceae is the only taxon starting its pollination in April, so it is excluded from further analysis. Since the pollen season of *Cannabis* and Chenopodiaceae starts in early and late June, these taxa are listed into the groups pollinating from May and July, respectively. In this way, the curve of the taxa pollinating from May (*Cannabis, Plantago, Rumex* and *Urtica*) indicate the most equalized course of weights in the study. For *Cannabis, Plantago* and *Rumex* the effect of the current weather conditions is more important from the beginning of the pollen-free season, while just before the start of the new pollen season the weights of the past climate elements are more remarkable, except *Urtica* (Fig. 1, Fig. 3, Table 1). *Ambrosia, Artemisia* and Chenopodiaceae comprise the highest weights of the past weather conditions of all taxa until at least three months before the start of the pollination that are characteristic

in determining the pollen production. However, some days or weeks before the start of the new pollen season the current climate elements have a higher importance (Fig. 1, Table 1).

. We should remark that water is much more essential to genera dominated by trees like *Quercus, Platanus, Pinus, Morus, Juglans, Betula* and *Alnus*. In this way, autumn and winter precipitation income influences their growth and pollen production potentials more than for herbaceous plants.

Note, that our findings for assessing the effect of the antecedent and current meteorological conditions on the current pollen concentration are valid only for variations of the daily pollen concentrations accounted for by the above-mentioned eight explanatory variables and nothing is known about the variance portion not explained by these variables.

REFERENCES

Bartková-Ščevková J (2003) The influence of temperature, relative humidity and rainfall on the occurrence of pollen allergens (Betula, Poaceae, Ambrosia artemisiifolia) in the atmosphere of Bratislava (Slovakia). Int J Biometeorol 48:1-5

Clot B (2003) Trends in airborne pollen: an overview of 21 years of data in Neuchâtel (Switzerland). Aerobiologia 19:227-234

Clot B (2008) Recent changes in airborne pollen and allergy risk. Environ Risque Sante 7:431-434

Cristofori A, Cristofolini F, Gottardini E (2010) Twenty years of aerobiological monitoring in Trentino (Italy): assessment and evaluation of airborne pollen variability. Aerobiologia 26:253-261

D'Amato G (2011) Effects of climatic changes and urban air pollution on the rising trends of respiratory allergy and asthma. Multidiscip Respir M 6:28-37

Damialis A, Halley JM, Gioulekas D, Vokou D (2007) Long-term trends in atmospheric pollen levels in the city of Thessaloniki, Greece. Atmos Environ 41:7011-7021

Deák JÁ (2010) Csongrád megye kistájainak élőhely-mintázata és tájökológiai szempontú értékelése. [Habitat-pattern and landscape ecological evaluation of the microregions of Csongrád country. (in Hungarian)] PhD thesis. University of Szeged, Szeged, Hungary

Deák JÁ (2011) Vegetáció-monitoring vizsgálatok Kunpeszéren a rákosi vipera védelmi programhoz kapcsolódóan 2010. Kutatási jelentés. [Vegetation-monitoring studies on Kunpeszér, associated with the protecting programme for rákosi viper 2010. Research report. (in Hungarian)] Magyar Madártani és Természetvédelmi Egyesület

Deák JÁ (2012) Vegetáció-monitoring vizsgálatok Kunpeszéren a rákosi vipera védelmi programhoz kapcsolódóan 2011. Kutatási jelentés. [Vegetation-monitoring studies on Kunpeszér, associated with the protecting programme for rákosi viper 2011. Research report. (in Hungarian)]) Magyar Madártani és Természetvédelmi Egyesület

Feehan J, Harley M, van Minnen J (2009) Climate change in Europe. 1. Impact on terrestrial ecosystems and biodiversity. A review (Reprinted). Agron Sustain Dev 29:409-421

Galán C, Cariñanos P, García-Mozo H, Alcázar P, Domínguez-Vilches E (2001) Model for forecasting Olea europaea L. airborne pollen in South-West Andalusia, Spain. Int J Biometeorol 45:59-63

Galán C, Alcázar P, Cariñanos H, Garcia E, Domínguez-Vilches (2000), Meteorological factors affecting daily Urticaceae pollen counts in southwest Spain. Int J Biometeorol 43:191-195

Herke S (1934) Szeged-Kiskunhalas környéke belvizes és szikes területeinek talajviszonyai. [Soil conditions of inland inundation and saline areas of the Szeged-Kiskunhalas region. (in Hungarian)] In: Sajó E, Trummer Á (eds) A magyar szikesek. (Saline areas in Hungary.) Pátria Nyomda, Budapest

Hirst JM (1952) An automatic volumetric spore trap. Ann Appl Biol 39:257-265

Hjelmroos M, Burkhead T, Egen NB, Spangfort M, Schumacher MJ (1999) Effects of automobile pollution and sunlight on variation of Bet v I content of birch pollen. J Allergy Clin Immun 103:S91-S91. Part 2, Meeting Abstract 347

Horváth F, Dobolyi ZK, Morschhauser T, Lőkös L, Karas L, Szerdahelyi T (1995) Flóra adatbázis 1.2. [Flora Database. (in Hungarian)] MTA-ÖBKI, Vácrátót

Jahn W, Vahle H (1968) Die Faktoranalyse und ihre Anwendung. Verlag die Wirtschaft, Berlin

Jolliffe IT (1993) Principal component analysis: A beginner's guide – II. Pitfalls, myths and extensions. Weather 48:246-253

Kasprzyk I (2008) Non-native Ambrosia pollen in the atmosphere of Rzeszow (SE Poland): Evaluation of the effect of weather conditions on daily concentrations and starting dates of the pollen season. Int J Biometeorol 52:341-351

Lindner M, Maroschek M, Netherer S, Kremer A, Barbati A, Garcia-Gonzalo J, Seidl R, Delzon S, Corona P, Kolström M, Lexer MJ, Marchetti M (2010) Climate change impacts, adaptive capacity, and vulnerability of European forest ecosystems. Forest Ecol Manag 259:698-709

Liu PWG (2009) Simulation of the daily average PM10 concentrations at Ta-Liao with Box-Jenkins time series models and multivariate analysis. Atmos Environ 43:2104-2113

Makra L, Sánta T, Matyasovszky I, Damialis A, Karatzas K, Bergmann KC, Vokou D (2010) Airborne pollen in three European cities: Detection of atmospheric circulation pathways by applying three-dimensional clustering of backward trajectories. J Geophys Res-Atmos115:D24220

Makra L, Matyasovszky I (2011) Assessment of the daily ragweed pollen concentration with previous-day meteorological variables using regression and quantile regression analysis for Szeged, Hungary. Aerobiologia 27:247-259

Margóczi K, Aradi E, Papp M (2008) A dél-kiskunsági semlyékek vegetációjának hidrogeográfiai háttérfaktorai. Aktuális Flóra- és Vegetációkutatás a Kárpát-medencében, VIII. Konferencia, Összefoglalók. [Hydrogeographical background factors of the vegetation of blow-out areas over the Southern-Kiskunság region. Actual Flora and Fauna Research in the Carpathian Basin, VIIIth Conference, Absracts. (in Hungarian)] Gödöllő-Debrecen. Kitaibelia 13:115

Miháltz I (1966) Az Alföld déli részének földtani és vízföldtani viszonyai. [Geological and hydrogeological relationships of the southern part of the Great Hungarian Plain. (in Hungarian)] Hidrológiai Tájékoztató 1:107-119.

Motta AC, Marliere M, Peltre G, Sterenberg PA, Lacroix G (2006) Traffic-related air pollutants induce the release of allergen-containing cytoplasmic granules from grass pollen. Int Arch Allergy Imm 139:294-298

Parry ML, Canziani OF, Palutikof JP, van der Linden PJ, Hanson CE (eds) (2007) IPCC. Climate Change 2007. Impacts, Adaptation and Vulnerability. Contribution of Working Group II to the Fourth Assessment Report of the Intergovernmental Panel on Climate Change. Cambridge University Press, Cambridge, UK

Rónai A (1975) A talajvíz és a rétegvíz kapcsolata az Alföldön. [Relationship of ground water and formation water in the Great Hungarian Plain. (in Hungarian)] Hidrológiai Közlöny 55:49-53

Štefanič E., Kovačevič V, Lazanin Ž (2005) Airborne ragweed pollen concentration in north-eastern Croatia and its relationship with meteorological parameters. Ann Agr Env Med 12:75-79

Ziska LH, Gebhard DE, Frenz DA, Faulkner S, Singer BD, Straka JG (2003) Cities as harbingers of climate change: Common ragweed, urbanization, and public health. J Allergy Clin Immun 111:290-295

SOME ASPECTS OF INDICATOR DEVELOPMENT FOR MAPPING MICROCLIMATE REGULATION ECOSYSTEM SERVICE OF URBAN TREE STANDS

Á TAKÁCS, M KISS and Á GULYÁS

Department of Climatology and Landscape Ecology, University of Szeged, P.O.Box 653, 6701 Szeged, Hungary
E-mail: takacsagi@geo.u-szeged.hu

Summary: In the light of the changing climate the urban heat island effect delineates important tasks for researchers and for urban planners. One choice of the adaptation possibilities is to preserve and extend urban green surfaces. The quantitative assessment of the ecosystem services of green surfaces is required to meet policy objectives. In our study, we summarize the available experiences concerning the evaluation and indication of climate regulation based on results from the literature. This is followed by a brief summary of the micro- and local-scale climatic effects of urban trees, with particular regard to the modification of the factors which affect human thermal comfort. Finally we make some suggestions concerning the mapping of urban green surfaces from the aspect of human thermal comfort with regard to indicator-development aspects.

Key words: urban heat island, ecosystem services, indicators, trees, microclimate regulation

1. INTRODUCTION

In the light of the changing climate the urban heat island effect marks important tasks for researchers and for urban planners. Because of the increasing number of urban citizens, proper adaptation features need to be worked out. Of these features the most important are the protection and the increasing coverage of urban trees and green places, because the vegetation affects the microclimatic conditions and thus human thermal comfort. These positive properties of green areas can be interpreted as ecosystem services, together with e.g. carbon sequestration, energy saving and the recreational value of parks (Gómez-Baggethun and Barton 2013). This environmental assessment methodology in addition to the many scientific results of the various regional-scale planning processes is also expected to significantly determine the future. According to the European Commission communication of „Green Infrastructure – Enhancing Europe's Natural Capital" in 2013, the various national and international regional development programs have to serve the development of a Green Infrastructure. This document highlights urban green areas as highly important elements of the Green Infrastructure. The assessment and mapping of ecosystem services are in most cases carried out by developing indicators, which describe the processes well. Accordingly, indicators have been developed concerning the climate regulation of urban tree vegetation, in different urban evaluations. Dobbs et al. (2011) set a general framework to work out indicators for urban ecosystem services. They assessed 11 (primarily regulating) services and 3 disservices based on available or on easily obtainable spatial data for other cities as well.

The 'maintenance of favourable climate' service, which has primary importance in terms of our topic, was indicated with the cooling effect of the trees, which was calculated through the effect by tree cover in each land multiplied by m^2 of plot trees cover in °C. Some socio-economic indicators were also part of this analysis, which were compared to the full range of services. They also mentioned the limited usage of the indicators in different geographical regions because the biomass growth and climatic factors strongly affect the services, and they depend on the geographical location (Dobbs et al. 2011). Similarly to the previous study Bastian et al. (2012) described different urban places with the temperature reduction and its spatial extrapolation using the tree crown area. The specific of this work is that he included the climate control service in the ecosystem properties-potentials-services system, and by relatively easily obtainable spatial data, he could evaluate land use change scenarios with regard to the prevalence of a particular service. The work of Breuste et al. (2013) was also based on relationships with land use forms, where the data of parks and other land use types were created on the basis of remotely sensed data. Mean annual temperature was calculated on a large time scale, based on a dataset of nearly five decades.

Table 1 Characteristics of studies that have indicated climate regulation (temperature modification) in urban ecosystem service assessments

Citation	Urban area	Indicating method
Dobbs et al. (2011)	Gainesville (Florida, USA)	Temperature reduction effect by tree cover in each land multiplied by m^2 of plot trees cover in °C
Bastian et al. (2012)	Leipzig (Germany)	Shading potential (based on temperature measurements in shaded and non-shaded places) extrapolated to the whole city, using an urban tree GIS data layer
Breuste et al. (2013)	Karachi (Pakistan)	Temperature reduction effect of different urban green spaces, in relation to land use pattern/characteristics of built-up areas
McPherson et al. (2012)	New York City (USA)	Decreasing temperature (calculated based on latent enthalpy hours/cooling degree days ratio), multiplied with the percent of the total lot covered by coarse vegetation
Schwarz et al. (2011)	Leipzig (Germany)	Combined use of land surface emissivity (based on a case study-specific look up table) and evapotranspiration potential (based on empirical estimations and site specific calculations)

McPherson et al. (2012) also treated this specific service as temperature regulation, but the quantification of the indicator was based on the ratio of latent enthalpy hours (LEH) to cooling degree days (CDD) in the city. Based on the particularity of the urban climate, they defined the rate of temperature decrease from the spatial data of the tree canopy cover. Local climate regulation prevails in an integrated manner through several modified climatic factors, and according to this, Schwarz et al. (2011) developed indicators for urban-scale evaluations. One of the most important factors, which help in defining the temperature influencing effect of the different land uses, is land surface thermal emission. He developed this indicator with land use-specific look-up tables from remotely sensed data. Latent heat also plays an important role in affecting the air temperature. He indicated this with an evapotranspiration potential parameter, because evapotranspiration is in a linear relationship with latent heat. The quantification of land use class was based on empirical estimations, taking local environmental conditions into consideration. In this article urban planning policies and their effect to climate regulation were defined with two different indicators. The

result was that in most cases the value of the two indicators moved together, but in certain land use types showed significant differences, so if these indicators are used together it becomes possible to more exactly define the extent and spatial pattern of local climate regulation. We summarized the results in Table 1.

The above examples of different-scale evaluations have given spatial indicators for urban trees, or in broader aspect to other land use types, for defining climate regulation using air temperature decrease as an indicator base unit. Air temperature is an important factor for human thermal comfort (as a welfare factor, in the ecosystem services framework); however it is affected by several climatic parameters. Human bioclimatology is the discipline which deals with this. It uses the results to clarify the theoretical basis and to make different regional-scale analysis, and specific models to typify the thermal comfort in numbers (Gulyás et al. 2006, Gulyás and Matzarakis 2009). It's a fundamental law, that besides air temperature, relative humidity, wind speed, and the mean radiant temperature (T_{mrt}) also play an important role, influence the urban environment and have a significant spatial variability because of the heterogeneous urban environment. The above factors are affected by urban trees in a complex way, but the goal is not an accurate process-based modelling, only indicating an ecosystem service or function. Using together the models applied by human bioclimatology and the GIS methods with which we can define the location and ecological characterization of urban vegetation it is possible to work out indicators which will better describe human thermal comfort, and serve as a good basis for urban planning.

Based on the above our objectives are the follows:
– to give a brief summary of the micro- and local-scale climatic effects of urban trees based on the results of the recent literature, with particular regard to the modification and the spatial assessment opportunities of the factors, which affect human thermal comfort.
– to provide methodological proposals for developing indicators better describing human thermal comfort and its spatial pattern in the frames of the generally used system of ecosystem properties-functions-services.

2. CLIMATE REGULATION EFFECTS OF URBAN TREES

2.1. Temperature decreasing and shading in micro scale

One of the most important effect of urban trees on the modification of urban human comfort especially in hot summer days is the shading effect. Shading, the alteration of radiation energy balance, has two basic human bioclimatic impacts. Firstly, reducing the short wave radiation input the temperature increase of shaded surfaces is reduced and additionally the air temperature close to the surface remains lower. Secondly, reduced direct radiation impact of a body reduces the impact of the physiological load. These two effects together result in the significant increase of human comfort situation during sunny days (Ali-Toudert and Mayer 2007, Lee et al. 2013) Numerous comparative measurements showed in the last decade that arboreal vegetation – as a consequence of the above – reduces the air temperature (especially at daytime) at micro-scale (Table 2).

The mean near-surface air temperature in the shade (T_{air}) is less by 0.8-1.7°C than the ambient air temperature (min 0.4, max. 4.5°C, depending on the background climate, measurement method, type of surface cover, etc.). Most of the field measurements were carried out in summer (with warm-hot ambient temperature) at daytime. This decrease seems

subtle, compared to the 25-35°C air temperature. In such a hot summer the impact of direct radiation on human comfort has emphasized importance that can be described by mean radiant temperature (T_{mrt}) value. T_{mrt} is the most important parameter in the human energy balance during summer conditions, since most human biometeorological thermal indices have special interest in this parameter (Hodder and Parson 2007, Thorsson et al. 2007, Kántor et al. 2013). Our studies show that the T_{mrt} (obtained from human bioclimate models or globe thermometer) differs in higher extent than (16-34.1°C) the air temperature between open and shaded (by single trees or small trees group) areas. This fundamentally affects the energy balance of the body and thus the degree of physiological stress (Shashua-Bar et al. 2010).

Table 2 Characteristics of studies that have indicated micro-scale temperature (near-surface layer) and radiation modification between open spaces and under tree (shown only the summer daytime data) * no data, **simulated environment

city	ΔT_{air} (°C) max/mean	ΔT_{mrt} (°C) max/mean	details	citation
Freiburg (Germany)	2.2 / 0.9	34.1 / 20.1	summer, daytime, small group of trees (deciduous)	Streiling and Matzarakis (2003)
	1.7/ n.d.*	29.3 / n.d.	summer, day- and nighttime, small group (dec.)	Lee et al. (2013)
Lisbon (Portugal)	4.5 / 1.7	33 / 26	summer, winter daytime small group and single (dec.)	Andrade and Vieira (2007)
Saitama** (Japan)	1.9 / 0.8	24 / n.d.	summer, daytime single trees along the road (coniferous)	Park et al. (2012)
Szeged (Hungary)	2.1 / 1.6	31.4 / 22	summer, daytime single tree (dec.)	Gulyás et al. (2006)
Taipei City (Taiwan)	2.5 / 1.4	n.d. / n.d.	summer, daytime small group of trees (dec.)	Lin and Lin (2010)
Tel-Aviv (Israel)	3.1 / 1.6	29.2/n.d.	summert, winter, day- and nighttime (dec. con.)	Cohen et al. (2012)

The canopy of a tree can (i) reflect, (ii) absorb or (iii) transmit a certain percentage of the incoming solar radiation (Kotzen 2003, Hunter Block et al. 2012). At the local scale, the question is whether there is woody vegetation, or not. If there is, tree planting density, canopy coverage level and extension of the shaded area can be observed in the area (see in Section 2.3.). At micro-level the individual tree characteristics (e.g. species, age, size, canopy structure, etc.) and the differences of their transmissivity arising from these factors are more important. Some of these individual parameters differ between species thus for precise microclimatic characterization and more precise characterization of the ecosystem services their study may produce valuable information for city planning purposes and the decision makers. Lin and Lin (2010) examined the temperature decreasing effect of only 12 species. In Dimoudi and Nikolopoulou (2003) the light transmission of tree canopies was used for calculation only as a standard value. In other studies transmission was calculated from measured global and diffuse radiation data (Cantón et al. 1994, Shahidan et al. 2010, Konarska et al. 2013). Every study, including our unpublished data show that canopy transmission shows huge differences (depending on the density of crown, angle of sunbeam, etc.) reaching 4-30% in summer and 40-80% (deciduous trees) in winter (Shashua-Bar et al. 2010, Konarska et al. 2013).

The shading of trees has a positive effect on not only the outdoor thermal comfort; the shading of exposed walls of buildings (especially W and S oriented) reduces the warming up

of interiors. In a hot climate, trees planted around buildings (the species corresponding to the right place) can positively influence the energy balance and reduce cooling energy requirements of particular buildings through sheltering windows, walls, and rooftops from strong direct solar radiation and radiation reflected from the surroundings (Nakaohkubo and Hoyano 2011, Berry et al. 2013).

Previously, only few studies addressed the micro-scale examination of temperature differences between shaded and non-shaded surfaces. These papers mainly focused on the comparison of thermal relations of surfaces covered with asphalt or grass (Ca et al. 1998, Spronken-Smith et al. 2000). Another study compared the tree canopy surface temperature values of different species but did not examine the relationship between the air and surface (under the trees) temperature (Meier and Scherer 2012). Land surface temperature can be examined using remote sensing techniques, thus it is usually studied at a larger (e.g. local) scale.

2.2. Evapotranspiration

Another important process as trees contribute to the reduction of negative effects of the urban heat island is evapotranspiration (ET), which is the sum of evaporation (movement of water to the air from different surfaces such as the soil, canopy interception, and water surfaces) and transpiration (conversion of water within the leaf to water vapor, which is then released to the atmosphere through the stomata, thus cooling the leaf and the surrounding local microclimate (Hunter Block et al. 2012). This mechanism plays an important role in the water cycle, and as such, it contributes to the provision of ecosystem services by the trees (Georgi and Dimitriou 2010).

The rate of evapotranspiration depends on various features of the local weather and climatological conditions (which are given in the Penman-Monteith equation, the general formula for ET calculations) and the characteristics of the vegetation. The latter are important from the point of view of ecosystem service indicating. One general vegetation attribute used in evapotranspiration calculations is the leaf area index, which is used in assessments on different spatial scales (Lee and Park 2008, Georgi and Dimitriou 2010). It should be noted that there are several morpho-anatomical and physiological features (leaf structure, stomata control, etc.) of the plants that characterize the complex phenomenon of evapotranspirative cooling, which should ideally be incorporated in exact referring indicators of the trees (Hunter Block et al. 2012). Though, knowing that LAI can be treated as an integrated indicator for different ecosystem services and that measurement methods of it are well-developed also for urban assessments, it will probably be considered as a general indicator of evapotranspiration and latent heat flux in most assessments in the future as well. Another important vegetation parameter in evapotranspiration calculations is the species-specific crop factor (K_c) which is an experimental ratio and its exact determination should be carried out specifically for the geographical region. In the multiparametric model for park cooling island by Vidrih and Medved (2013), LAI was used as general indicator in the thermal model (through the index of LAI_{sp} for integrative representation of trees and grass), with the evaporative heat flux incorporated. For the direct measurement of evapotranspiration (and thus for validation of other methods) there are several field-based techniques; the one which can be considered the most frequent is the eddy correlation method (Oke 1987).

Remote sensing methods provide useful assessment opportunities for calculating evapotranspiration in urban green spaces or other wider areas, enabling the analysis of spatial variations. In remote sensing approaches, spectral information is used mainly for defining

empirical relationships to predict a parameter for the calculations (e.g. crop coefficients, surface temperature) (Nouri et al. 2013). These methods can probably form a good basis for ecosystem service assessments as well, when evapotranspiration is directly handled as an indicator in spatial assessments.

2.3. Local scale effects of green spaces

The previous overviewed climatic effects prevail in bigger urban green spaces in the phenomenon of Park Cool Island (PCI). In urban scale studies, in the past few years several studies examined its different aspects (Bowler et al. 2010). The generally measured parameters in PCI studies are air temperature and relative humidity, but there examples also for radiation measurements and bioclimate index calculations (Oliveira et al. 2011).

The influence of green areas in the urban environment depends on a wide variety of factors, such as size and vegetation structure, season and time of the day, sky obstruction, and weather conditions in the built-up and green areas, and the climatic zone where the green area is located (Oliveira et al. 2011). These connections can be analysed in targeted models to estimate the PCI intensity or indicators of the effect. Feyisa et al. (2014) investigated statistical relationships between different characteristics of the vegetation of parks (species group, NDVI, size and shape parameters, etc.) and some chosen characteristics of the PCI (mean hourly temperatures inside the park, park cooling distance, etc.) The multiple linear regression found many valuable informations on the effects of the studied parameters, though it should be noted that these (and every kinds of) statistical models have to be developed for every cases. For this reason, they are useful primarily in the baseline study phase for indicator development and other decision making-oriented works.

Another modelling approach was introduced by Vidrih and Medved (2013), who developed a multiparametric CFD model for estimating the cooling effect. The heat fluxes were calculated for the tree and grass layers separately. One of the parameters of the vegetation was the leaf area index, for which a constant value was given in the case of the grass layer, and a species-specific growth curve was used for the trees. Another was transmissivity, which was calculated based on the actual LAI value (for the tree layer). The model was well-verified with field temperature measurements; this fact highlights the usefulness of these types of indicating the vegetation structure.

The surface temperature (and thus the differences between parks and built-up areas) can be detected using remote sensing techniques, based on data of the thermal band of multispectral imagery. For these types of analyses the most often used datasets are from Landsat and ASTER sensors (Cao et al. 2010, Ren et al. 2013). From an ecosystem service aspect, the surface temperature does not represent the total effect of urban trees and green spaces on human thermal comfort, and the spatial resolution of the above-mentioned data is irrelevant in micro-scale studies. But, owing to the widely available data, remote sensing based PCI studies can have an important role in urban scale assessments.

3. METHODOLOGICAL ASPECTS OF ECOSYSTEM SERVICE INDICATOR SELECTION

As the above-mentioned examples show, a numerical link can be established between the determinable and measurable parameters of urban trees and tree stands and human heat

stress as a direct indicator of the well-being of citizens. All the parameters which determine human comfort are only available from point-like calculations; therefore integrated heat stress maps have so far only been created by interpolating micro-scale calculations or point-like data (Égerházi et al. 2013, Takács 2013). However when the task is to choose and develop suitable indicators for the climate regulation effect of urban tree stands, or in a wider context, urban ecosystems, all the steps of the cascade model (Potschin and Haines-Young 2011) elaborated to represent the supply side of the ecosystem services can be expressed.

Several frameworks have been worked out recently for the indicator development (Dobbs et al. 2011, Bastian et al. 2012, van Oudenhoven et al. 2012). It is common in these frameworks that indicator development should be carried out in a hierarchical order (Fig. 1), where different yet quantitatively related indicators characterize the ecosystem properties, ecosystem functions (the latter is called ecosystem capacity by Bastian et al. (2012) and the utilization-based ecosystem services. In bioclimate-based evaluations the property-indicator can be the leaf area, or leaf area index, which characterizes foliage density which describes the shading effect as well as the whole biomass independently from the built-up environment or the land use. For a function indicator (in order to express the potential service supply) we suggest a shading-index possibly taking into account the effect of the buildings since human-made structures also affect the amount of ecosystem services, besides the ecosystem characteristics. One of the most important components of thermal human comfort is radiant temperature, which can be well modelled at the local scale (Lindberg and Grimmond 2011). Service indicators should be chosen possibly with regard to their further usage. In the case of urban green places, which are visited by the urban citizens with recreational purposes, this is possible since in such places the bioclimatic conditions are statistically related to the usage of the visitors (Égerházi and Kántor 2011). This system is similar to the framework where indicators are classified as either state or performance indicators (de Groot et al. 2010). Ecosystem property indices can be used as state indicators while performance indicators describe the rate of service supply.
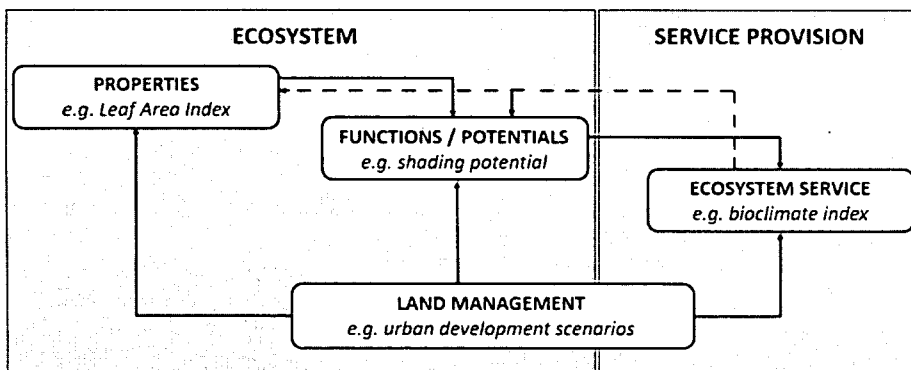

Fig. 1 Possible bioclimate-oriented indicators for mapping microclimate regulation of urban trees, in the framework by van Oudenhoven et al. (2012) for defining links between ecosystem and service provision, and based on Bastian et al. (2012)

The criteria of suitable ecosystem service indicators (van Oudenhoven et al. 2012), can be easily fulfilled in this indicator system. Temporal extensibility is possible, with the use of solid data (tree crown and building databases, meteorological data) which are available

or can be calculated for most of the cities. Therefore bioclimate-based indicators can form the basis of the evaluation if considering data availability. These data types also define the local climate zones, so they can serve as a basis for aggregation e.g. by creating transfer functions for each zone (already used for the mapping of other services) therefore a given indicator can be considered scalable (McPherson et al. 2013). In the evaluation and mapping of ecosystem services the use of aggregated indicators is always an option, and through these, it is possible to visualize ecosystem service bundles (UNEP-WCMC 2011, for example: in fast evaluations, mapping different services). Leaf area index, or canopy projection area (CPA), which represents the amount of biomass, can serve as indicators for several climatological services of urban tree stands. In several studies which involve the mapping and modelling of ecosystem services, it arises that the chosen indicator must be sensitive to land management (Petz and van Oudenhoven 2012), because such decisions significantly influence the state of the ecosystem, and the amount of the available services. It also makes it possible to analyze the amount of ecosystem services in different management intensity scenarios. In the case of urban green areas, land management not only means the usage of the service providing unit (e.g. the tree stand), but also the proportion of built-up areas which affects the amount of the services too. According to our previous statements socio-economic scenarios which are realized in the changing of land management intensity, will be different urban scenarios.

4. CONCLUSIONS

In the above literature review we highlighted the need to develop suitable spatial indicators describing the micro-climate regulation role of urban trees, which significantly affects human thermal comfort. If the mapping of this ecosystem service is intended the indicators need to be selected according to the complex nature of the phenomenon. For the shading effect of the trees there are several quantitative models with bioclimatological indices and for the mean radiant temperature there is an existing model which allows medium-scale mapping. At the same time, these works also highlight the species- and individual-specific variability of parameters which affect the shading effect (e.g. transmissivity). This requires further detailed field examinations in different geographical areas, and cities with frequent urban tree species, representing the age, structure and condition of the urban trees and the seasonal variability as well as possible. Another important task is to fit these factors into city- or district-scale evaluations. The evapotranspirational effect of the trees and larger green places appears in the bioclimatological measurements, but for the calculation of the latent heat flux, and meso-scale urban climate modelling it is necessary to choose and define the appropriate indicator (leaf area index) precisely, and relevant methodological background investigation is needed as well. In many studies the researchers use remotely sensed data to examine the climatic effects of large urban green places. The study of the intensity and extension of Park Cool Islands needs specific data types and knowledge, but for a certain parameter (surface temperature) it is possible to obtain reliable data on large areas. The urban climate phenomenon and the condition of green surfaces can be significantly different in various geographical regions, partly due to the differences in the vegetation; so many more studies are needed to be carried out in several places in order to work out appropriate indicators for this task.

REFERENCES

Ali-Toudert F, Mayer H (2007): Effects of asymmetry, galleries, overhanging façades and vegetation on thermal comfort in urban street canyons. Sol Energy 81:742-754

Andrade H, Vieira R (2007) A climatic study of an urban green space: the Gulbenkian park in Lisbon (Portugal). Finisterra 17:27-46

Bastian O, Haase D, Grunewald K (2012) Ecosystem properties, potentials and services – The EPPS conceptual framework and an urban application example. Ecol Indicat 21:7-16

Berry R, Livesley SJ, Ayeb L (2013) Tree canopy shade impacts on solar irradiance received by building walls and their surface temperature. Build Environ 69:91-100

Bowler DE, Buyung-Ali L, Knight TM, Pullin AS (2010) Urban greening to cool towns and cities: A systematic review of the empirical evidence. Landscape Urban Plan 97:147-155

Breuste J, Qureshi S, Li J (2013) Applied urban ecology for sustainable urban environment. Urban Ecosys 6:675-680

Ca VT, Asaeda T, Abu EM (1998) Reductions in air conditioning energy caused by a nearby park. Energ Buildings 29:83-92

Cantón MA, Cortegoso JL,Derosa C (1994) Solar permeability of urban trees in cities of western Argentina. Energ Buildings 20: 219-230

Cao X, Onishi A, Chen J, Imura H (2010) Quantifying the cool island intensity of urban parks using ASTER and IKONOS data. Landscape Urban Plan 96:224-231

Cohen P, Potchter O, Matzarakis A (2012) Daily and seasonal climatic conditions of green urban open spaces in the Mediterranean climate and their impact on human comfort. Build Environ 51:285-295

de Groot RS, Alkemade R, Braat L, Hein L, Willemen L (2010) Challenges in integrating the concept of ecosystem services and values in landscape planning, management and decision making. Ecol Complex 7:260-272

Dimoudi A, Nikolopoulou M (2003) Vegetation in the urban environment: microclimatic analysis and benefits. Energ Buildings 35:69-76

Dobbs C, Escobedo FJ, Zipperer WC (2011) A framework for developing urban forest ecosystem services and goods indicators. Landscape Urban Plan 99:196-206

Égerházi LA, Kántor N (2011) Area usage of two outdoor public places with regard to the thermal conditions – observation-based human thermal comfort study in the centre of Szeged. Acta Climatol et Chorol Univ Szegediensis 44-45:73-81

Égerházi LA, Kovács A, Unger J (2013) Application of microclimate modelling and onsite survey in planning practice related to an urban micro environment. Adv Meteorol 2013:251586

Feyisa GL, Dons K, Meilby H (2014) Efficiency of parks in mitigating urban heat island effect: An example from Addis Ababa. Landscape Urban Plan 123:87-95

Georgi JN, Dimitriou D (2010) The contribution of urban green spaces to the improvement of environment in cities: Case study of Chania, Greece. Build Environ 45:1401-1414

Gómez-Baggethun E, Barton DN (2013) Classifying and valuing ecosystem services for urban planning. Ecol Econ 86:235-245

Gulyás Á, Unger J, Matzarakis A (2006) Assessment of the microclimatic and human comfort conditions in a complex urban environment: modelling and measurements. Build Environ 41:1713-1722

Gulyás Á, Matzarakis A (2009) Seasonal and spatial distribution of physiologically equivalent temperature (PET) index in Hungary. Időjárás 113:221-231

Hodder SG, Parsons K (2007) The effects of solar radiation on thermal comfort. Int J Biometeorol 51: 233-250

Hunter Block A, Livesley SJ, Williams NSG (2012) Responding to the urban heat island: A review of the potential of green infrastructure.Victorian Centre for Climate Change Adaptation Research

Kántor N, Lin TP, Matzarakis A (2013) Daytime relapse of the mean radiant temperature based on the six-directional method under unobstructed solar radiation. Int J Biometeorol DOI 10.1007/s00484-013-0765-5

Konarska J, Lindberg F, Larsson A, Thorsson S, Holmer B (2013) Transmissivity of solar radiation through crowns of single urban trees—application for outdoor thermal comfort modelling. Theor Appl Climatol DOI 10.1007/s00704-013-1000-3

Kotzen B (2003) An investigation of shade under six different tree species of the Negev desert towards their potential use for enhancing micro-climatic conditions in landscape architectural development. J Arid Environ 55:231-74

Lee SH, Park SU (2008) A vegetated urban canopy model for meteorological and environmental modelling. Bound-Lay Meteorol 126:73-102

Lee H, Holst J, Mayer H (2013): Modification of human-biometeorologically significant radiant flux densities by shading as local method to mitigate heat stress in summer within urban street canyons. Adv Meteorol, 2013:312572

Lin BS, Lin YJ (2010) Cooling effect of shade trees with different characteristics in a subtropical urban park. Hortscience 45:83-86

Lindberg F, Grimmond CSB (2011) The influence of vegetation and building morphology on shadow patterns and mean radiant temperatures in urban areas: model development and evaluation. Theor Appl Climatol 105:311-323

McPherson PT, Kremer P, Hamstead Z (2012) Urban ecosystem services in New York City: A social-ecological multi-criteria approach. In: Ecological Economics and Rio+20: Challenges and Contributions for a Green Economy, Rio De Janeiro, Brazil

McPherson EG, Xiao Q, Aguaron E (2013) A new approach to quantify and map carbon stored, sequestered and emissions avoided by urban forests. Landscape Urban Plan 120:70-84

Meier F, Scherer D (2012) Spatial and temporal variability of urban tree canopy temperature during summer 2010 in Berlin, Germany. Theor Appl Climatol 110: 373-384

Nakaohkubo K and Hoyano A (2011) Development of passive designe tool using 3D-Cad compatible thermal simulation – prediction of indoor radiation environment considering solar shaving by surrounding trees and buildings. In Proc. of Building Simulation 2011: 12th Conference of International Building Performance Simulation Association, Sydney. 2711-2717

Nouri H, Beecham S, Kazemi F, Hassanli AM, Anderson S (2013) Remote sensing techniques for predicting evapotranspiration from mixed vegetated surfaces. Hydrol Earth Syst Sci Discuss10:3897-3925

Oke TR (1987) Boundary layer climates, Methuen, New York

Oliveira S, Andrade H, Vaz T (2011) The cooling effect of green spaces as a contribution to the mitigation of urban heat: A case study in Lisbon. Build Environ 46:2186-2194

Park M, Hagishima A, Tanimoto J, Narita K (2012) Effect of urban vegetation on outdoor thermal environment: Field measurement at a scale model site. Build Environ 56:38-46

Petz K, van Oudenhoven APE (2012) Modelling land management effect on ecosystem functions and services: a study in the Netherlands. Int J Biodivers Sci Ecosys Serv Manage 8:135-155

Potschin MB, Haines-Young RH (2011) Ecosystem services: Exploring a geographical perspective. Prog Phys Geogr 35:575-594

Ren Z, He X, Zheng H, Zhang D, Yu X, Shen G, Guo R (2013) Estimation of the relationship between urban park characteristics and park cool island intensity by remote sensing data and field measurement. Forests 4:868-886

Schwarz N, Bauer A, Haase D (2011) Assessing climate impacts of local and regional planning policies – quantification of impacts for Leipzig (Germany). Environ Impact Asses 31,97-111

Shahidan MF, Shariff MKM, Jones P, Salleh E, Abdullah AM (2010) A comparison of *Mesua ferrea* L. and *Hura crepitans* L. for shade creation and radiation modification in improving thermal comfort. Landscape Urban Plan 97:168-181

Shashua-Bar L, Potcher O, Bitan A, Boltansky D, Yaakov Y (2010) Microclimate modelling of street tree species effects within the varied urban morphology in the Mediterranean city of Tel Aviv, Israel. Int J Climatol 30: 44-57

Spronken-Smith RA, Oke TR, Lowry WP (2000) Advection and the surface energy balance across an irrigated urban park. Int J Climatol 20:1033-1047

Streiling S, Matzarakis A (2003) Influence of single and small clusters of trees on the bioclimate of a city: a case study. J Arboricult 29:309-316

Takács Á (2013) Mikro-bioklimatológiai vizsgálatok egy szegedi sétálóutca példáján. [Micro-bioclimatological assesments in a pedestrian street in Szeged. (in Hungarian)] MSc thesis, University of Szeged, Szeged, Hunary

Thorsson S, Lindberg F, Eliasson I, Holmer B (2007) Different methods for estimating the mean radiant temperature in an outdoor urban setting. Int J Climatol 27:1983-1993

UNEP-WCMC (2011) Developing ecosystem service indicators: Experiences and lessons learned from sub-global assessments and other initiatives. Secretariat of the Conventionon Biological Diversity, Montréal, Canada. Technical Series No. 58

van Oudenhoven APE, Petz K, Alkemade R, Hein L, de Groot RS (2012) Framework for systematic indicator selection to assess effects of landmanagement on ecosystem services. Ecol Indicat 21:110-122

Vidrih B, Medved S (2013) Multiparametric model of urban park cooling island. Urban Forest Urban Green 12:220-229

--